Lubricated Dynamic Friction Measurement of Thermoplastic Polyurethane

A thesis submitted in fulfillment of the requirements

for the degree of Doctor of Philosophy

in

Faculty of Mathematics, Informatics and Natural Sciences

Department of Chemistry

at

University of Hamburg

by

Xiangyun Kong

Hamburg 2019

The experimental work described in the present thesis has been carried out at the Institute of Technical and Macromolecular Chemistry, University of Hamburg, in the research group of Professor Dr. G. A. Luinstra, between October 2015 and December 2018.

1st Reviewer: Prof. Dr. Gerrit. A. Luinstra

2nd Reviewer: Prof. Dr. Berend Eling

Date of disputation: 06.09.2019

Print approval: 09.09.2019

The highest form of human intelligence is to observe yourself without judgement.

- Jiddu Krishnamurti

Table of Contents

Abbreviations and nomenclature

(in the order in which they appear in the text)

PU	polyurethane		v	sliding velocity [m/s]
TPU	thermoplastic polyurethane		σ	thickness parameter [-]
SSC	soft segment components		h_c	central film thickness [m]
HSC	hard segment components		λ	fluid film-thickness to roughness ratio
MDI	methylene diphenyl diisocyanate			
F_T	total friction force		R_a	arithmetic mean roughness [μm]
$F_{adhesive}$	adhesive friction force		R_q	root-mean-square roughness [μm]
$F_{hysteresis}$	hysteresis friction force		U	entrainment speed [m/s]
F_{wear}	wear or abrasion friction force		U_m	mean sliding velocity [m/s]
E^*	complex modulus of elasticity [Pa]		SD	standard deviation
E'	storage modulus of elasticity [Pa]		R_{tm}	mean peak-to-valley roughness [μm]
E''	loss modulus of elasticity [Pa]		T_g	glass transition temperature [°C]
CoF	coefficient of friction		$\tan \delta$	loss factor
CoF_A	adhesion component of CoF		G^*	complex shear modulus [Pa]
CoF_H	hysteresis component of CoF		G'	storage shear modulus [Pa]
p	nominal pressure [Pa]		G''	loss shear modulus [Pa]
p_0	maximum contact pressure [Pa]		DSC	Differential Scanning Calorimetry
P	average contact pressure [Pa]		BPST	British Portable Skid Tester
Gu	Gumbel number		MTM	Mini-Traction-Machine
Ω	angular sliding velocity [rad/s]		PDMS	polydimethylsiloxane
η	dynamic viscosity [Pa·s]		F_f	friction force [N]
EHL	elastohydrodynamic lubrication		M	torque [N·m]

r arm [m]

W load [N]

F_A axial force [N]

POM polyoxymethylene

S_m average spacing parameter [μm]

CoF_{min} minimum of CoF in the Stribeck curve

$a_T(T)$ time-temperature shift factor

TTS time-temperature superposition

T_{ref} reference temperature [°C]

f_{ref} reference frequency [Hz]

T environment temperature [°C] (Section 5.1)

T relevant temperature in the temperature dependent DMA curve [°C] (Section 5.2 and 5.3)

f deformation frequency [Hz]

R^2 linear correlation coefficients [-]

E_e equivalent modulus of a tribo-system [Pa]

E_1, E_2 (or E in general) Young's modulus of contacting bodies [Pa]

υ Poisson's ratio [-]

PTHF polytetrahydrofuran

l_N evaluation length [mm]

l_r cut-length [mm]

σ_s surface free energy of solid [mN/m]

θ contact angle [°]

σ_l surface tension of liquid [mN/m]

γ_{sl} interfacial tension [mN/m]

a contact radius [m]

d indentation depth [m]

1. Zusammenfassung

Moderne Rheometer können mit speziellem Zubehör ausgestattet werden, um Reibungsmessungen durchführen zu können. Solche in der Tribologie verwendete Aufbauten hat bei entsprechenden Studien an weichen Materialien Eingang gefunden. Eine neuartige Messmethode wurde nun entwickelt, um den Gleitreibungskoeffizienten (CoF) auf der Grenzfläche zwischen Stahlkugel und thermoplastischem Polyurethan mittels eines Rotationsrheometers mit einem „Drei-Kugel-auf-Platte"-Zubehör zu messen. Das Prüfverfahren wurde unter Verwendung von Polyoxymethylen (POM) und thermoplastischem Polyurethan (TPU) als repräsentativen Materialien entwickelt. Die Reibungseigenschaften wurden durch das Auftragen der CoF gegen die Gumbel-Zahl (Stribeck-Kurve) evaluiert.

Das Verfahren kann für die Bewertung der Nassrutschfestigkeit von Polyurethan-Elastomeren, z.B. bei Schuhsohlenmaterial, benutzt werden. Daher wurden die Testbedingungen so festgelegt, dass die biomechanischen und tribologischen Parameter die tatsächliche Situation des Rutschens von Schuhen auf nassen Oberflächen darstellen können. Die CoFs wurden bei verschiedenen Gleitgeschwindigkeiten von 3,3 bis 335 mm/s und einer konstanten Last von 1 N in drei verschiedenen Glycerin-Wasser-Gemischen gemessen. Die Stribeck-Kurve für POM zeigte drei verschiedene Schmierregime, nämlich die Grenzschmierung, die gemischte und die elastohydrodynamische Schmierung (EHL), während die Stribeck-Kurve für TPU das gemischte und das elastohydrodynamische Schmierregime sowie ein Übergangsregime zwischen den beiden zeigte. Die Messungen weisen eine gute Reproduzierbarkeit auf, und die erhaltenen CoFs beider Benchmark-Materialien zeigen eine gute Übereinstimmung mit den Werten in der Literatur.

Diese Arbeit berichtet über den Einfluss der Oberflächeneigenschaften sowie der Härte von TPU auf die Nassgleitreibung. Die Stribeck-Kurven für TPU-basierte Tribosysteme zeigten die Reibung in den Misch- und EHL-Regimen und belegten zugleich, dass die Oberflächeneigenschaften des TPUs die Reibung in beiden Schmierregimen beeinflussen können. Der Einfluss im gemischten Schmierregime ist für das Material deutlicher und die Stribeck-Kurven sind differenzierbarer als beim EHL-Regime. Die TPU-Oberflächen wurden mittels Sandpapier-Prägung unter Verwendung eines Heißpress-Protokolls behandelt, um zwei Kategorien von Oberflächenparametern zu erhalten: den durchschnittlichen Abstandsparameter (S_m), der die Unregelmäßigkeiten in horizontaler Richtung charakterisiert,

1. Zusammenfassung

und die arithmetische mittlere Rauheit (R_a) bzw. die mittlere Spitze-zu-Tal-Rauheit (R_{tm}), die die Rauheit in vertikaler Richtung zeigt. Auf den Oberflächen mit variierenden S_m (20 - 300 µm) und ähnlichen R_a (1 - 2 µm) und R_{tm} (4 - 7 µm) nahm der CoF mit zunehmendem S_m ab, bis er sich dem gleichen minimalen Pegel näherte, der auf einer glatten Referenzfläche erreicht wurde. Ein größerer Abstand zwischen Oberflächenunebenheiten förderte das Mitreißen von Flüssigkeit in die Kontaktzone und verringerte somit die Reibung. Eine einfache Analyse der Gleitfrequenzabhängigkeit von der „Hysterese-Reibung" zeigte, dass ein geringeres S_m mit einer höheren Verformungsfrequenz des Elastomers während des Nassrutschens einherging und zu einem höheren Energieverlust führte. Dies kann zu einem höheren Energieverlust der Hysterese führen, der zur Reibung beiträgt. Es konnte eine Korrelation zu den höheren Werten des Verlustmoduls oder Verlustfaktors bei der relevanten Temperatur in den temperaturabhängigen DMA-Kurven gefunden werden. Auf zwei Oberflächen mit verschiedenem R_a (2 gegen 3,4 µm) und R_{tm} (6 gegen 10 µm) und einem ähnlichen S_m (210 ~ 260 µm) stieg der CoF mit zunehmendem R_a oder R_{tm} an. Eine zunehmende Rauheit führte zu einem höheren Energieverlust (Hysterese) bei dem Kontakt zwischen Oberflächenunebenheiten der Stahlkugeln und des Polymers.

Die geschmierte Reibung von fünf TPU-Proben mit Shore-Härten von A80 bis A97 wurde ebenso untersucht. Um zu verhindern, dass die Oberflächenrauigkeit die Ergebnisse beeinträchtigt, wurden die Proben mit dem Heißpressverfahren vorbehandelt, um gleiche Oberflächeneigenschaften zu erhalten ($S_m \approx 200$ µm, $R_a \approx 2$ µm, $R_{tm} \approx 7$ µm). Innerhalb des getesteten Härtebereichs nehmen die CoFs im Mischschmierbereich mit zunehmender TPU-Härte zu. Die CoFs bei einer Gleitgeschwindigkeit von 11 mm/s wurden mit den viskoelastischen Eigenschaften der TPUs bei einer relevanten Temperatur von ca. 10ºC in Verbindung gebracht, die den temperaturabhängigen DMA-Kurven bei einer Verformungsfrequenz von 1 Hz entnommen wurden. Die CoFs wurden mit dem Verlustmodul und dem Verlustfaktor bei 10°C, 1 Hz und mit der mechanischen Hysterese bei 10% der maximalen Dehnung korreliert. Eine Linearität der Korrelation ist für den Verlustmodul und die Materialhysterese feststellbar.

2. Summary

2. **Summary**

Modern rheometers can be equipped with accessories to perform frictional measurement and the technology has gained popularity in tribology studies on compliant contact. A novel frictional method was developed to measure the lubricated dynamic coefficient of friction (CoF) on the steel-thermoplastic polyurethane contact, using a rotational rheometer in combination with a three ball-on-plate accessory. The testing procedure using polyoxymethylene (POM) and thermoplastic polyurethane (TPU) as representative materials was established and the frictional properties were evaluated using the Stribeck curve, i.e. plotting the CoF against the Gumbel number.

The method aims at the evaluation of wet slip resistance of polyurethane elastomers as shoe soling material. Therefore, the test conditions were defined to represent the biomechanical and tribological parameters involved in actual shoe slipping events. Precisely, the CoFs were measured at varying sliding velocities between 3.3 to 335 mm/s and a constant load of 1N in three different glycerin-water mixtures. The Stribeck curve for POM shows three distinguishable lubrication regimes-the boundary, mixed and elastohydrodynamic lubrication (EHL), while the Stribeck curve for TPU shows the mixed and elastohydrodynamic lubrication regimes and a transitional regime between the two. The obtained CoFs on both benchmark materials show good measurement repeatability and are in good agreement with literature.

This work also comprises a study of the effect of surface characteristics and bulk hardness of TPU on the wet sliding friction. The Stribeck curves for the TPU based tribo-systems show the frictional properties in the mixed and EHL regimes and demonstrate that the surface characteristics of the TPU can influence the friction in both lubrication regimes. The effect in the mixed lubrication regime is more noticeable and the Stribeck curves are more differentiable than in the EHL regime.

The TPU surfaces were treated by sandpaper imprinting using a hot-pressing protocol to obtain two categories of surface parameters: the average spacing parameter (S_m) characterizing the irregularities in the horizontal direction, and arithmetical mean roughness (R_a) and mean peak-to-valley roughness (R_{tm}) characterizing the roughness in the vertical direction. On the surfaces with varying S_m (20 to 300 µm) and similar R_a (1~2 µm) and R_{tm} (4~7 µm), the CoF decreases with increasing S_m until approaching a same minimum level as obtained on a smooth referential surface. Larger spacing between surface asperities promotes

2. Summary

fluid entrainment into the contact zone and hence reduces friction. A brief analysis of the sliding frequency dependence on hysteresis friction shows that a smaller S_m is associated with higher deformation frequency of the elastomer during wet sliding. This may cause more hysteresis energy loss contributing to the friction. Latter is correlated to the higher values of loss modulus or loss factor obtained from temperature dependent DMA curves using the time temperature superposition principle. On two surfaces with differentiable R_a (2 vs. 3.4 µm) and R_{tm} (6 vs.10 µm) and a similar S_m (210~260 µm), the CoF increases with increasing R_a or R_{tm}. Increasing roughness results in more energy loss during the contact between surface asperities of the polymer and the steel balls.

The lubricated friction of five TPU samples with hardnesses from 80 to 97 Shore A was investigated. To prevent the surface roughness from complicating the results, the samples were pre-treated with the hot-pressing protocol to obtain the same level of surface characteristics ($S_m \approx 200$ µm, $R_a \approx 2$ µm, $R_{tm} \approx 7$ µm). Within the considered range of hardnesses, the CoFs in the mixed lubrication regime increase with increasing TPU bulk hardness. The CoFs at the sliding velocity of 11 mm/s were associated with the viscoelastic properties of TPUs at the relevant temperature of ca.10°C taken from the temperature dependent DMA curves at a deformation frequency of 1Hz. The CoFs were correlated to the loss factor and loss modulus at 10°C, 1Hz and with the mechanical hysteresis at 10% maximum strain. A linear correlation was found for the loss modulus and material hysteresis.

3. Introduction and Background

3.1 Thermoplastic polyurethane elastomers in the footwear industry

Polyurethane elastomers are block copolymers comprised of alternating soft segments and hard segments, and display high reversible deformation. Such materials possess highly flexible chains with a low degree of intermolecular interaction as well as crosslinks which prevent sliding of the chains against their neighbors causing plastic flow. The basic chemical process of polyurethane preparation was discovered by Otto Bayer et al. in 1937 [1]. The soft segments (SS) are obtained by reacting polyether or polyester polyols with diisocyanates, and the hard segments (HS) usually consists of diisocyanates and chain extenders [2] (Figure 3.1). Polyols in elastomers are often based on polytetrahydrofuran diols, polyester polyols, or polyether polyols. The chain extenders can be either short-chain glycols or diamines. The isocyanate components are usually bifunctional, typically such as MDI (methylene diphenyl diisocyanate, 4,4'-MDI(**1**) and 2,4'-MDI(**2**)), TDI (toluene diisocyanate, 2,4-TDI (**3**) and 2,6-TDI (**4**)), NDI (1,5-naphthalene diisocyanate)(**5**), PPDI (1,4-*para*-phenylene diisocyanate)(**6**), TODI (3,3'-dimethyl-4,4'-biphenylene diisocyanate)(**7**), and hydrogenated MDI (H_{12}MDI (**8**)) (Figure 3.2). The isocyanates are generally manufactured as prepolymers, produced from the whole amount or part of the polyol in reaction with the diisocyanate. Additives typically include colorants, anti-hydrolysis agents (such as carbodiimides), plasticizers, abrasion-resistance enhancers (such as silicone oils or polyethylene) and flame retardants [3].

Because of rigidity and hydrogen bonding, the hard segment components (HSC) form hard domains acting as physical crosslinks and as filler particles within the rubbery soft segment components (SSC) matrix (Figure 3.3). The HSC are incompatible with the SSC due to the different polarity and chemical nature, which results in phase separation in most polyurethane elastomers. The degree of phase separation and domain formation depends on the macromolecular structure of the constituting monomers of polyurethane (PU), the molecular weight and sizes of the hard and soft domains, and the hydrogen bonding formation between the urethane linkages, and also influenced by the manufacturing process and reaction conditions [4]. By changing the formulation, polyurethanes can be produced with diverse properties from soft to relatively hard elastomers. The physical crosslinks provided by the hard domains in PU can be melted, allowing the material to be molded or extruded.

Polyurethane elastomers have found a broad and wide spectrum of applications in soft-contact tribology by virtue of their exceptional abrasion and chemical resistance, excellent mechanical and elastic properties, blood and tissue compatibility, and other specific properties. Representative examples of applications are in wheels, coatings, footwear, medical tubes and sieves in the mining industry [5]–[7].

$$n+m \ \ O=C=N-R-N=C=O \ \ + \ \ n \ HO-R'-OH \ \ + \ \ m \ HO\left(\overset{H_2}{C}\right)_x OH \longrightarrow$$

$$\left[\begin{array}{c}\overset{O}{\overset{\parallel}{C}}-\overset{H}{\overset{\mid}{N}}-R-\overset{H}{\overset{\mid}{N}}-\overset{O}{\overset{\parallel}{C}}\left[O\left(\overset{H_2}{C}\right)_x O-\overset{O}{\overset{\parallel}{C}}-\overset{H}{\overset{\mid}{N}}-R-\overset{H}{\overset{\mid}{N}}-\overset{O}{\overset{\parallel}{C}}\right]_m O-R'-O\end{array}\right]_n$$
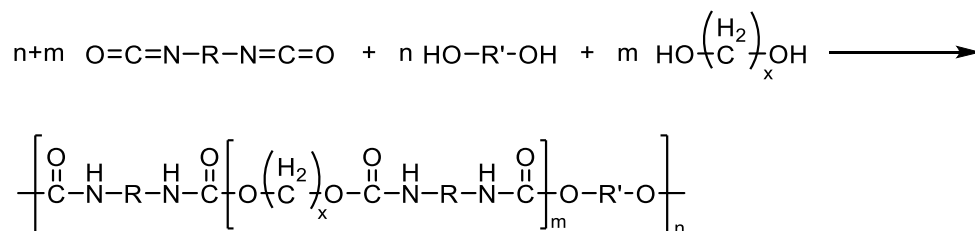
Figure 3.1 General structure of polyurethane elastomers. The representative structure shown in this figure is linear, single-phase (m=0) and phase-separated (m≠0) polyurethanes generated from bifunctional monomers.
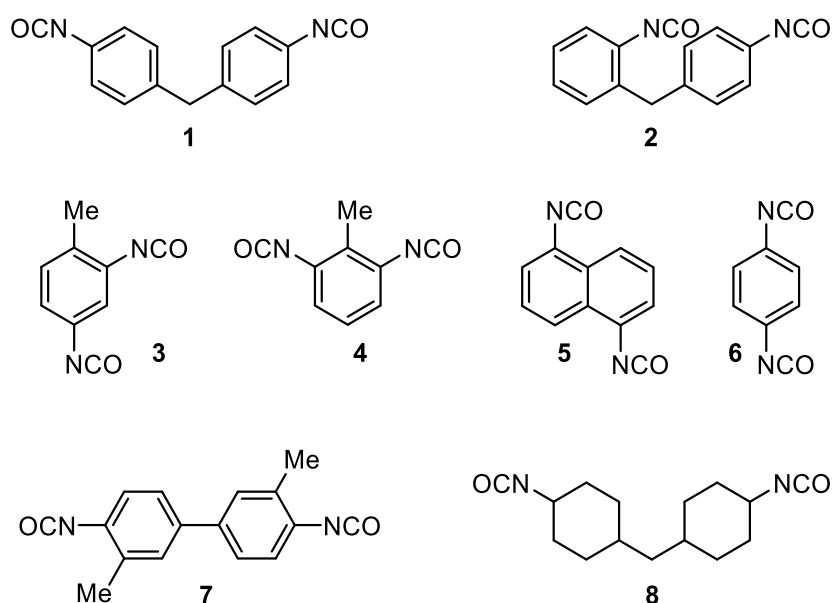

Figure 3.2 Industrially relevant diisocyanates used for manufacturing of polyurethane elastomers
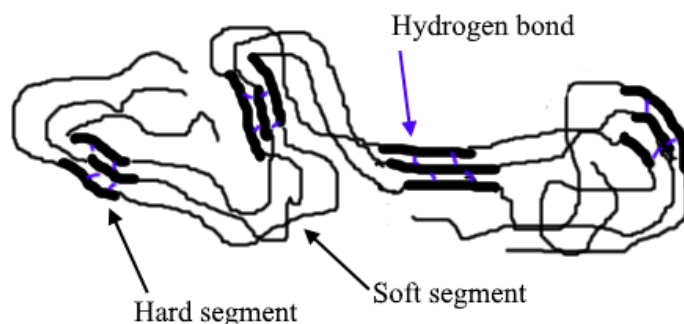
Figure 3.3 Alternating hard segment (HS) and soft segment (SS) structure of PUs

Polyurethanes are used in a wide range of footwear types. Although best known for sports and trekking shoes and boots, they are also extensively used for business and fashion shoes, as well as high-quality safety shoes [8]. Compared to other sole materials like rubber, PVC [(poly (vinyl chloride)] and EVA (ethylene vinyl acetate), polyurethanes have pronounced advantages: improved long-term flexibility, tear strength, resistance to puncture, hydrolysis resistance and flexibility over a broad temperature regime and high design flexibility. The features of commonly used polymeric sole materials are summarized in Table 3.1.

Table 3.1 Polymeric material used in shoe soles [9]

Material	Features
Latex/Crepe	Not vulcanized natural rubber, compact, low density (0.85-0.95 g cm^{-3}) and less stiff. Good slip resistance properties.
Natural rubber (NR) - polyisoprene	Sole material with good properties of resistance to abrasion and flexing.
Polyisoprene (IR)	Synthetic rubber with the same constitution of natural rubber.
Polybutadiene (BR)	Synthetic rubber with high resilience, abrasion and flexion resistance. Often used in mixtures with NR and SBR to improve its properties or to reduce production costs.
Styrene-butadiene rubber (SBR)	Similar characteristics of natural rubber (can be mixed). Density between 1.10-1.25 g cm^{-3} and a hardness between 60 to 80 Shore A.

	Good abrasion resistance, good mechanical properties and slip resistance.
Nitrile rubber (NBR)	Acrylonitrile-butadiene copolymer. Density between 1.10-1.25 g cm^{-3} and a hardness between 60 to 80 Shore A. It can be blended with PVC to improve resistance to oil and temperature. Good abrasion and slip resistance.
Polychoroprene (CR)	Correspond to the neoprene brand. It is especially used when improved resistance to oils is required.
Neolite	The base polymer is a styrene-butadiene copolymer, but with a higher styrene content (50 to 85%). High hardness (88 Shore A) and high density (1.25-1.40 g cm^{-3}). Low tensile strength and flexing. Typically used in classic shoe soles or/and covers.
SEBS (Styrene-Ethylene/Butylene-Styrene)	High resistance to UV radiation, good resistance to high temperature and good processing stability. Mostly used in hospital footwear.
Rubber thermoplastic (SBS)	Styrene-butadiene-styrene copolymer. High strength, a large range of hardness and low melt viscosity. Density of 0.90-1.20 g cm^{-3}, for compact shoe soles.
Acrylonitrile-butadiene-styrene (ABS)	Thermosetting plastics with good resistance to solvents and more thermostable than polystyrenes. Typically used in the production of heels, heel of high fashion shoes.
Polyvinyl chloride (PVC)	Used in thermoplastic form. It is a hard polymer, colorless solid resin and melts at temperatures between 170-180 $^{\circ}$C. Its thermal instability can be problematic due to release of HCl. Often has a reasonable/good wear resistance.
Polyurethane (PU)	There are two types of polyurethane used in shoe soles: polyester and polyether based. Density may vary from 0.06-1.25 g cm^{-3}. It can reproduced in expanded (microcellular) and compact (TPU) form. The expanded PU soles have properties such as lightness, softness, good low temperature flexibility and good slip resistance.

Ethylene Vinyl Acetate (EVA)	Can be used in its expanded form (microcellular) or as compact material (less usual). Some grades can be slippery and possess low tear and wear resistance and slow recovery after compression. Used mostly in sports shoes.

Two types of polyurethane elastomers are commonly used in the production of footwear: microcellular cast elastomer and thermoplastic polyurethane (TPU). Microcellular cast elastomers have a density ranging between 0.3 and 0.7 g cm^{-3}, which is considerably higher than that of conventional PU foam (e.g. flexible polyurethane foam). In contrast, solid cast elastomers (e.g. TPU) are not foamed and typically have a density of 1.2 g cm^{-3}[3][10]. Microcellular polyurethanes have excellent physical properties in combination with simple processing. It is predestined for the production of high-quality midsoles as well as for non-skid and compact running soles and beach mules [11]. TPUs are highly abrasion-resistant, oil, hydrolysis and microbe-resistant, and have high flexibility at low temperature and therefore particularly suited to the production of heavy-duty soles.

The differences in composition, processing and performance of polyurethanes produced with polyester polyol or polyether polyol provide different options for producers and designers of shoes. Polyester systems are favored in shoe soles due to their increased resistance to abrasion, tear, traction, greases and solvents. The excellent abrasion resistance makes them the preferred material for high durability soles. When resistance to oils and solvents is a requirement for applications such as safety shoes, the polyester-based systems are the preferred choice. However, as polyester-based polyurethanes are more sensitive to hydrolysis, with aging the physical properties may deteriorate. Anti-hydrolysis additives can be used as stabilizers, but it may impact the cost. Another option for manufacturing low-density soles with improved resistance to hydrolysis is the use of polyether polyols [12].

3.2 The lubricated friction of elastomers

3.2.1 General friction mechanisms in elastomeric friction

Elastomeric friction on working surfaces can be divided into at least three components:

Equation 3.1

$$F_T = F_{adhesive} + F_{hysteresis} + F_{wear}$$

F_T is the total friction force. $F_{adhesive}$ is the adhesive component. $F_{hysteresis}$ is the hysteresis component. F_{wear} is the wear or abrasion component.

The adhesion occurs in the regions of real contact and is described by modern theories of adhesion as a thermally activated molecular stick-slip process[13][14], as illustrated in Figure 3.4. The flexible chains in the elastomer structure are in a constant state of thermal motion. During relative sliding between an elastomer and a hard surface, the separate chains in the surface layer attempt to link with molecules in the hard base, thus forming local junctions like van der Waals bonds and hydrogen bonds, and is further enhanced by the flexible polymer molecules locking into the mating surface crevices [15]. The increase in pressure or temperature enhances adhesion, while the contamination, either due to surface film or lubricant, decreases it. Sliding action causes these bonds to stretch, rupture and relax before new bonds form so that effectively the elastomer molecules jump a molecular-scale distance to their new equilibrium position. Thus, a dissipative stick-slip process on a molecular level is fundamentally responsible for adhesion.
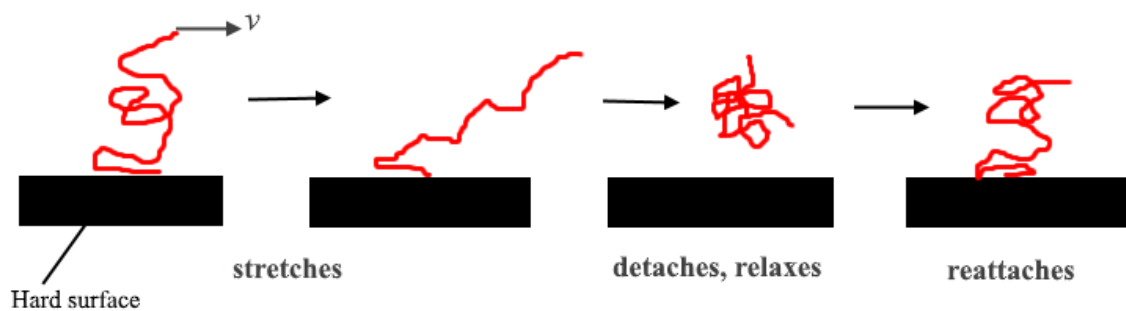

Figure 3.4 The classical description of a polymer chain in contact with a lateral moving countersurface. The chain stretches, detaches, relaxes, and attaches to the surface to repeat the cycle.

A conventional visualization of the hysteresis component of elastomeric friction is displayed in Figure 3.5. The contact area between an elastomer and a rough surface is characterized by a draping of the elastomer about individual asperities in the rigid base. Consider here the case of an elastomer sliding on a rounded, symmetrical asperity. In the absence of relative motion, a symmetrical draping of the elastomer about the asperity is produced. The pressure distribution normal to the contour of the asperity can be resolved into vertical and horizontal components. The summation of the vertical components must be in equilibrium with the load while the horizontal components cancel. If, however, the elastomer is moving with a finite velocity relative to the base surface, it tends to accumulate or "pile up" at the leading edge of the asperity and to break contact at a higher point on the download slope. Thus, the contact arc moves forward compared with the static situation, leading to an unsymmetrical pressure distribution. Now the horizontal pressure components give rise to a net force, which opposes the sliding motion.
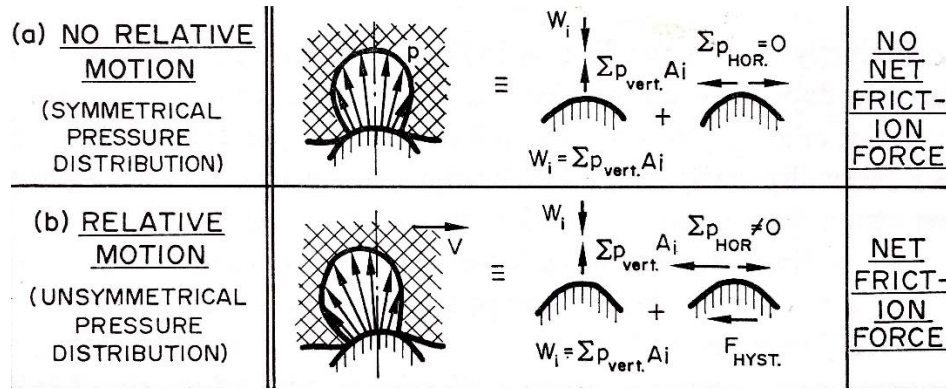

Figure 3.5 Effects of asperity interaction on hysteresis force in sliding (Reprinted from Ref. [14])

On a macroscopic level, both adhesion and hysteresis depend on the viscoelastic properties of the elastomer. Assume a sinusoidally oscillating strain is applied to an elastomeric body, a stress develops in direct response to the applied strain. The stress must also be sinusoidally oscillating in the linear viscoelastic region. The complex modulus of elasticity E^* as the ratio of stress to strain for the elastomeric body can be expressed as:

Equation 3.2

$$E^* = E' + iE''$$

where E' is the storage modulus for the component of stress in phase with the applied strain, and E'' is the loss modulus for the component of stress out of phase with the applied strain. The ratio of energy dissipated to energy stored per cycle is defined as the loss factor, where:

Equation 3.3

$$tan\ \delta = \frac{E''}{E'}$$

For a given elastomer and surface combination, the adhesion component of the coefficient of friction is given by the relationship [14][16]:

Equation 3.4

$$CoF_A = K_2 \frac{E'}{p^m} tan\ \delta$$

where p is the nominal pressure, m an exponent with a value about 0.2 and K_2 a constant dependent on the particular sliding combination. This equation shows the viscoelastic nature of adhesion.

The following equation is valid for the hysteresis component of the coefficient of friction [14]:

Equation 3.5

$$CoF_H = K_3 \left(\frac{p}{E'}\right)^n tan\ \delta \quad (n \geq 1)$$

where p is again the nominal pressure and K_3 is a constant. Both CoF_A and CoF_H depend directly on the loss factor, so that both components of friction may be attributed to the same viscoelastic mechanism. By combining *Equation 3.4* and *Equation 3.5*, we obtain the total coefficient of friction:

Equation 3.6

$$CoF = K_2 \left[\frac{E'}{p^m} + K_4 \left(\frac{p}{E'}\right)^n\right] tan\ \delta \qquad (K_3 = K_2 K_4)$$

Additionally, an abrasion can happen when an elastomer slides on a rigid substrate. There is evidence that irreversible deformation and some physical degradation of the sliding surfaces occurs, and it is often accompanied by a high coefficient of sliding friction. In the case of elastomers, three distinct mechanisms of wear can be identified, dependent on the nature of the surface texture [14]. For very sharp surfaces, abrasive wear produces micro-cutting and

longitudinal scratches on the elastomer surface. When the surface asperities are rounded rather than sharp, the surface of elastomer undergoes cyclic deformation and failure eventually occurs as a result of fatigue wear. On smooth surfaces, wear by roll formation occurs at the sliding interface, accompanied by continuous tearing of the rolled fragment [17].

3.2.2   The Stribeck curve as the evaluation tool of frictional properties

The Stribeck curve is a useful plot to show the frictional properties of a lubricated system over conditions usually spanning the boundary, mixed and hydrodynamic (or elastohydrodynamic for compliant[1] material) lubrication regimes. It must be determined experimentally for a specific tribological system ("tribo-system"). The earliest systematic study of the variation of friction between two liquid-lubricated surfaces as a function of speed for different loads on journal bearings was conducted by Thurston [18], Stribeck [19] and Martin [20] in the late 19th century. Around ten years later, Gümbel [21] and Hersey [22] plotted the friction coefficient against the dimensionless lubrication parameter ("*Gu*", the Gumbel number)

Equation 3.7

$$Gu = \frac{\Omega \eta}{P}$$

where η is the viscosity, Ω is the angular velocity, P is the load per unit projected area onto the geometrical surface[2], which forms the classic Stribeck curve (Figure 3.6). Originally developed for journal bearings, the Stribeck curve now has been extensively used for contacts with counterformal geometry such as a ball-on-three plate. The advantage of using the Stribeck curve in tribology research is that the non-dimensional lubrication parameters such as *Gu* allow a single curve to represent the same tribo-system under varying sliding velocities and normal loads.

---

[1] The word "compliant" is used as a synonym of "soft" throughout the text.
[2] In this work, P denotes the average contact pressure (see Appendix A.1).
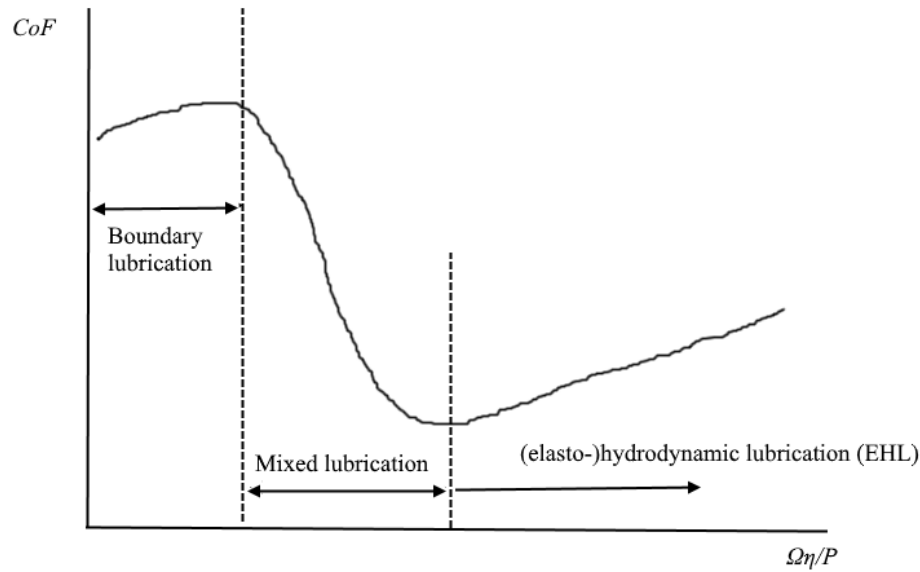
Figure 3.6 A typical Stribeck curve illustrating the three main regimes of sliding lubrication: (1) boundary lubrication; (2) mixed lubrication; (3) (elasto)hydrodynamic lubrication.

The three main lubrication regimes indicated in the Stribeck curve are illustrated Figure 3.7. Each regime is characterized by different flow and pressure conditions and governed by various friction mechanisms [23].
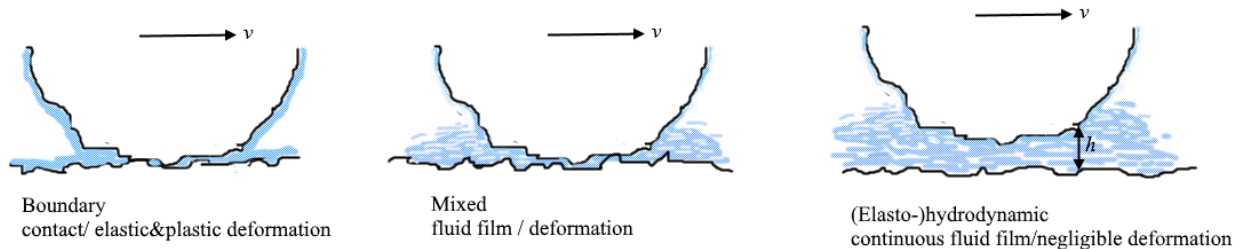

Figure 3.7 Illustration of three main lubrication regimes of sliding friction

The boundary lubrication regime can be found at lower values of Gu, and is often characterized by high coefficients of friction. The occurrence of low values of Gu is either due to high normal load or low sliding velocity, or low lubricant viscosity. At low Gu, the lubricant film between the sliding surfaces cannot support the applied load, and the two interacting surfaces are almost in solid-solid contact but still separated by a molecular-scale boundary layer of the lubricant. As the result of close contact of surface asperities, the friction is significantly influenced by material hysteresis and surface adhesion which is proportional

to the real contact area. The nominal area of asperity contact is only a fraction of the real contact area. At the microscopic level, surfaces are composed of asperities that themselves are composed of hundreds of micro-scale asperities, as illustrated in the surface profile in Figure 3.8. In addition, the friction can be accompanied by the breaking of surface asperities and the transference of surface residues. These worn particles lead to friction and wear by "plowing" across the surfaces [23], resulting in high friction. On the other hand, the detached material may form a solid lubricating layer to reduce the friction [24]. The interfacial junctions together with products of their fracture and the highly deformed layers where shear deformation is localized are named as "a third body." The term implies that the polymer involved in the friction process may possess the properties which differ drastically from its bulk properties [25]–[27].
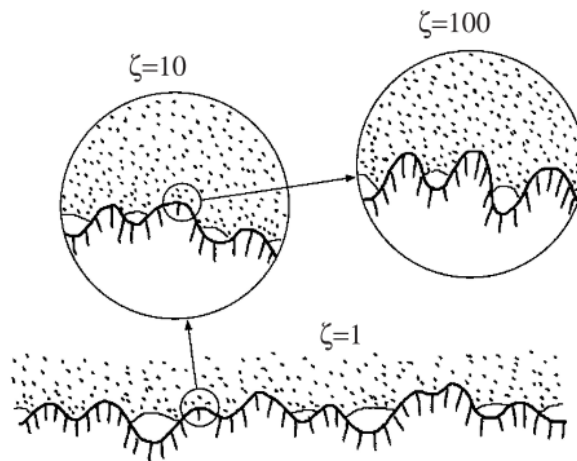

Figure 3.8 A rubber block (dotted area) in adhesive contact with a hard-rough substrate (dashed area). The substrate has roughness on many different length scales and the rubber makes partial contact with the substrate on all length scales. When a contact area is studied at low magnification (ζ=1) it appears as if complete contact occurs in the macro-asperity contact regions, but when the magnification is increased it is observed that only partial contact occurs. (Reprinted from Ref. [28])

High values of Gu lead to the establishment of a full lubricant film between the sliding surfaces. The regime is either called elastohydrodynamic lubrication or hydrodynamic lubrication, depending on the surface properties of material [29]. There is no interaction between the contact surfaces and therefore very little wear occurs. The feature of elastohydrodynamic lubrication is that a force is transmitted through the liquid and the

surfaces deform elastically under the load. Elastohydrodynamic lubrication typically occurs at lower Gu than hydrodynamic lubrication and depends on the bounding surface material characteristics. The frictional properties in this lubrication regime are mainly determined by fluid hydrodynamics and rheological properties (fluid viscosity).

There is a transitional regime between the boundary lubrication and elastohydrodynamic regime at intermediate Gu, named as the mixed lubrication regime [30]. The sliding surfaces enter the mixed lubrication regime when the thickness of the fluid film is less than or equal to the height of the tallest surface asperities [31]. The fluid film is pierced by sharp micro-peaks on the surface; the lubricant becomes trapped in some of the micro-valleys and is capable of helping to sustain some of the load between the two surfaces. As the film thickness decreases due to reduced hydrodynamic support, more asperities come into contact until reaching the boundary lubrication, where the asperities support the entire load between the two surfaces.

Other parameters similar to the Gumbel number are also usually applied in the Stribeck curve [32][33]. One of them is $v\eta/P\sigma$ (v is the sliding speed) by Dizdar and Andersson [34]. The thickness parameter σ can be calculated as $\sigma = \sqrt{R_{a1}^2 + R_{a2}^2}$, where R_{a1} and R_{a2} are the arithmetic mean roughnesses of the two interacting surfaces. Another widely used lubrication parameter is the fluid film thickness to roughness ratio (Lambda ratio) $\lambda = h_c/\sigma$, where h_c is the central film thickness. The criteria for the different lubrication regimes are [35]:

- Boundary lubrication, $\lambda < 1$
- Mixed lubrication, $1 < \lambda < 3$
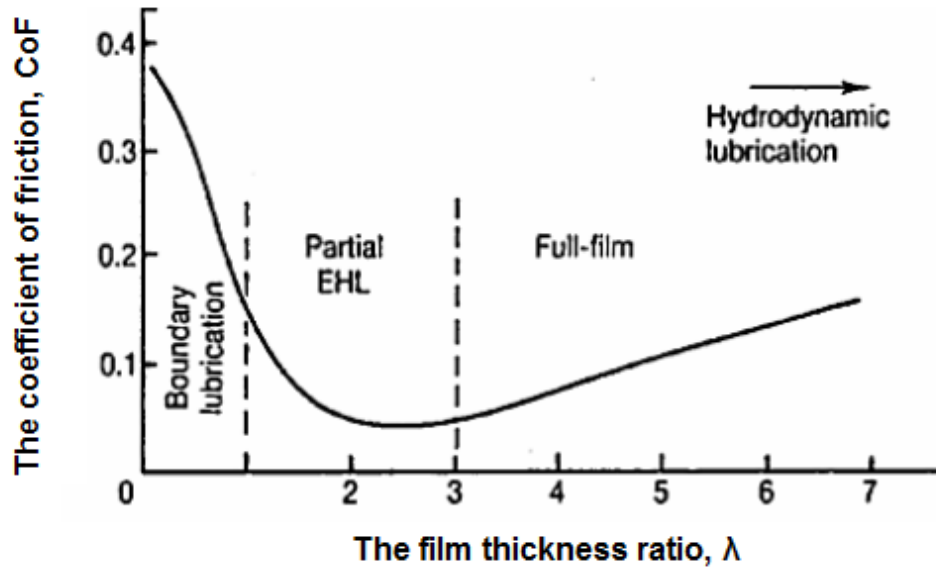- Hydrodynamic lubrication, $3 < \lambda < 10$

Figure 3.9 Lubrication regimes as a function of λ (fluid film thickness to roughness ratio or Lambda ratio) (Reprinted from Ref. [36])

3.2.3 The influential factors in lubricated friction of elastomers – surface roughness and bulk viscoelastic properties

Roughness, among other physical quantities, has been shown to play a key role in the frictional properties of soft contacts [37]. However, there have been only a few studies on the effect of roughness in lubricated soft contacts [38]–[40]. To reveal factors governing lubrication in soft contacts, Bongaerts et al. investigated the influence of surface roughness and hydrophobicity [38]. The Stribeck curves are acquired for a hydrophobic PDMS sphere (root-mean-square roughness R_q=26 nm) in relative motion on a rotating hydrophobic PDMS disk of varies roughness (R_q at 8.6 nm, 382 nm, 3.6 μm) under the load of 1.3N in the presence of aqueous lubricants. The entrainment speed U is between 1 mm/s and 2.4 m/s. The research reveals that surface roughness has no effect on the CoF in the EHL regime. However, in the mixed lubrication regime, the minimum in the Stribeck curve[3], which indicates the transition from mixed lubrication to EHL, is shifted to a higher critical value of $U\eta$ for rougher disks and the minimum of CoF increases. In the boundary regime, the CoF decreases

---

[3] In Figure 3.10 and Figure 3.11, the Stribeck curve is the plot of friction coefficient as a function of the product of lubricant viscosity and velocity, because the authors used a single type of material and applied a fixed load. Hence the contact pressure (P) was also fixed irrespective of the effect of surface roughness. Therefore, the "P" in the lubrication parameter Uη/P was omitted. But I used the Gumbel number (Equation 3.7) throughout the work.

as the surface becomes rougher. In addition, the hydrophobicity of the PDMS surfaces affects the position of the Stribeck curve. For a hydrophilic PDMS-PDMS tribopair with two values of disk roughness, the Stribeck curve of the hydrophilic rough contact lies below that of the hydrophobic rough contact but is above that of the hydrophilic smooth contact in the mixed and boundary lubrication regime.

Research by Scaraggi et al. shows that for a setup consisting of a smooth (mirror-finished) steel ball in lubricated steady-sliding contact with a fixed rough PDMS substrate characterized by anisotropic roughness, the transition from the mixed to hydrodynamic lubrication regime is observed to deviate strongly from the classical shape of the Stribeck curve [39]. The applied load is 1 N while the mean velocity U_m is between 0.002 and 0.25 m/s. The lubricants are mixtures of glycerin and water for adjusting the range of viscosity. As shown in Figure 3.11, a conventional Stribeck curve is obtained on the smooth (R_q= 0.1 µm) PDMS substrate. In contrast, for the rough ($R_q \approx 10$ µm) PDMS substrate with grooves aligned in a direction perpendicular to the ball sliding, two hydrodynamic regimes appear. The first increase in the CoF initiates at about $\eta U_m = 10^{-4}$ Pa·m. The second increase in CoF occurs at about $\eta U_m = 0.1$ Pa·m and rapidly follows the classical EHL Stribeck curve for smooth bodies. The first transition is considered as a consequence of the micro-EHL conditions which occur locally at the individual asperities while the macroscopic EHL contribution coming from the ball curvature radius is still negligible.
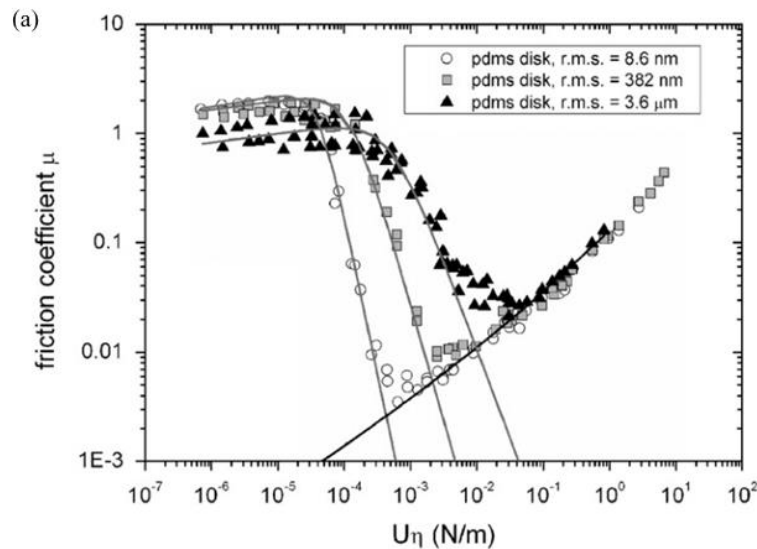

Figure 3.10 Stribeck curves for the hydrophobic PDMS-PDMS tribopairs with three different values of disk roughness, lubricated by Newtonian fluids. (Reprinted from Ref.[38])
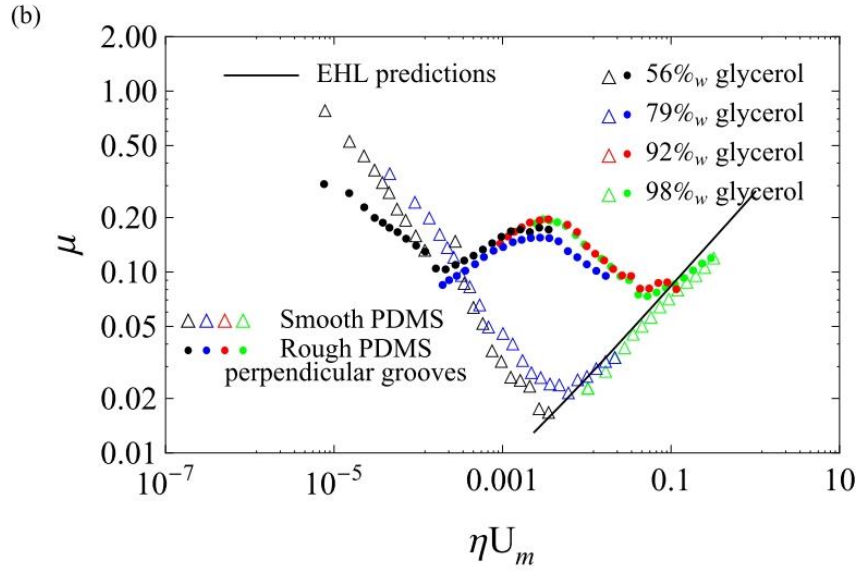
Figure 3.11 Friction coefficient as function of the product of dynamic viscosity η and mean velocity U_m for a smooth steel ball rotating on the fixed PDMS substrates with smooth or rough surfaces, lubricated with glycerin-water mixtures. On the rough substrate, the grooves were perpendicular to the sliding friction. (Reprinted from Ref.[39])

In the applied research of slip resistance of footwear, the contact interface between footwear and floor can be generally divided into the squeeze-film, draping and traction zones [41]. In the draping and traction zones where the footwear has direct contact with the floor, the interface is in the boundary lubrication region where the normal load is supported by both the lubricant and the solid-to-solid contact. The floor surface roughness plays a more critical role in friction in these two zones than in the squeeze-film zone. Beschorner et al. [42] proved that increased floor roughness raised the lubricated friction between an elastomer and a hard floor surface by increasing the contribution of hysteresis friction. A rough surface profile assists penetration of a liquid film on the floor and enables the asperities of footwear and floor to make contact, which causes more energy loss during the internal damping cycle. This finding indicates that increasing hysteresis friction through floor roughness and material selection may reduce the prevalence of slip and fall accidents.

In addition to floor surface roughness, studies have revealed that the surface roughness of soling material is also a major determinant of slip resistance on lubricated surfaces [43][44]. Increasing material surface roughness has an inverse effect on hysteresis and adhesion friction; it benefits hysteresis friction due to the greater penetration depth of surface asperities.

3.2 The lubricated friction of elastomers

Manning et al. showed in a walking traction test that the abrasion of rubber in steps with an increasingly coarse grit on abrasive paper raised the roughness (mean peak-to-valley roughness R_{tm}= 4.4-19.1 μm) in parallel with an increase in the CoF on water-wet surfaces [43]. In the experiment, soling roughness was a more important factor than floor roughness. Another study found that the good slip resistance of a microcellular polyurethane was attributed to its high roughness after the cellular structure was broken open by wear (R_{tm}=35-50 μm) [45]. On the other hand, increasing the surface roughness of elastomer has an inverse effect on adhesion friction. A high roughness results in less real contact area and hence reduces adhesion friction which is proportional to the real contact area [46]. The change in total friction is a balanced outcome of the individual effect on hysteresis and adhesion friction and depends on material properties.

Chang et al. provided comprehensive reviews on the role of surface roughness in the measurement of slipperiness. It comes to the insight that the surface roughness parameter that has the highest correlation with friction is dependent on the material used, and that some surface parameters appear to have a good correlation with friction in general [44][47]. For laboratory-scale testing, the surface parameters R_a (arithmetic mean roughness) and R_{tm} (mean peak-to-valley roughness) are most relevant to friction and are widely used in research, although they have significant limitations in representing surface characteristics and are highly location-dependent [44]. On a roughened surface, hills and valleys are present and their distances are much larger than the micro-phase separation of an PU elastomer. If two bodies are in contact, friction will first take place on the summits of the irregularities and large contact areas will be separated by a distance greater than the molecular range of action. Therefore, the parameters featuring spatial wavelength, such as those defined in Chang's work, determine the frequency of deformation during sliding and are related to the hysteresis loss in shoe soling material [47]. Grosch's detailed study in 1963 described the relation between the friction and viscoelastic properties of rubber [48][49]. The hysteresis friction, as the dominating mechanism in friction on rough surfaces, in rolling friction or lubricated friction, is influenced by the loss factor of the polymer and the average spacing between adjacent peaks on the rough track. The adhesion friction, as the dominating mechanism in friction on smooth surfaces or in dry friction, is influenced by the loss modulus and the relaxation time of the polymer.

There are few studies reported on the influence of viscoelastic properties on the sliding friction of polyurethanes [50][51](The cited work is limited to dry friction). The related

experimental studies on tread rubber compounds are more numerous and systematic. Below are some examples showing the significance of tuning bulk viscoelasticity on wet sliding friction of rubbers. The studies are based on the widely accepted concept that wet sliding friction on rough surfaces arises primarily from the bulk hysteretic energy dissipation in the viscoelastic rubber compounds under dynamic deformation at high frequency (about 10^5 Hz at 40 ℃ in the case of tire traction). Both $tan\,\delta$ and G'' at 0°C have been used for predicting the wet traction performance of tread rubber [52]. The broad investigation on a collection of tread rubber compounds by Takino et. al [53] shows that the friction values (BPST wet skid resistance number) correlated nonlinearly with the T_g from DSC (Differential Scanning Calorimetry), $tan\,\delta$ and G'' at 0 ℃ and correlated linearly with the T_g determined by the maximum in the $tan\,\delta$ (peak value). Pan et al. [54] investigated the impact of the glass transition temperature on the wet sliding friction of rubber compounds made of high *cis*-polybutadiene with different degrees of sulfur vulcanization. With increasing glass transition temperature, the wet sliding friction values measured with the BPST increase to a maximum and then decrease. The rate of increase or decrease varies with the amount of filler in the rubber compounds. However, the friction values do not favor a good correlation with $tan\,\delta$ at 0 ℃ or -10 ℃. Another work by Pan [55] shows that with the proper application of the time-temperature superposition technique, the values of $tan\,\delta$ can predict a qualitatively reasonable ranking in wet sliding friction among two styrene-butadiene rubbers with similar microstructure but different macrostructure. However, he also raised an argument that the ranking of $tan\,\delta$ for different rubber compounds may vary with strain; the suitable level of strain that reflects the material deformation responsible for energy dissipation during wet BPST testing is not the same for each rubber compound. The correlation between viscoelastic properties of elastomers and their wet sliding friction may be material-dependent.

3.3 The frictional measurement techniques used in the study of lubricated friction of elastomers

Slips and trips are the most common cause of major injuries in the workplace with considerable economic damage. In Europe, slips, trips and falls on the same level accounted for approximately 15-20% of all reported over-three-day occupational injuries [56]. The direct cost of disabling workplace injuries in 2012 due to falls on the same level in the U.S. was estimated to be approximately US$9.19 billion or 15.4% of total injury cost, according to the data from the Liberty Mutual Workplace Safety Index [57]. Using flooring and footwear with adequate slip resistance can be an effective measure for the prevention of slips.

In the past few decades, numerous frictional measuring devices have been developed to assess the slipperiness between footwear and walking surfaces. The coefficient of friction (CoF), defined as the ratio of frictional force to normal force, has been widely used as a measure of slipperiness. The consensus is that surfaces with a lower CoF are more slippery than those with a higher CoF. The measuring techniques apply various methods including drag-sled methods, steady state dynamic methods, and impact methods, ranging from small portable devices for field tests to large whole-shoe devices for standardized laboratory tests. Chang et al. evaluated the validity and repeatability of different friction measurement methods using criteria based on biomechanical observations and friction mechanisms during actual slips [58][59].

Slipperiness measurement techniques mostly consider either static friction properties or steady-state/transitional dynamic friction properties as safety criteria. The measurement of static friction is only recommended for dry and clean surfaces [60]. If contaminated conditions are used to measure slip resistance of shoes or floors, the dynamic friction is preferred [41][61][62]. The following two sections (Section 3.3.1 & 3.3.2) briefly summarize the typical techniques for dynamic friction measurement. Steady-state dynamic friction properties are based on the traditional measurement of resistance to a steady-state motion and are more relevant for actual steady-state sliding motion between the foot and the walkway. There are also a few inclined-strut devices that measure the transitional friction properties of floor surfaces during a short contact time between the surfaces within hundreds of milliseconds. The transitional test alternative is important for simulating slipping initiated during early heel contact in gait [63][64].

3.3 The frictional measurement techniques used in the study of lubricated friction of elastomers

In Section 3.3.3, some studies on a kind of emerging friction measurement device, the tribo-rheometers that can measure both the rheological and frictional properties of the test system, are summarized. The technology has found widespread applications in soft tribology study not limited by shoe slip resistance.

3.3.1   The portable devices for field tests of slipperiness on shoe-floor surfaces

Field tests enable the evaluation of floors or shoes under field conditions at the same spots in a worksite. The devices used for this purpose are portable, but they can also be used in laboratory studies. Examples of portable test devices for onsite assessing the floor slipperiness are shown in Figure 3.12.
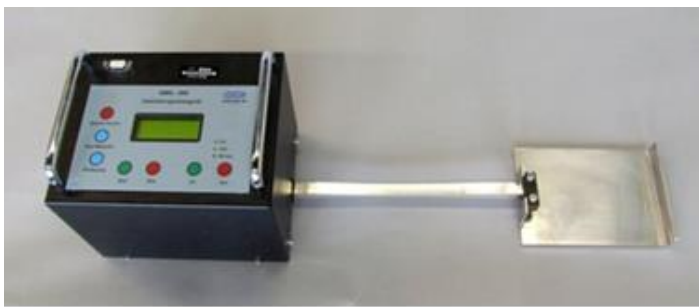
(a) GMG200

(b) BPST

(c) Brungraber Mark II

Figure 3.12 Examples of portable test devices for onsite assessing the floor slipperiness (Reprinted from Ref.[65][66])

Drag-sled type devices (e.g. Tortus, Schuster, FSC 2000, Gabbrielli SM, GMG200) are pushed at a constant speed by an operator or a motor drive over a length of the floor and measure the steady-state dynamic CoF [56], [64], [67]–[69]. Although they are recommended for use on both dry and wet surfaces, they tend to overestimate the CoF for wet surfaces due

to the inertial resistance to movement [59][70]. Some common problems exist for these type devices: the drive wheels have a tendency to slip on oily surface; the contact area is small, so that raised patterns can disrupt the friction measurement; the measurement is sensitive to oscillation, which in turn may enhance normal frictional vibrations (stick-slip) causing bias during testing [64][71].

Swing pendulum-type devices, such as the British Portable Skid Tester (BPST), measure residual energy as determined by the maximum height of the pendulum's center of mass during upswing after pavement contact and are widely used for assessing the slip resistance of flooring [72][73]. However, the sliding velocity of 2.8 m/s is above the relevant biomechanical range between zero to 1.0 m/s related to actual slipping accidents, making a reasonable correlation of these results to a single slip resistance value questionable. It tends to underestimate the CoF for wet surfaces in particular [64]. Like the Tortus, the pendulum cannot be used to obtain valid results on profiled surfaces or those with a gradient of more than five degrees [71]. On surfaces with raised patterns, measurements may be affected if the elastomer hits a bump in the relief of impact.

On the other hand, the inclined-strut slipmeters (e.g. Brungraber Mark II, English XL) investigate the transitional friction within short contact time (up to 250 ms) between shoe and floor, simulating initial frictional squeeze-film processes during a heel strike [58]. The shoe sample impacts the floor surface with a force and some momentum at an inclined angle from the vertical direction. The CoF is obtained from the angle at which a non-slip transitions to a slip. However, the Brungraber Mark II articulated strut was ever recorded to produce a frictional force that oscillated several times for a period of less than 50 ms each during a measurement. It may not be well suited for viscous contaminants such as glycerol, for which it tends to underestimate the CoF [64].

3.3.2 The laboratory-scale devices for the assessment of slipperiness on shoe-floor surfaces

Figure 3.13 Slip Resistance Tester STM603 (source: https://www.satra.cn/test_equipment)

Evaluation of the slip resistance of shoes can be best conducted under laboratory conditions where the operational and tribosystem conditions can be carefully controlled and thus standardized. Laboratory tests can be used to study the effect of operational conditions such as normal force, sliding speed, contact angle, or normal force build-up rate as well as the effect of tribosystem parameters such as surface roughness, sole stiffness or tread wear on friction [5], [57], [74]–[80]. These types of devices are usually not portable and cannot be used under real working conditions. One example is the Slip Resistance Tester STM603 (Figure 3.13) developed by the Shoe and Allied Trades Research Association (SATRA) to simulate a slip after a heel strike or before toe-off [81]. The shoe is mounted on a shoemaking last and lowered onto the floor surface which is pulled by a speed motor at a user-specified constant velocity. During sliding, the horizontal and vertical forces are measured, and the dynamic friction properties are determined. In the standard to determine the slip resistance of safety footwear EN 13287:2012(E), the operational conditions for STM603 are defined as the normal force of 400 or 500 N, the contact angle of 7°, the reference floors of ceramic tile and steel plate, the sliding velocity of 0.3 m/s, and the lubricants of sodium lauryl sulfate-water and glycerin [82]. For most of these types of device, a whole shoe is mounted on an artificial foot or a shoemaking last and slides against the floor. However, some devices also have a holder for material samples (e.g. BST2000 [59] and LABINRS[83]) allowing for sliders other than shoes to be tested. More whole-shoe test devices can be seen in the review by Chang et al.

[59] Due to a large number of variables like the normal force, contact angle and sliding speed across devices, the measured CoFs using different devices can show significant differences for the same shoe-floor-lubricant systems [84]. Clarke et al. conducted friction measurements on six common household surfaces in water contaminated conditions in compliance with two standardized tests using the BPST (according to BS 7976: Parts2:2002+A1:2013) and the STM603 (according to EN ISO 13287:2012) as measuring devices and found no correlation between the measured CoFs. The authors suggested different friction mechanisms for each testing method due to the differences in contact time and sliding speed [85].

Laboratory-scale tribometers that do not use whole shoes but sole materials as testing samples emerged in the field of soft tribology research in recent years. Beschorner et al. developed a pin-on-disk type tribometer to examine the mechanisms that contribute to shoe-floor friction in the boundary lubrication regime (Figure 3.14). The tribometer consists of a rate table (disk) containing the floor sample, which rotates at a constant speed relative to a stationary shoe sample (pin). The sliding speed of the floor relative to the shoe sample is set by adjusting the rotational speed of the rate table. They carried on systematic studies to identify the contributions of adhesion and hysteresis to friction in the boundary lubrication regime and to understand the influence of hydrodynamic properties, floor roughness and sliding speed on the friction of shoe-floor materials [42][86][87].
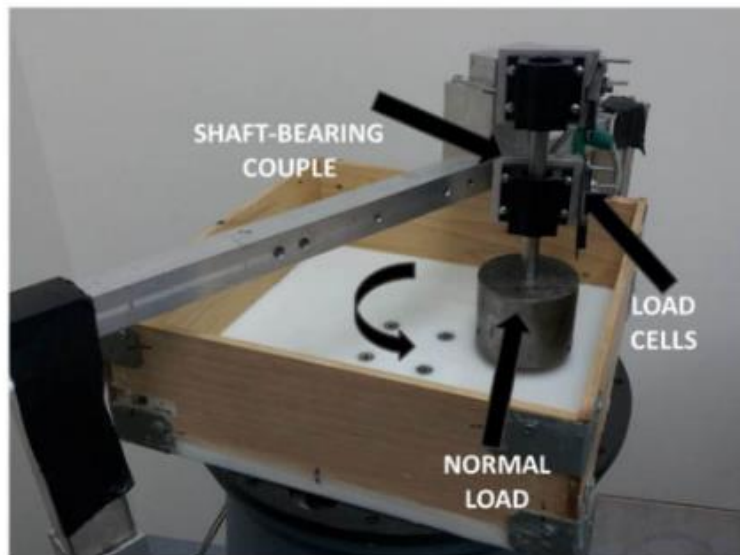

Figure 3.14 A custom developed pin-on-disk tribometer for the frictional study between the shoe and floor surfaces (Reprinted from Ref.[88])

Bongaerts et al. used a modified ball-on-disk type Mini-Traction-Machine (MTM, Figure 3.15) to study the influence of surface roughness and hydrophobicity on lubrication in a compliant

PDMS-PDMS (polydimethylsiloxane) contact [38]. The equipment consists of an independently driven ball and disc specimens, with the ball contacting the disc at an angle of 45°. A load beam controls the normal force acting through the ball, perpendicular to the disc at the point of contact. A force transducer located on the ball arm records the friction force. An experimental work followed to show the influence of lubricant viscosity and wetting on lubrication across multiple lubrication regimes within a viscoelastic contact. The distinct tribological behavior, generally characterized by a decrease in the CoF with increasing fluid viscosity and wettability, is explained in terms of lubricant dewetting and squeeze-out dynamics and their impact on viscoelastic dissipation on multiscales [89]. Scaraggi et al. also used the MTM to investigate the effects of roughness anisotropy on the mixed lubrication. In particular, they made a smooth steel rotating ball in lubricated contact with the fixed rough PDMS counter surfaces and showed that the shapes of friction curves were strongly affected by the roughness orientation and found the evidence of micro-EHL lubrication in rough, soft contacts [39]. In conventional lubrication studies, the MTM uses metal balls and discs, but in these studies, either the ball or the disc is an elastomer. The facts that the ball and the disc can be independently driven to achieve any desired rolling-sliding speed combination enables the separation of sliding friction component (primarily generated from surface adhesion and hydrodynamic effects) and rolling friction component (primarily generated from elastic hysteresis and hydrodynamic effects) [90]. The MTM has the potential for fundamental studies of the lubricated friction between the shoe and floor surfaces.
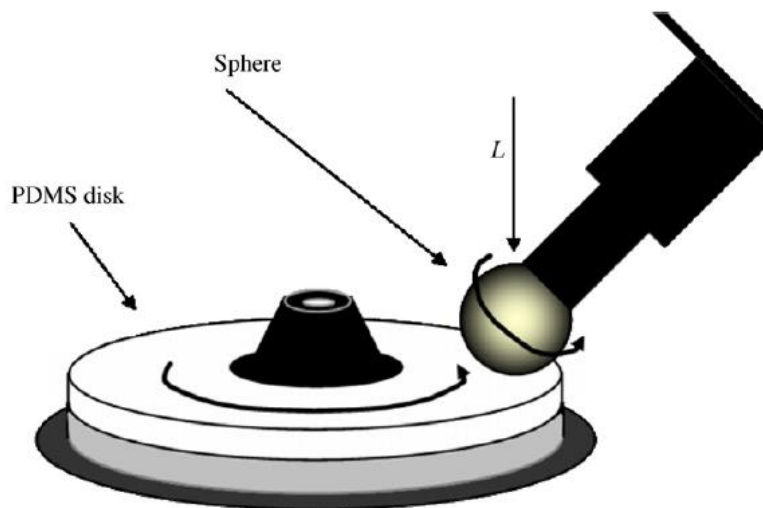

Figure 3.15 Schematic representation of the Mini-Traction-Machine (MTM) (Reprinted from Ref.[38])

The continuous development of tribometers for measuring the CoF in soft contacts offers more possibilities of assessing slip resistance of shoes on lubricated floors. However, we need to pay close attention to the fidelity of the tribometers [57]. Does the situation represented at the measurement interface with the device reflect the frictional phenomena at the shoe and floor interface of slip events? Due to the requirement of machine design and usability, the contact pressure, contact area, velocity or lubricating conditions applied with the test device may have to be altered and may not reproduce the movement of shoes at the critical instants of slip events. Further investigations are needed to understand the frictional mechanisms involved in wet sliding friction between shoe and floor.

3.3.3 The tribo-rheometry equipment used in frictional measurement

Traditionally, rheometers are used to measure the flow and deformation behavior of matter under the influence of stresses in the rotational and oscillatory mode. Modern rheometers are equipped with high-performance bearings, force transducers and position sensors, and therefore speed, torque and normal force can be precisely measured or controlled during a measurement. These features are also favored in frictional measurement. The first attempt to extend rheometer accessories to measure friction was made by Kavehpour and McKinley [91] who modified a traditional parallel plate configuration to explore the coupled rheological and frictional properties of complex fluids and solid-liquid systems. The lower bounding fixture is an annular disk, allowing for a range of materials to be placed on it, whilst the upper rotating fixture is a stainless-steel plate (Figure 3.16). The fixture is self-leveling by using a wax layer to fix the lower disk and both the normal load and the sample gap can be monitored or controlled. The effect of surface roughness of metal materials and the effect of variations in the normal force on the Stribeck curves were presented, along with data for commercial lubricants.
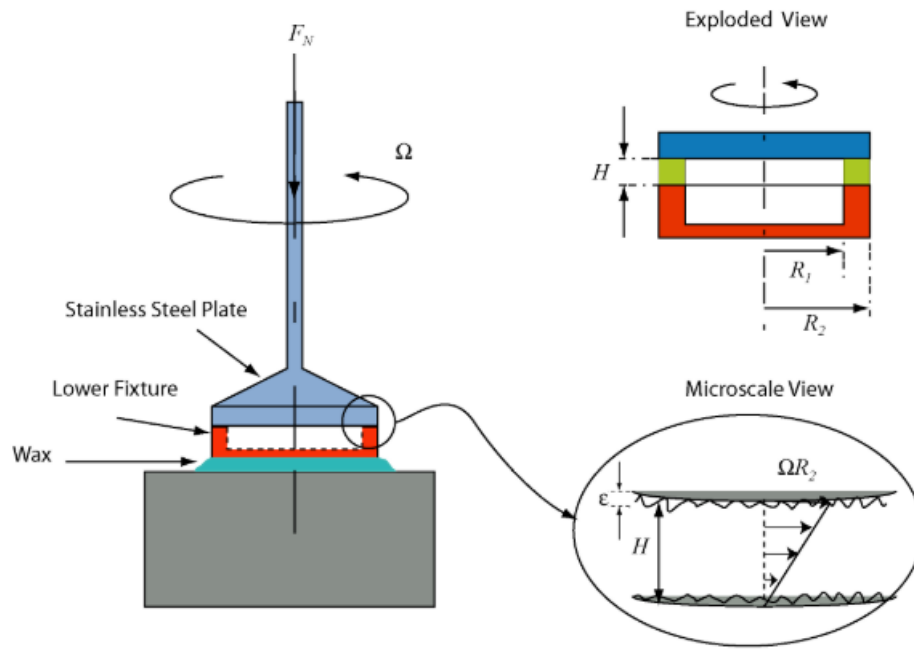
Figure 3.16 Schematic view of the tribo-rheometry accessary used in combination with the rheometer AR-2000 (TA Instruments Inc.), developed by Kavehpour and McKinley (Reprinted from Ref.[91])

The first commercial tribo-rheometry accessary was designed by Heyer and Läuger from Anton Paar [92]. The set-up consists of a steel ball loaded onto three flat plates arranged in the form of an inverted pyramid (Figure 3.17). A bottom stage is movable in all directions to get the same normal load acting evenly on all the three contact points of the upper ball. The ball, as well as the plates for the inset, can be exchanged so that the system is adapted to desired material combinations. The system has been used to investigate the rheological or frictional properties of greases, ball bearings and fluid dairy products [93]. In recent years, more reports have been published using the equipment for tribological testing of complex fluid or elastomer. The applications reported on are extensive, from tactile sensation testing of food products [40][94][95], water-based machinery lubrication [96], to the performance of asphalt pavement [97].
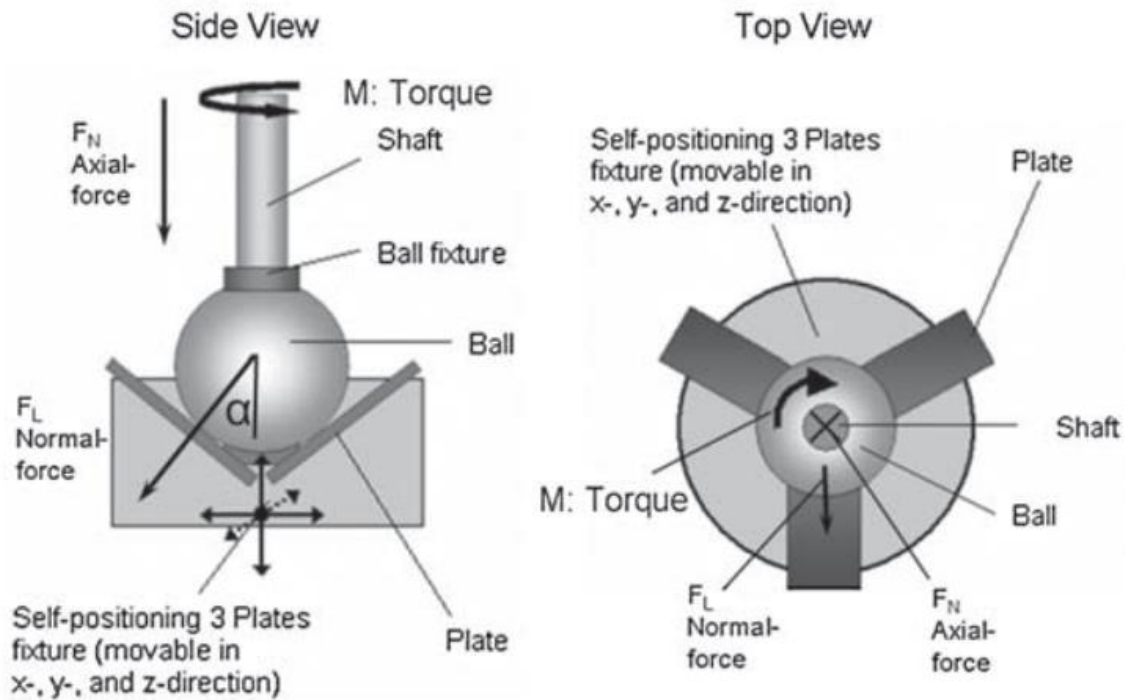
Figure 3.17 Schematics of the ball-on-three-plate tribo-rheometry accessory in side and top view. The accessory is used in combination with the Anton Paar MCR 301 rheometer. The torque and the normal force applied by the rheometer are indicated by arrows. (Reprinted from Ref.[93])

Goh et al. [98] have also developed a rheology accessary specifically for the study of frictional behavior of food systems. The upper contact probe consists of two balanced hemispheres equidistant from the central rheometer shaft, giving two contact points for measurement. The lower plate is unchanged, allowing for the attachment of any flat material (Figure 3.18).

Figure 3.18 Image of the tribometer cell used in combination with Physica UDS 200 (Anton Paar GmbH) (Reprinted from Ref.[98])

Prakash et al. used another commercial tribo-rheometry accessary developed by TA Instruments for measuring the CoF of representative dairy products as a function of sliding speed in order to assist the sensory research of food during complex oral processing [99]–[101]. The upper rotational half-ring geometry is coupled to the rheometer head through a coupling adapter and a beam coupling. The lower plate geometry is connected to a Peltier plate for accurate and stable temperature control. The half-ring geometry is a ring interrupted in three sections such that only half of the ring is in contact with the substrate, which helps the replenishment of lubricant in the solid-solid contact (Figure 3.19). The well-defined contact area between the half-ring and the substrate makes it possible for an accurate computation of the friction and normal stress.

The research progress on the development of tribo-rheometry equipment inspired to utilize a conventional rotational rheometer to measure the frictional properties of elastomer on lubricated surfaces in the application for assessing the wet slip resistance of shoe soling materials. The development of the method is described in detail in Chapter 5.1.
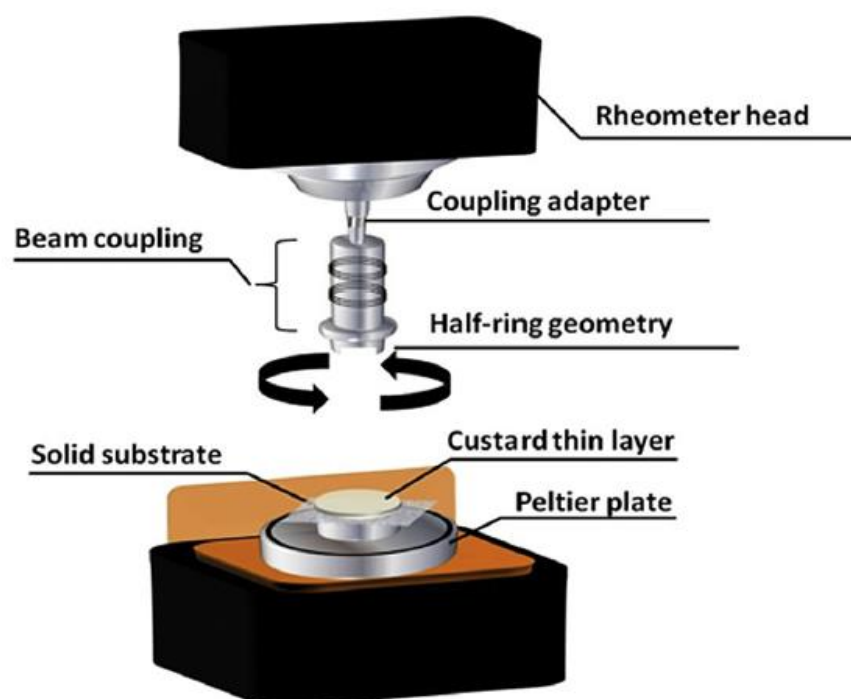
Figure 3.19 Schematic illustration of the ring-on-plate tribo-rheometer set-up (TA Instruments, Reprinted from Ref.[102])

4. Aim of the work

A rheometer combined with a three-ball-on-plate tribo-rheometry accessory will be used to develop a feasible testing method for measuring the friction coefficient of an elastomer based tribo-system at varying lubricated operation conditions. An application of the testing method is the assessment of the wet slip resistance of polyurethane soles. It may be beneficial to the design of footwear with adequate slip resistance which is an effective measure for the prevention of slip and fall accidents. Modern rheometers have found their extended application in tribology studies on compliant contact.

Two essential influential factors for the lubricated friction of thermoplastic polyurethane are investigated: surface roughness parameters and material bulk hardness. Either changing the roughness of the material surface or changing the bulk hardness can result in variations in the contribution of hysteresis friction to the lubricated friction. The work aims to develop the measurement method, to analyze the abovementioned effects, and to build the correlation of the coefficient of friction with the viscoelastic properties of the material. The finding may pave the way for a better understanding of the frictional mechanisms involved at the interface between the shoe and the floor in wet sliding.

5. Results and Discussion

5.1 The tribo-rheometer for frictional measurements

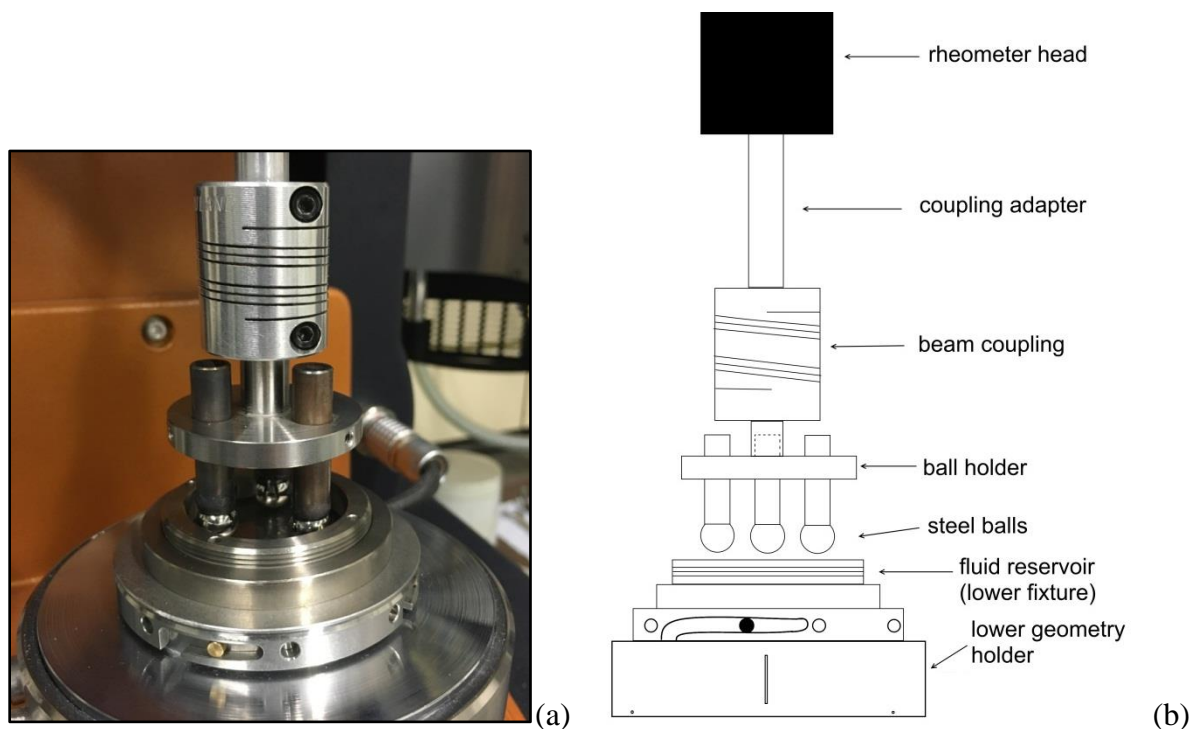#### 5.1.1 The features of the three-ball-on-plate accessary

Figure 5.1 (a) photograph and (b) schematic view of the three-ball-on-plate accessory used in combination with a DHR-2 rheometer

Friction measurements were made using a combined motor and transducer Discovery Hybrid Rheometer 2 ("DHR-2", TA Instruments Inc.) with a three-ball-on-plate tribo-rheometry accessory previously designed at BASF SE. The rheometer design highlights a patented Force Rebalance Transducer offering more accurate normal force measurements than conventional tribometers which usually use strain gauge and capacitive sensors to sense a force [103]. The photograph and schematic views of the three-ball-on-plate configuration are shown in Figure 5.1. The upper fixture is a ball holder fixing three steel cylinders. Three identical bearing steel spheres (radius = 4.5 mm) are glued to the circular ends of the cylinders with a two-component reactive adhesive. The R_a (arithmetic mean roughness) of the steel sphere is 0.027±0.006 µm. To ensure that the load (axial force) is distributed evenly on the contact surface, the upper ball fixture is connected to the rheometer shaft through a flexible beam coupling (Ruland Manufacturing Co., Inc.) to perform rotation movement. The beam coupling

5.1 The tribo-rheometer for frictional measurements

is manufactured from a single piece of aluminum and utilizes a system of spiral cuts to accommodate misalignment and transmit torque. The lower fixture is a static fluid reservoir containing test fluid and a fixed disk sample with 40 mm in diameter. The set-up operates at room temperature and room humidity. The spherical geometry in the ball-on-plate contact allows for a quick replenishment of lubricant after the balls pass the solid surface and can prevent the squeeze and stack of the elastomer at the leading edge of the contact.

The spheres provide point contacts with the rigid substrate or circular contact area with the compliant substrate. The contact surface depends on the moduli of the substrate and spheres. During the test, the torque and the axial force are recorded by the rheometer; the friction force and the CoF are calculated as follows:

Equation 5.1

$$F_f = M/r$$

Equation 5.2

$$CoF = \frac{F_f}{W} = \frac{M}{r \cdot F_A}$$

In the above equations r denotes the arm which is the radius from the axis of rotation to the point of application of the load and equals 11.15 mm. F_f is the friction force, given by the ratio of the torque M to r. The axial force F_A equals the load W for the particular geometry.

5.1.2   The setting of test conditions

A laboratory-scale frictional measurement that targets the application in shoe manufacturing sector should reproduce the relevant biomechanical and tribological parameters during actual slipping events such as a heel slide when slipping during normal walking. It was suggested that [59] the following operational parameters should be considered. These are based on the biomechanical observations during normal walking and fiction mechanisms involved at the interface between the shoe and the floor: (1) the normal force build-up rate should be at least 10 kN s^{-1} for whole-shoe devices; (2) the normal contact pressure should be between 200 and 1000 kPa; (3) the sliding velocity at the interface should be between zero and 1.0 m/s; (4) the maximum time of contact prior to and during the CoF computation should be 600 ms. Because this investigation focuses on steady-state sliding friction rather than transitional

friction, the testing conditions should about fulfill the requirement stated in criteria (2) and (3). Criteria (1) and (4) are out of the scope of the work.

Table 5.1 Test conditions

Test variable	Abbreviation	Setting
Angular sliding velocity	Ω (rad/s)	Ω = 0.3; 0.5; 1; 2; 3; 5; 10; 14; 20; 30 rad/s
Corresponding linear sliding velocity	v (mm/s)	v = 3.3; 5.6; 11.2; 22.3; 33.5; 55.8; 111.5; 156.1; 223.0; 334.5 mm/s
Axial force (load)	F_A (N)	F_A=1.0 ±0.1 N
Lubricant	glycerin-water mixtures	40 wt%; 60 wt%; 86.6 wt% glycerin in water
Environment temperature and humidity	T (ºC); H (%RH)	24-33 ºC; 21-53% RH

The Stribeck curve is used to evaluate and visualize the frictional properties of the tribo-system. In order to make the Gumbel number in the Stribeck curve span several orders of magnitude, the CoF was measured under a constant axial force and varying sliding speeds in three different glycerin-water mixtures. The test conditions are presented in Table 5.1. The sliding angular velocities are set to ten discrete values ranging from 0.3 to 30 rad/s, corresponding to the linear sliding velocities ranging from 3.3 to 334.5 mm/s which are derived from

Equation 5.3

$$v = \Omega \cdot r$$

where v is the linear sliding velocity and r denotes the arm (11.15 mm). Within the velocity range, it can be reasonably assumed that the interfacial heating effect related to the local increase in contact temperature is negligible [49]. The normal (axial) force of 1.0 N is applied. The normal force transducer installed in the rheometer can detect the change in normal force and commend an adjustment of the head position to keep the accuracy of normal force within ±0.1 N. Although the instrument has a high force resolution and can work well at a lower normal force, 1.0 N is regarded as the minimum practicable normal force because further attempts to reduce the force may introduce vigorous data vibration especially under a low

sliding velocity. The Hertzian contact theory is used for estimating the static contact pressure between the ball-on-disk interfaces, and the result depends on the elastic modulus of polymer. The calculated average contact pressure between the steel ball and POM substrate is 22.3 MPa and those between the steel ball and the TPU substrates with varying hardnesses range from 840 to 3300 kPa. The calculative process is described in Appendix A.1.

Glycerin-water mixtures were used as lubricants in the friction measurements because glycerin is a Newtonian fluid and can be easily mixed with water to achieve different viscosities. The friction measurements were done in a temperature range of 24 -33 ᵒC (the temperature range in the laboratory). The viscosities of the test fluids with different glycerin water ratios at 25 ᵒC and 30 ᵒC were measured respectively and shown in Table 5.2. The influence on the shape of the Stribeck curve and the conclusions by the viscosity variation in the concerned temperature range is negligible. Therefore, the set of viscosities measured at 25 ᵒC was used for the data analysis throughout the work.

Table 5.2 Test fluid

Fluid	Viscosity at 25 °C (mPa·s) (used in this work)	Viscosity at 30 °C (mPa·s)
40 wt% glycerin-water	3.25	2.91
60 wt% glycerin-water	9.17	7.80
86.6 wt% glycerin-water	101	73.8

In the early phase, two representative materials were chosen to demonstrate the feasibility of the method - TPU and POM. TPU is an example of polyurethane elastomer used as shoe sole material and the main experimental object of the work. POM is used as an example of engineering thermoplastic material, characterized by high stiffness and strength, low friction, excellent wear resistance and dimensional stability. Its low friction is attributed to the flexibility of the linear molecular chains, and its excellent wear resistance is attributed to its crystallinity and high bond energy [104]. POM has been widely used as self-lubricating engineering components such as in pumps, gearwheels, bearings, lock systems, and fan propellers. The surfaces of the two material used in this work are both mirror-like smooth and have the same level of surface roughness. Their surface and mechanical properties along with the average contact pressures are presented in Table 5.3.

**Table 5.3** Material properties and surface roughnesses of the TPU and POM samples

	Shore hardness	Young's modulus E (MPa)	Average contact pressure[4] P (kPa)	R_a (µm)
TPU	86A	37.8	1339	0.025 ±0.005
POM	84D	2811	22325	0.029 ±0.003

5.1.3 The CoF and axial force profiles

Figure 5.2 shows the profiles of the CoFs for one TPU sample and the axial force in a single frictional measurement in 40 wt% glycerin-water under three different sliding velocities: 223 mm/s; 33.5 mm/s; 5.6 mm/s (Ω=20 rad/s; 3 rad/s; 0.5 rad/s, respectively). The axial force was well-controlled within the tolerance range. In the beginning 10 seconds of the measurement, the tribo-system often experiences a running-in phase during which the torque decreased to stable values from a higher initial value. Therefore, the profile of CoF also showed the same pattern, which can be seen in Figure 5.2 (a) and (c). The first CoF recorded when the sliding was initiated indicates that the static friction was much higher, and the following running-in effect is characteristic for elastomeric material. During the subsequent time, the CoF approached to a stable value. The result was taken as the averaged value of the CoF recorded in the last 100 seconds out of the 120-second measurement. The degree of data deviation varies from experiment to experiment, but generally larger data deviations were observed at lower sliding velocities.

---

[4] The calculation is based on Hertzian contact theory (see Appendix A.1).
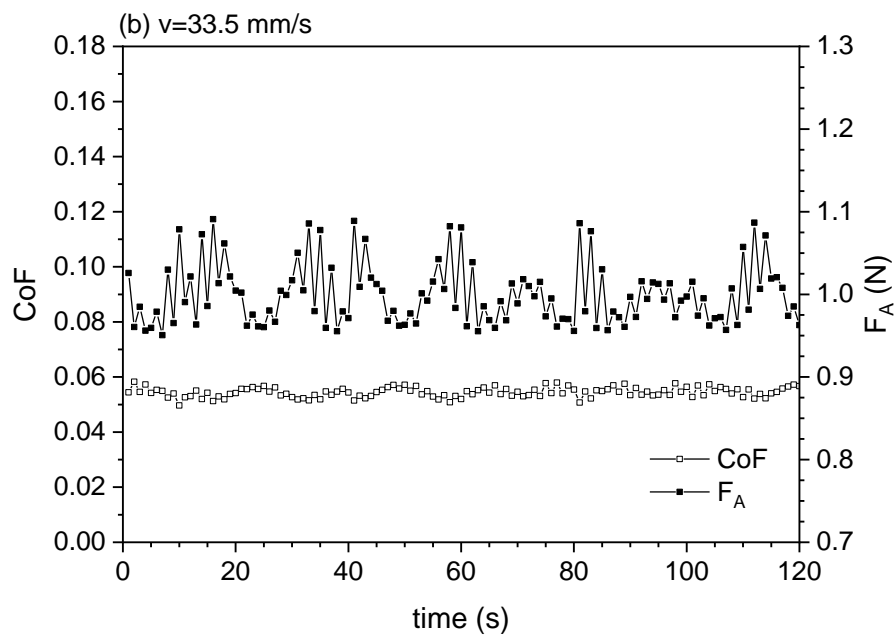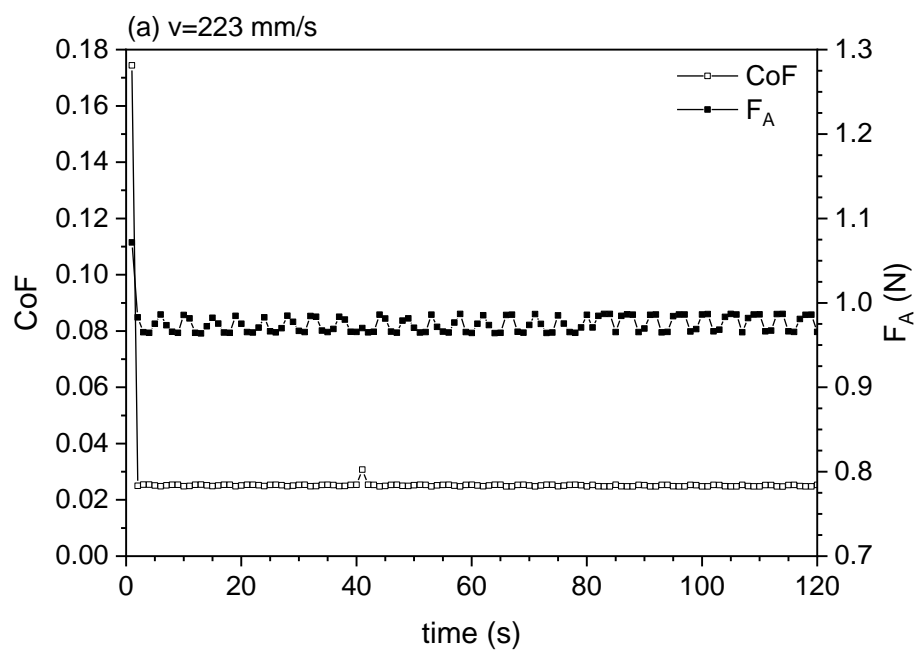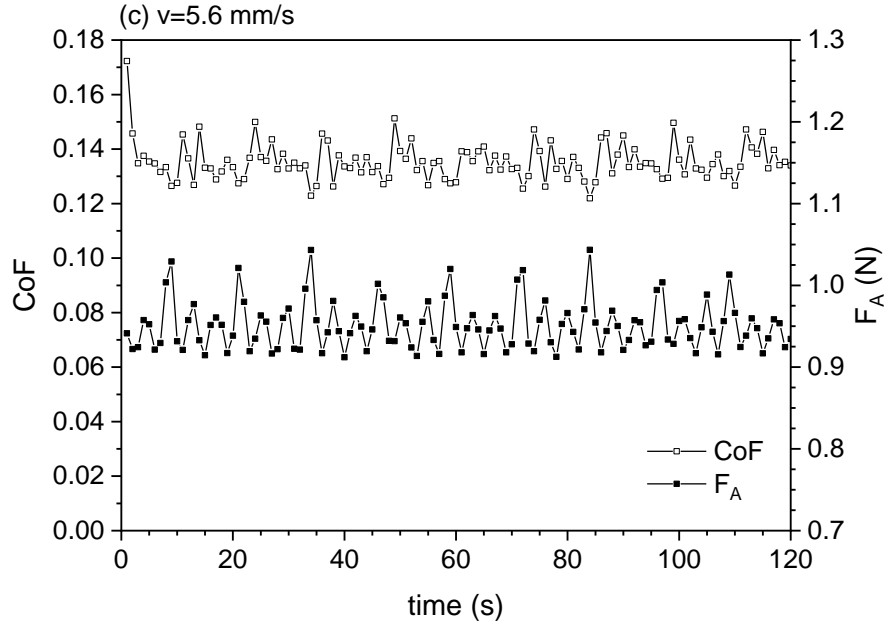
(a) v=223 mm/s

(b) v=33.5 mm/s

Figure 5.2 Friction of one TPU sample and the axial force F_A as a function of time in a single frictional measurement in 40 wt% glycerin-water at three different sliding velocities: (a) $v = 223$ mm/s (Ω=20 rad/s); (b) $v = 33.5$ mm/s (Ω=3 rad/s); (c) $v = 5.6$ mm/s (Ω=0.5 rad/s). F_A=1 N. One measurement lasted for 120 seconds and the result was taken as the averaged value of the CoF recorded in the last 100 seconds.
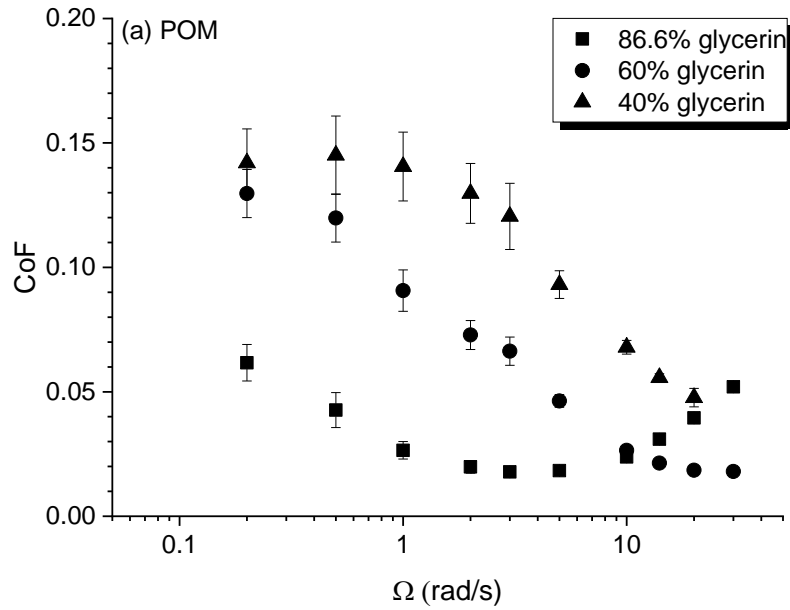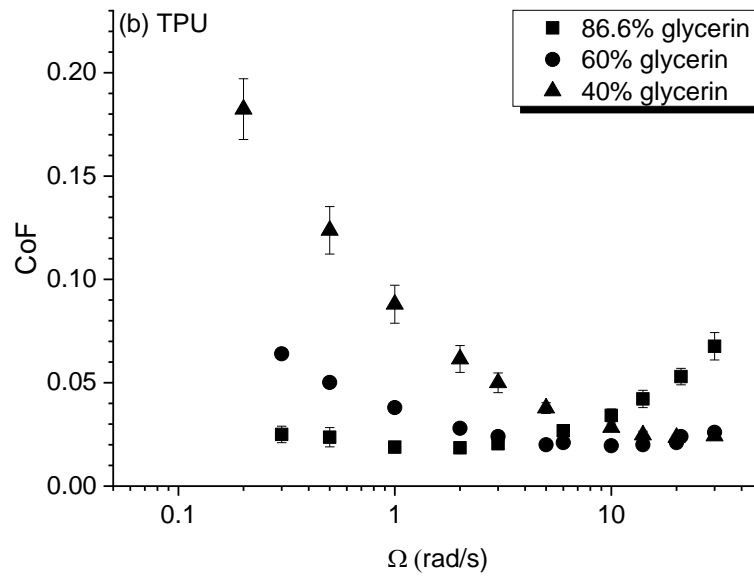
Figure 5.3 Friciton as a function of angular velocity in three glycerin-water mixtures: 40 wt% glycerin (triangle); 60 wt% glycerin (circle); 86.6 wt% glycerin (square) (a) POM; (b) TPU.

Figure 5.3 shows the CoF as a function of angular velocity in three glycerin-water mixtures for a POM and a TPU sample. For the POM-steel contact, the data point measured at 334.5 mm/s (Ω=30 rad/s) in 40 wt% glycerin was excluded due to the frictional noise coming from the contact interface during the measurement. The noise may be caused by the collision of surface asperities as the sliding velocity increased. The phenomenon confines the upper limit of sliding velocity and is more likely to happen for a lubricant with a lower viscosity. An effort was also put to measure CoF in a less viscous fluid with 10 wt% glycerin in water. The results on two POM disks, however, differed greatly and were not shown in the graph. Shallow circular marks were observed on the disks measured in 40 wt% glycerin and 10 wt% glycerin, indicating the surface wear of POM took place to a visible level for the two liquids. No wear was traced on the TPU disk samples after measurement. The wearing effect on the two materials can be explained from the perspective that the contact pressure for POM is 35 times higher than that for TPU, facilitating a more severe abrasion of surface asperities when the interactive surfaces are in close contact. For the 40 wt% and 60 wt% glycerin, the error bars shown in Figure 5.3 denote the standard deviations of CoF calculated from the repetitive measurements on three samples; due to the excellent data repeatability for the 86.6 wt% glycerin, only two measurements were sufficient and the error bars denote the variations of CoF calculated from the repetitive measurements on two samples. The variation ranged from 1% to 13% for POM and from 0 to 16% for TPU and were generally larger at the lower

velocities (See Table 5.4 for the CoFs and their variations under three representative velocities). At lower sliding velocities, the fluid film thickness between the surfaces reduces [105], allowing the formation of more asperity junctions [106] which have more time to form and break as the surfaces slide across each other, hence giving the more scattered data.

Table 5.4 Averaged coefficients of friction and variations of the frictional measurements at different test conditions

Sliding velocity (mm/s)	Averaged CoF (±variation) POM-steel ball	Averaged CoF (±variation) TPU-steel ball
In 40 wt% glycerin		
5.6	0.145 (±0.016)	0.124 (±0.012)
33.5	0.121 (±0.013)	0.050 (±0.005)
223	0.048 (±0.004)	0.024 (±0.002)
In 60 wt% glycerin		
5.6	0.120 (±0.010)	0.050 (±0.002)
33.5	0.066 (±0.006)	0.024 (±0.001)
223	0.019 (±0.000)	0.021 (±0.000)
In 86.6 wt% glycerin		
5.6	0.043 (±0.007)	0.024 (±0.005)
33.5	0.018 (±0.002)	0.021 (±0.003)
223	0.040 (±0.002)	0.053 (±0.004)

To check whether any surface wear had affected the result, after all friction measurements were done on one sample another single measurement was made immediately using the same sample at v of 33.5 mm/s ($\Omega = 3$ rad/s) and the obtained CoF was compared with the one measured previously at that velocity. As seen from Table 5.5, under all lubricating conditions, the CoFs at v of 33.5 mm/s in the middle and at the end of one test series did not exhibit significant differences and therefore showed the trivial effect of surface wear.

Table 5.5 Repeated frictional measurement: after all friction measurements were done on one sample another single measurement was made immediately using the same sample at v of 33.5 mm/s and the obtained CoF was compared with the one measured previously at v of 33.5 mm/s.

Material	Lubricating condition	CoF in the middle of the test series	CoF at the end of the test series
POM	40 wt% glycerin	0.121 (±0.013)	0.134 (±0.014)
	60 wt% glycerin	0.066 (±0.006)	0.065 (±0.005)
	86.6 wt% glycerin	0.018 (±0.002)	0.016 (±0.002)
TPU	40 wt% glycerin	0.050 (±0.005)	0.049 (±0.003)
	60 wt% glycerin	0.024 (±0.001)	0.023 (±0.001)
	86.6 wt% glycerin	0.021 (±0.003)	0.021 (±0.002)

5.1.4　The Stribeck curve used as the evaluation tool of frictional properties

The CoF is plotted against the Gumbel number (Gu) for the two tribo-systems. The CoFs in the series of glycerine-water mixtures overlap and the friction-speed curves can be collapsed onto a single master curve presenting a typical shape of the Stribeck curve [107][108]. The curve of the POM-steel tribo-system (Figure 5.4(a)) exhibits the three lubrication regimes of the boundary lubrication, mixed lubrication and hydrodynamic lubrication over four decades of Gu. A small part of the boundary lubrication regime is observed as $Gu < 7.3 \times 10^{-11}$. The CoF has a maximum value of around 0.15. In this regime, the lubricant is insufficient to build up a continuous fluid film to separate the surfaces. Instead, fluid film exists in close proximity to the boundary of the surfaces, which is typically 10^{-7} m in thickness [109], and the asperities of the surfaces are in direct contact. The friction of the tribo-system is largely determined by the surface roughness and the viscoelastic properties of the contacting materials [89]. The mixed lubrication regime is observed in the range of $7.3 \times 10^{-11} < Gu < 1.3 \times 10^{-8}$, where the CoF decreases to a minimum value of 0.016. In this regime where either the sliding velocity or the fluid viscosity increases, more fluid is entrained in the contact zone and thus there is less solid to solid contact and a reduction in friction appears. The hydrodynamic lubrication regime is observed as $Gu > 1.3 \times 10^{-8}$, where the CoF increases with increasing Gu. In this regime, the fluid fully separates the surfaces. The increase in either sliding velocity or fluid viscosity increases the viscous drag within the fluid layer and leads to the increase in friction. The lubrication friction is markedly affected by hydrodynamic properties of the lubricant. Heyer and Läuger reported the CoFs of engine oil-lubricated POM-steel tribo-system using a tribo-rheometer equipped with a ball-on-three-plate accessory [93]. Although the test device and the test conditions (i.e. normal load, lubricant, velocity) applied in their work are different from that in this study, the averaged CoFs vary from 0.02 to 0.11. The

CoFs below 0.10 in lubricated POM-steel contact were also reported [110][111]. Thus, the measured CoFs in the work are in good agreement with literature.

The Stribeck curve of the TPU-steel tribo-system (Figure 5.4(b)) exhibits the regimes of mixed and elastohydrodynamic lubrication as well as a short transitional region between the two. Not like POM, the maximum of CoF at low Gu indicating the appearance of the boundary lubrication regime does not appear. One explanation is that the compliance of TPU enhanced entrainment of the liquid into the contact zone. The mixed regime is observed as $Gu < 3.5 \times 10^{-8}$, where the CoF reduces with increasing Gu and approaches a minimum value of 0.019. The elastohydrodynamic regime is observed as $Gu > 1.5 \times 10^{-7}$, where the CoF increases with increasing Gu. There is also a transitional flat region between the two regimes, where the CoFs remain the same minimum level in the range of Gu of 0.02. The friction values obtained in the experiment range between 0.02 and 0.2. The similar range of CoFs between 0.05 to 0.51 on rubber-ceramic tile systems were reported in a previous study using another methodology [42]. The higher hysteresis friction in the later was the result of higher levels of floor roughness (R_{tm} between 16 and 35 μm). The lower hysteresis friction observed here is attributed to the close to mirror-like smoothness of both the TPU and steel surfaces.

When the friction curves for the two materials are presented together in a single graph (Figure 5.4(c)), the curve for POM is located to the left side. The smaller Gu characterizing the boundary and mix lubrication regimes for POM is associated with the higher contact pressure (P_{POM}=22325 kPa; P_{TPU}=1339 kPa; refer to Table 5.3) applied in the POM-steel interface which had become necessary on account of POM's higher elastic modulus. The transition towards EHL takes place at lower Gu values for POM, but the minimum of CoF is almost identical to that for the TPU. At the same value of Gu around 1.3×10^{-8} where the POM-steel tribo-system begins to enter into the EHL regime, the TPU-steel tribo-system is still in the mixed lubrication regime and shows a higher lubricated friction. Although the surfaces of the two materials are similar in roughness, the compliance of the TPU surface results in a larger contact area (See Appendix A.1 for the supporting data) and hence a higher level of friction coming from surface adhesion is expected.
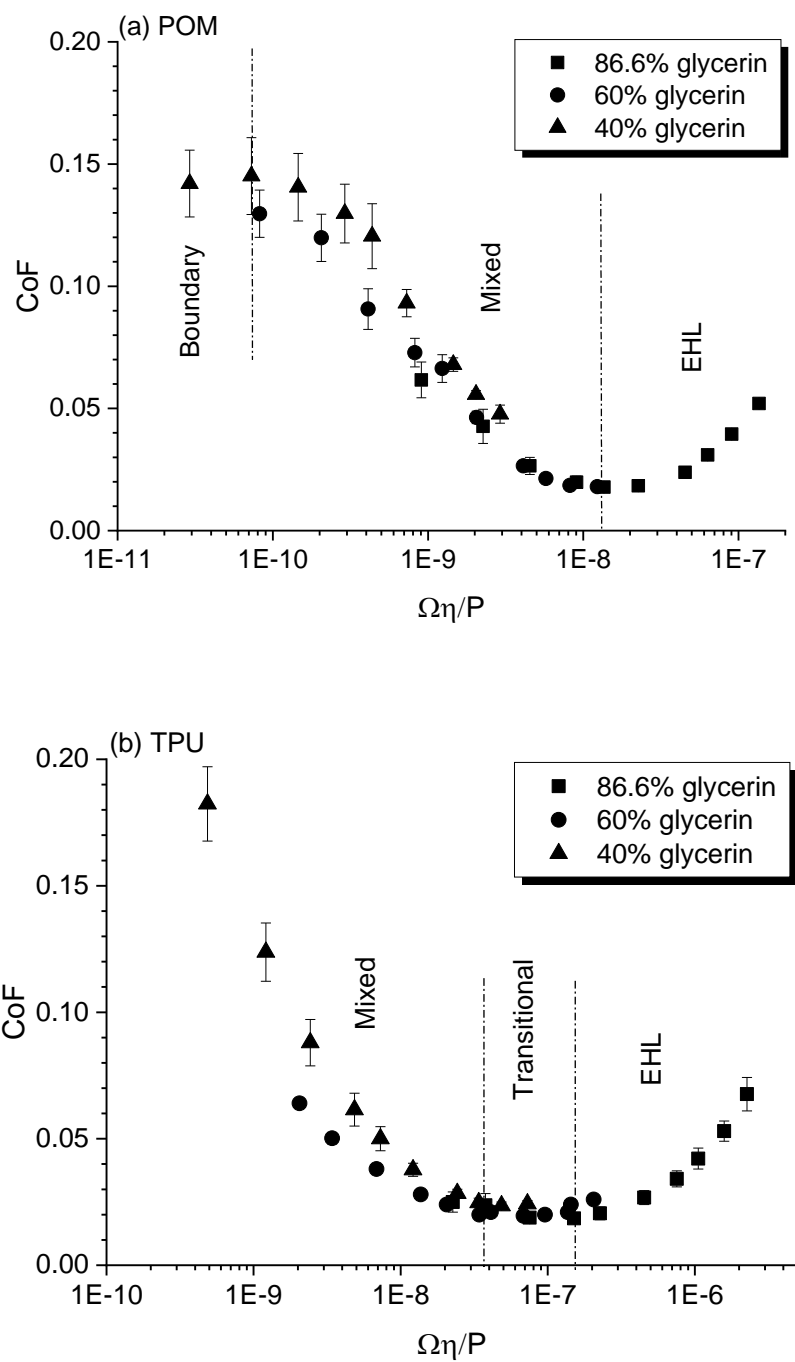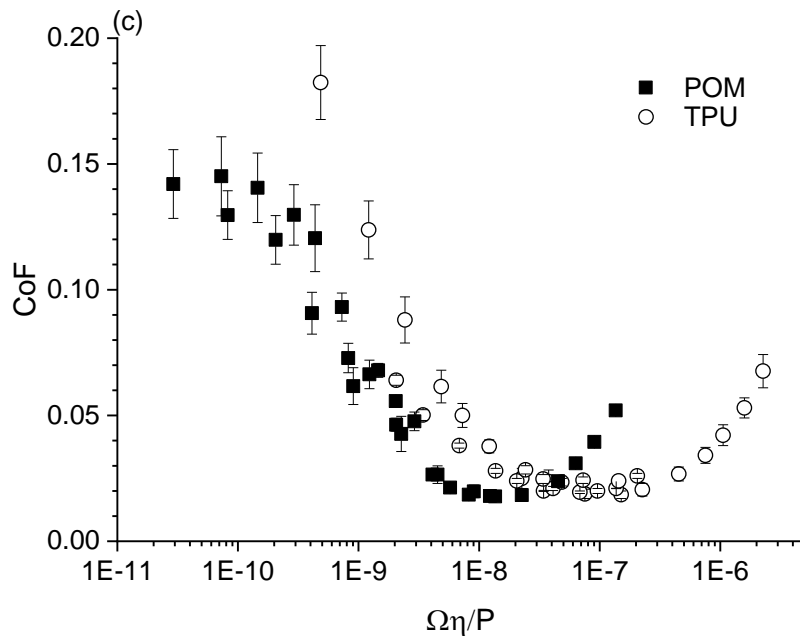
Figure 5.4 The Stribeck curves for the (a) POM-steel and (b) TPU-steel tribo-systems: 40 wt% glycerin (triangle); 60 wt% glycerin (circle); 86.6 wt% glycerin (square); (c) the Stribeck curves of the two tribo-stystems presented in one graph.

5.1.5   Intermediate summary

A novel method for measuring the steady-state wet sliding friction on compliant contact has been developed, using a rotational rheometer in combination with an accessory based on a three ball-on-plate geometry. The tribo-rheometer enables the accurate control of axial force, torque and sliding angular velocity. The testing procedure and evaluation method using POM and TPU as representative materials is established. The test conditions are defined in consideration of the relevant biomechanical and tribological parameters during actual shoe slipping events. The friction coefficients between the material and steel surfaces are measured under a constant axial force and varying sliding velocities in three different glycerin-water mixtures. The Stribeck curves are constructed by plotting the CoFs against the Gumbel number. The Stribeck curve for POM shows three distinguishable lubrication regimes-the boundary, mixed and elastohydrodynamic lubrication while the Stribeck curve for TPU showed the mixed and elastohydrodynamic lubrication regimes and a transitional regime between the two. The method shows good measurement repeatability and the obtained friction values are in good agreement with literature. When the Stribeck curves for POM and TPU are presented in one graph, due to the influence of material stiffness on the contact pressure, the curve for a relatively stiffer material (e.g. POM) is located to the left side and the curve for a

relatively softer material (e.g. TPU) is located to the right side. A definite range of Gumbel number corresponds to different lubrication regimes for the different materials. The new method shows the reliability and applicability to the assessment of wet slip resistance of elastomer.

5.2 Effect of surface characteristics of TPU on the coefficient of friction

5.2.1 The surface roughness parameters and their role in frictional measurements

The morphology and surface profile of TPUs depend not only on the chemical architecture but also on synthesis and processing conditions such as mixing efficiency of components, reaction temperature, reactivity and the experience of the technician and the machine set up. Small changes can make a big difference. The surface profile of TPUs can be strongly influenced by the mold finish and can vary significantly under the same processing condition. Figure 5.5 shows two white-light-interferometry images of the TPU Elastollan® 1185A (BASF Polyurethanes GmbH) produced by belt casting and then injection molding under same operation condition, one with a mirror-like smooth surface profile (a) and the other with visible parallel ridges at microscopic scale (b) Some preliminary experiments showed that the difference in surface characteristics resulted in a considerable change in the CoF. To gain a definite view of the effect of surface characteristics on the friction of TPU, surfaces of the material were roughened by hot-pressing and changed the roughness in either horizontal direction or vertical direction.
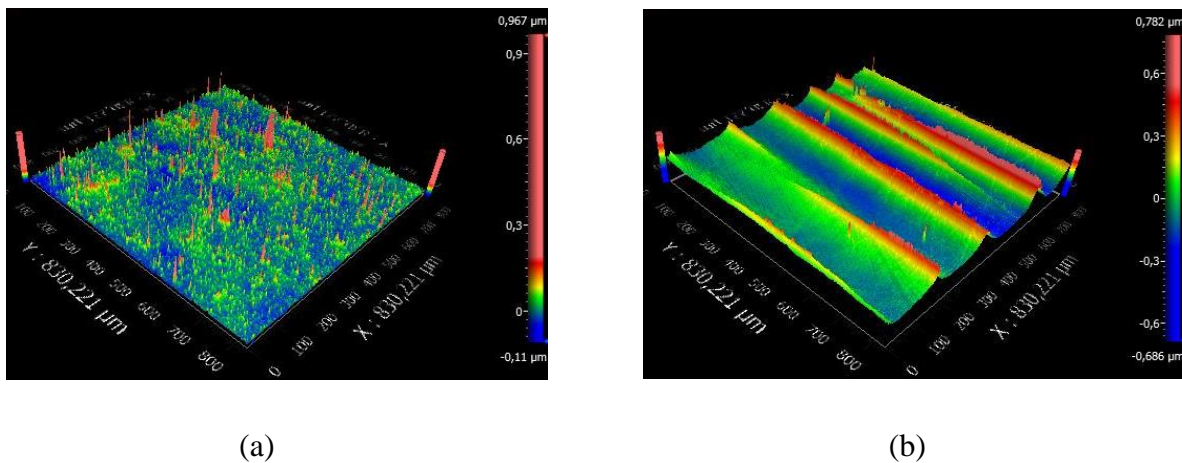

(a) (b)

Figure 5.5 White-light-interferometry images of TPU Elastollan®1185A

High-pass filtering is performed on the measured profile with a proper selection of a filtering length (the cut-off length, l_r) to obtain the surface roughness profile, also known as the surface heights. The surface roughness parameters are calculated from the filtered roughness profile. A typical surface roughness profile is shown in Figure 5.6. The evaluation length l_N is usually integral multiples of the cut-off length ($l_N = N \times l_r$). Discrete points (x_i, i=1,...,n)

with an equal increment Δx are described by *Equation 5.4* and the corresponding surface heights (z_i, i=1,...,n) are described by a mathematical function $z(x)$ [44].

Equation 5.4

$$x_i = x_1 + (i - 1) \times \Delta x$$

Equation 5.5

$$z_i = z(x_i)$$

There are various surface roughness parameters generated from a surface profile representing its geometric characteristics. The three commonly used surface characteristics are defined below [44][112]. The average spacing parameter (S_m) is the average spacing between the peaks at the mean line over the evaluation length. It can be calculated as $S_m = \frac{1}{n}\Sigma_i^n S_i$, i=1,..., n. It characterizes the surface irregularities in the horizontal direction. R_a and R_{tm} characterize the surface roughness in the vertical direction. Arithmetical mean roughness (R_a) is the arithmetic average of the absolute values of the surface heights, and can be calculated as
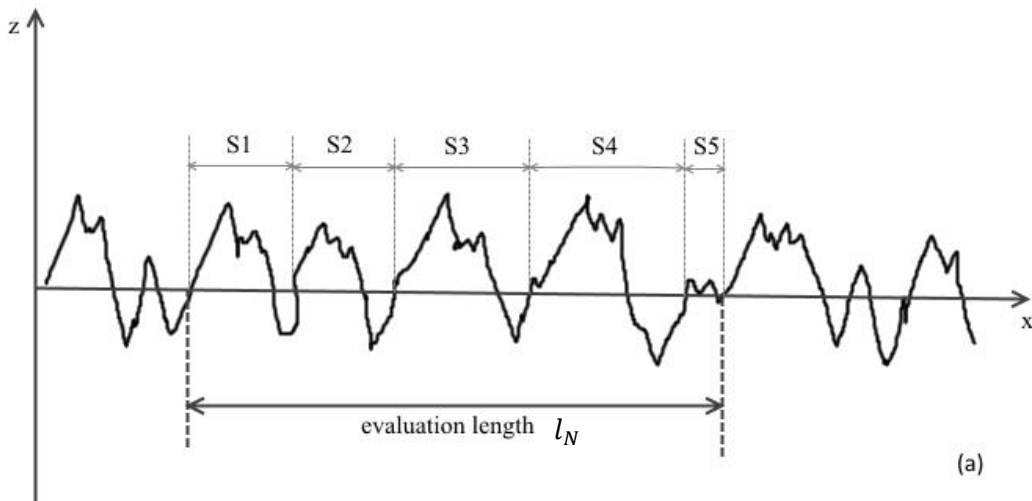
Equation 5.6

$$R_a = \frac{1}{n}\Sigma_i^n |z_i|, \qquad i=1,..., n.$$

Mean peak-to-valley roughness (R_{tm}) is determined by the difference between the highest peak and the lowest valley (denoted as Z) over the evaluation length, and can be calculated as

Equation 5.7
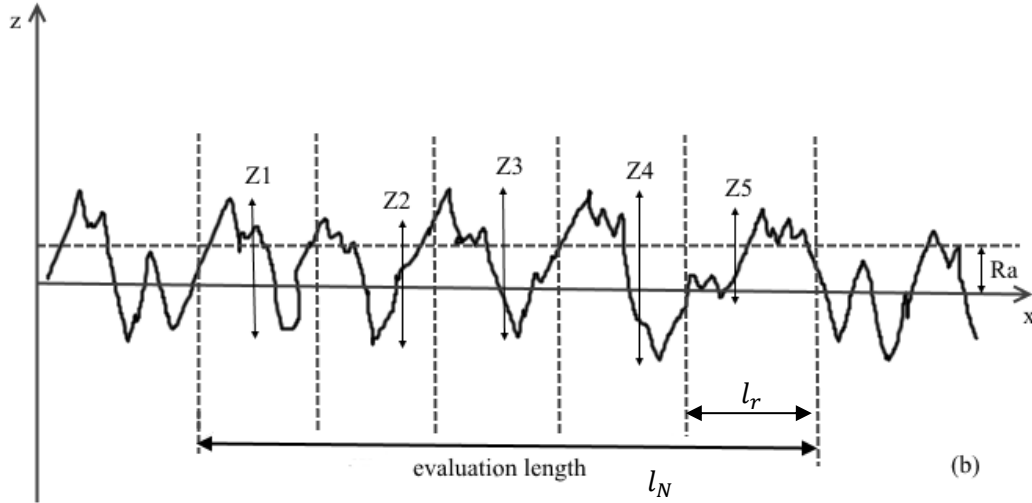
$$R_{tm} = \frac{1}{n}\Sigma_i^n Z_i, \qquad i=1,...,n.$$

49

Figure 5.6 A typical surface roughness profile and the illustration of (a) the average spacing parameter $\boldsymbol{S_m}$; (b) arithmetical mean roughness $\boldsymbol{R_a}$ and mean peak-to-valley roughness $\boldsymbol{R_{tm}}$

The TPU samples are divided into two groups and the surface characteristics are shown in Table 5.6. The nomenclature of the TPU samples consists of the capital letters PU followed by the grade of the sandpaper. For the grade P180, two different levels of roughness are further discriminated by the capital letters "S" and "R". The surface morphology of the samples is shown in Figure 5.7 and Figure 5.8. The TPU surfaces from group (i), as shown in Figure 5.7(a)-(e), have similar values of the vertical roughness parameters (R_a and R_{tm}) while the spacing parameter (S_m) generally increases as the particle size of the sandpaper increases. A smooth surface PUS (Figure 5.7 (f)) without the hot-pressing treatment is used as a reference for comparison to other surfaces, and it has extremely low R_a and R_{tm} at the nanometer scale and a smaller S_m than all the other samples. The TPU surfaces from group (ii), as shown in Figure 5.8(a)-(b), have similar values of S_m but differ in R_a and R_{tm} (PU180S < PU180R).

5.2 Effect of surface characteristics of TPU on the coefficient of friction

Table 5.6 Surface parameters of the TPU samples

Sample	R_a (μm)	R_{tm} (μm)	S_m (μm)
Group (i)			
PUS	0.024 ±0.004	0.208±0.055	21 ±3
PU800	1.11 ±0.13	5.86± 0.77	54 ±5
PU400	1.10 ±0.10	5.20± 0.62	77 ±6
PU240	1.33 ±0.16	4.47 ±0.46	170 ±26
PU180S	1.99 ±0.40	6.18 ±1.09	266 ±62
PU120	1.89 ±0.30	5.13 ±0.94	301 ±50
Group (ii)			
PU180S	1.99 ±0.40	6.18 ±1.09	266 ±62
PU180R	3.40 ±0.53	10.66 ±1.65	215 ±73

(a)   (b)

(c)   (d)

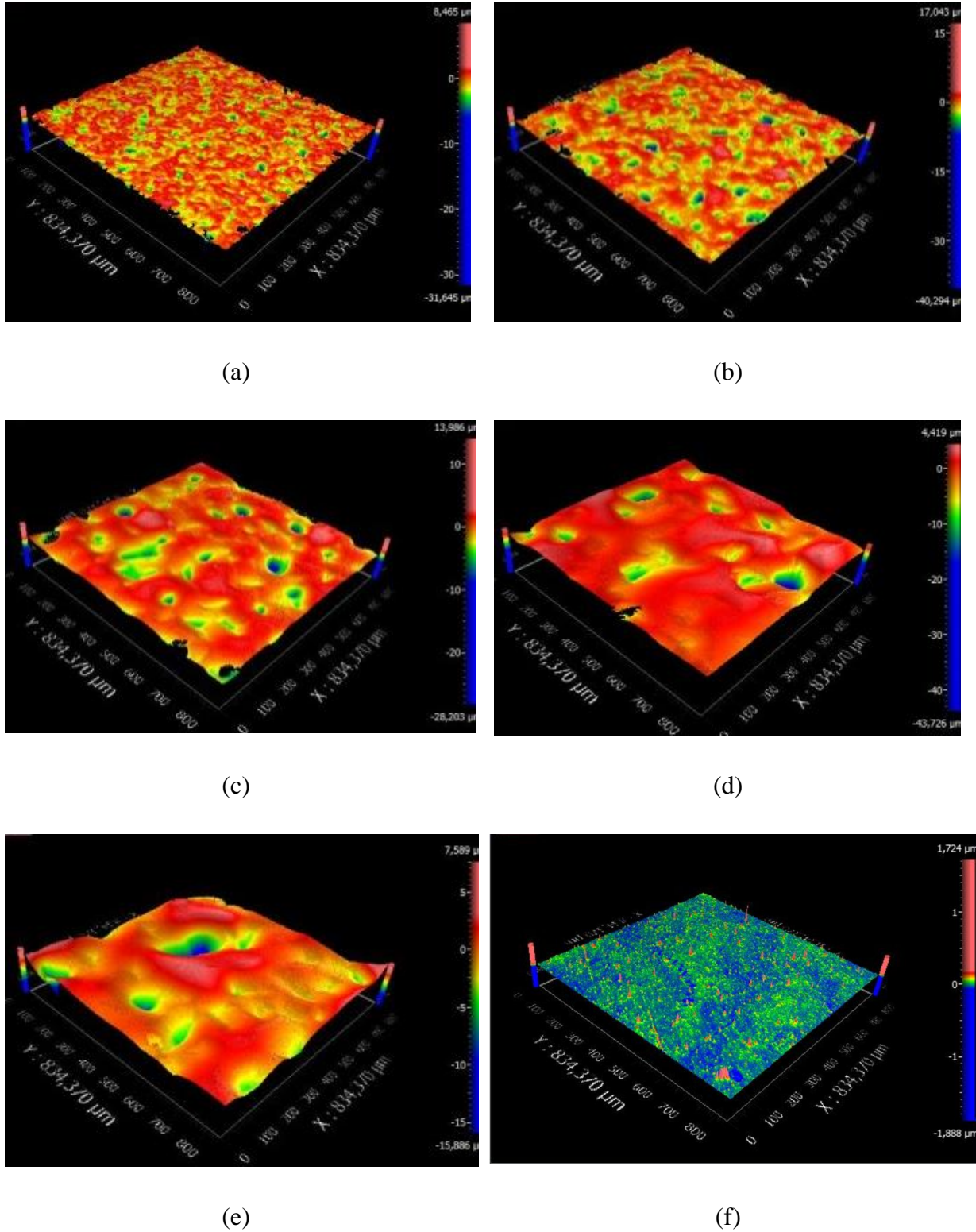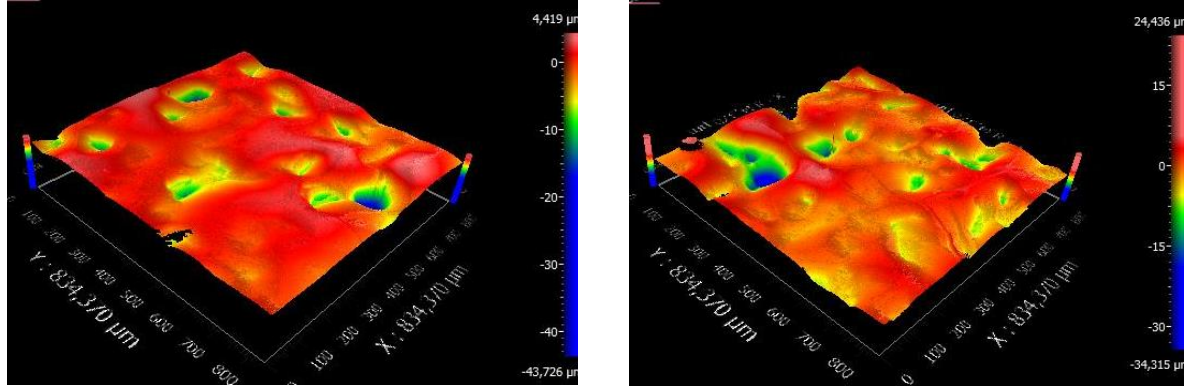(e)   (f)

Figure 5.7 White-light-interferometry images of the surfaces of the TPU samples roughened respectively by sandpaper imprinting with the grade (a) P800 (b) P400 (c) P240 (d) P180 (e) P120 and (f) a smooth referential surface without the hot-pressing treatment.

<div align="center">(a)   (b)</div>

Figure 5.8 White-light-interferometry images of the surfaces of the TPU samples roughened by sandpaper imprinting with the grade of P180 under different load to obtain two levels of roughness. (a) PU180S, the smoother surface; (b) PU180R, the rougher surface.

5.2.2 Effect of S_m on the coefficient of friction

5.2.2.1 The frictional properties presented by the Stribeck curve

The CoFs of the five TPU surfaces with varying S_m and similar R_a and R_{tm} were measured. In addition, the CoF of an untreated smooth surface (PUS) was measured as a reference for comparison to the others. The Stribeck curves of these samples are shown in Figure 5.9, exhibiting the mixed lubrication regime at low Gu, the EHL regime at high Gu and a transitional flat region where the minimum values of CoF (CoF$_{min}$) appear. The CoFs of different tribo-systems are more clearly distinguished in the mixed lubrication regime than in the EHL regime. In the mixed regime, the sample surface PU800 with the smallest S_m shows the highest CoF, followed by the surface PU400 with a larger S_m. As the S_m further increases on PU240, PU180S and PU120, the CoFs for the three surfaces become lower and approach the same level as obtained on the referential smooth surface. In the EHL regime, although the CoFs measured on different surfaces are less differentiated, a general trend still exists that the CoFs of PU800 and PU400 are higher than those obtained on the other surfaces, indicating the surface characteristics of TPU also have influence on the friction in the lubrication regime where the interacting surfaces are supposed to be separated by liquid. The CoF$_{min}$ in all the Stribeck curves and the corresponding ranges of Gu within which CoF$_{min}$ appears are listed in Table 5.7. The entry values of Gu for the surfaces with larger S_m are slightly lower than those for the surfaces with smaller S_m, indicating that a larger spacing between surface asperities promotes fluid entrainment into the contact zone. On a defined TPU surface, the CoFs obtained in 86.6 wt % glycerin are always slightly higher than those overlap points obtained

in 40 wt % glycerin at the same value of Gu, suggesting that hydrodynamic effect of the lubricant (viscosity) also plays a role. The scattered values of CoF$_{min}$ in the Stribeck curve for one sample is the consequence of scaling the curves with the lubricant viscosity. The scattered presence of the data while constructing the Stribeck curve was also observed by others [94][113].

The CoFs of the six TPU surfaces from group (i) measured at the angular sliding velocity of 23 mm/s in different lubricants are compared in Figure 5.10. The three columns for each surface represent the CoFs measured in 40 wt %, 60 wt % and 86.6 wt % glycerin, respectively. These data can also be found in the Stribeck curves at $Gu = 4.8 \times 10^{-9}$, $Gu = 1.4 \times 10^{-8}$, $Gu = 1.5 \times 10^{-7}$ from Figure 5.9. The values of CoF obtained in 40 wt % and 60 wt % glycerin decrease with increasing S_m and eventually approach the same minimum level as obtained on the referential smooth surface. The trend still exists but is less obvious for the CoFs measured in 86.6 wt % glycerin. The effect of S_m on friction is smaller and the influence of fluid properties become dominating in 86.6 wt % glycerin. In the next section, an explanation is provided for the descending trend of the CoF with increasing S_m.
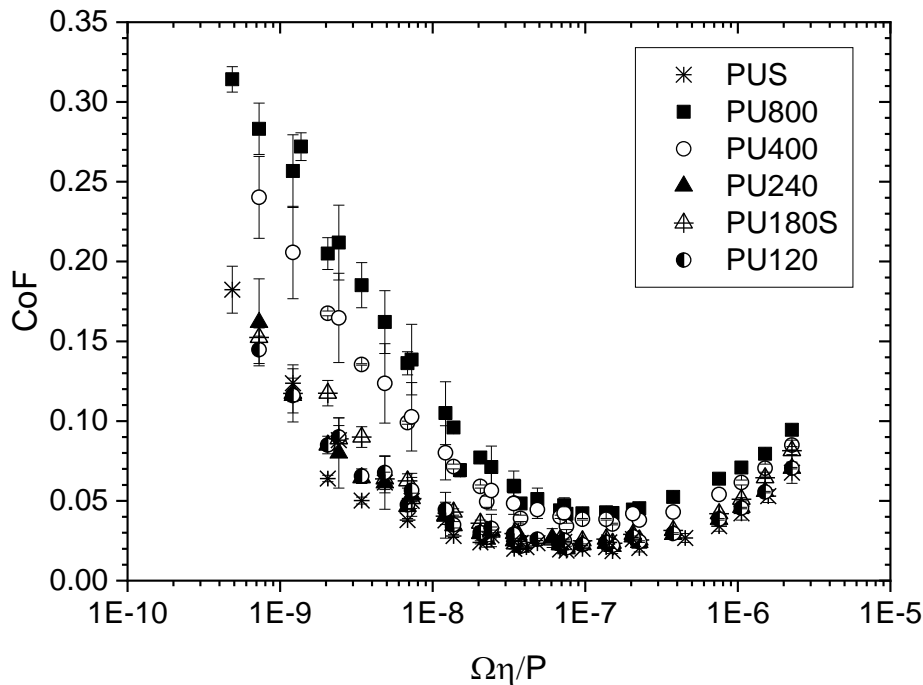

Figure 5.9 Stribeck curves for the five TPU surfaces with different S_m and similar roughness (R_a and R_{tm}), and for a smooth TPU surface (PUS) as reference.

Table 5.7 Minimum values of CoF and the corresponding ranges of *Gu* in the transitional flat region in the Stribeck curves

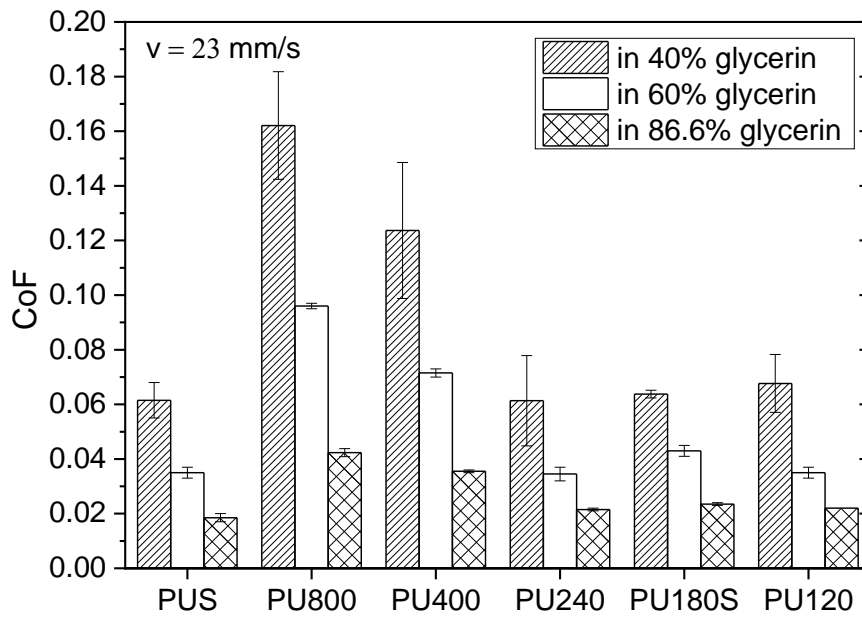| Sample	The range of *Gu* in the transitional region where the CoF_{min} appears	CoF_{min}
PUS	3.5×10^{-8} - 1.5×10^{-7}	0.017 - 0.020
PU800	6.8×10^{-8} - 1.6×10^{-7}	0.041 - 0.045
PU400	6.8×10^{-8} - 1.6×10^{-7}	0.032 - 0.040
PU240	3.8×10^{-8} - 1.6×10^{-7}	0.021 - 0.024
PU180S	5.0×10^{-8} - 1.9×10^{-7}	0.021 - 0.026
PU180R	8.8×10^{-8} - 1.9×10^{-7}	0.038 - 0.054
PU120	7.0×10^{-8} - 1.8×10^{-7}	0.020 - 0.023

Figure 5.10 Friction for the five TPU surfaces with different S_m and similar roughness (R_a and R_{tm}), and for a smooth TPU surface (PUS) as reference measured in three lubricants at the angular sliding velocity of 23 mm/s (Ω=2 rad/s).

5.2.2.2 The correlation between viscoelastic properties of TPU and the coefficient of friction

A steel ball slides over the asperities on a roughened elastomeric surface and causes a local deformation of the elastomer at the sliding frequency

Equation 5.8

$$f = \frac{v}{S_m}$$

where *v* denotes the linear sliding velocity. Although modern rubber friction theories point out that a realistic surface is essentially fractal and therefore the wet sliding involves multiple length scales[37][114], - as a brief and somewhat oversimplified summary of the on going discussion - it is decided to still use a single averaged value of S_m as the characteristic length scale in the sliding motion.

For the correlation between elastomer viscoelasticity and hysteresis friction, the frequency dependence on viscoelastic properties is required. These may be obtained from DMA measurements. DMA measurements are usually performed at a constant deformation frequency (typically at 1 Hz) and a temperature sweep is applied to analyze transitions such as the glass transition temperature and the softening of materials. The obtained curves show the viscoelastic properties of the material as a function of temperature. Because direct reliable dynamic testing at a high frequency is still difficult to achieve with common rheometers, the time-temperature superposition (TTS) principle [115] is (uncritically) used to transform the relevant sliding frequency at the test (reference) temperature T_{ref} into the relevant temperature *T* using the temperature dependent DMA curve measured under a fixed reference frequency f_{ref}. The following equations are used for the TTS transformation [116]:

Equation 5.9

$$H\big(a_T(T) \cdot f_{ref}\big) = H\big(a_T(T_{ref}) \cdot f\big); \quad H \text{ denotes } G'' \text{ or } tan\delta$$

or

Equation 5.10

$$a_T(T) \cdot f_{ref} = a_T(T_{ref}) \cdot f$$

$a_T(T)$ is the Williams-Landel-Ferry (WLF) time-temperature shift factor and is given through the WLF equation [117] with the two constants C1 and C2:

Equation 5.11

$$\log\big(a_T(T)\big) = \frac{-C1 \cdot (T - T_{ref})}{C2 + T - T_{ref}}$$

The constants C1 and C2 vary with the chosen reference temperature and the tested polymer. We use the universal constants C1= 8.86 and C2 = 101.5 for $T_{ref} \cong T_g + 50$ °C [48]. T_g is the glass transition temperature of the polymer. The T_g of the tested TPU is -45 °C as determined by the maximum of the loss modulus. For f_{ref} of 1 Hz, the relevant temperature is obtained from *Equation 5.10* and *Equation 5.11*:
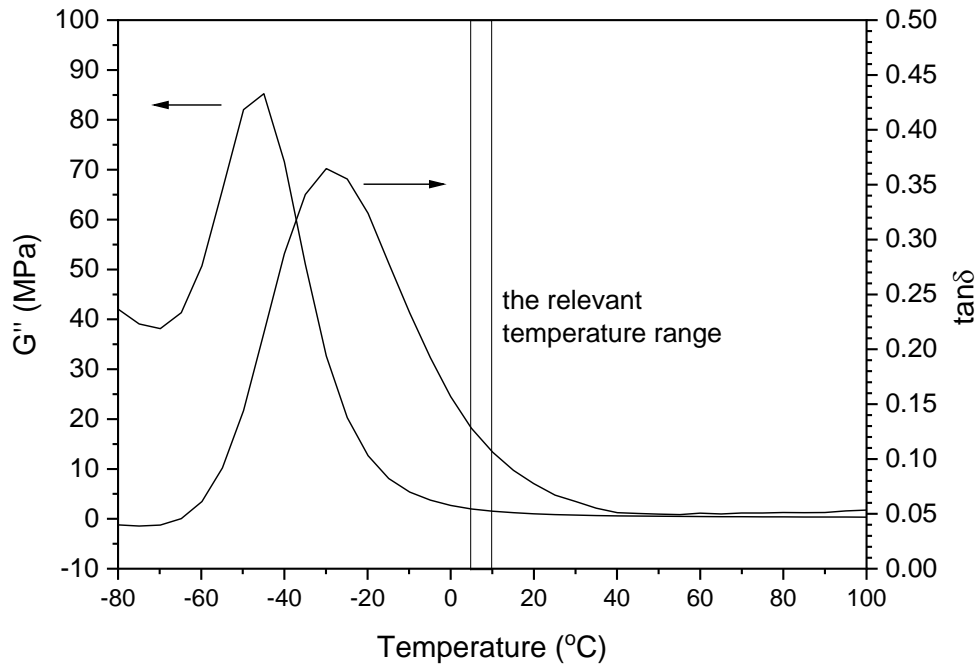
Equation 5.12

$$T = \frac{\log(f) \cdot \big(C2 - T_{ref}\big) - C1 \cdot T_{ref}}{-C1 - \log(f)}$$

The relevant frequencies of dynamic deformation on the TPU surfaces corresponding to the sliding velocity of 23 mm/s and the calculated relevant temperatures in the temperature dependent DMA curves according to the TTS are shown in Table 5.8.

As the average spacing becomes larger, the relevant frequency of surface deformation becomes lower and is transformed into a higher relevant temperature. The whole range of sliding frequency involved in the friction measurements is linked to a relevant temperature range of 5 to 10 °C at the f_{ref} of 1 Hz, marked in the temperature dependent DMA curves shown in Figure 5.11. The loss modulus and the loss factor are monotonically decreasing functions of temperature in the relevant temperature range. At a lower temperature, the material experiences more hysteresis energy loss (contributing to the hysteresis friction). In other words, a higher coefficient of friction is expected at a higher relevant deformation frequency during wet sliding, which is related to a smaller S_m. The reference surface PUS is not compared to the others in the context of friction-viscoelasticity correlation because of its much lower R_a and R_{tm}. For this surface, the low friction is the results of the low degree of hysteresis deformation and the fast surface wetting by the test liquid.

Table 5.8 Relevant frequencies of dynamic deformation during wet sliding and corresponding relevant temperatures in the temperature dependent DMA curves according to the TTS

Sample	Average value of S_m (µm)	Relevant frequency(Hz) of deformation during sliding as v = 23 mm/s	Relevant temperature(°C) on the temperature dependent DMA curves (see Figure 5.11)
PU800	54	413	5
PU400	77	290	6
PU240	170	131	8
PU180S	266	84	10
PU120	301	74	10

Figure 5.11 Loss modulus (G") and loss factor (tanδ) as a function of temperature for the TPU Elastollan® 1185A. f_{ref} =1 Hz; strain = 0.3%

5.2.3 Effect of R_a and R_{tm} on the coefficient of friction

The Stribeck curves for two TPU surfaces (PU180R(ough) vs. PU180S(mooth)) with varying values of R_a and R_{tm} and a similar S_m are shown in Figure 5.12, exhibiting the mixed lubrication regime at low Gu, the EHL regime at high Gu and a transitional flat region between the two where the CoF$_{min}$ values appear. The rougher surface (PU180R) exhibits higher CoFs in all lubrication regimes and the difference in the friction is more noticeable in

the mixed regime, as expected. The CoFmin on the smoother surface (PU180S) at Gu of 1.0×10^{-7} is 0.02 and the CoFmin on the rougher surface at the same Gu increases two-fold to reach 0.04 when the roughness values have increased by a factor of around 1.7. The results demonstrate that the surface roughness of TPU can influence the friction in both the mixed and EHL regimes. Increasing roughness results in more hysteresis energy loss during the collision between surface asperities of the steel balls and the polymer, which contributes to the hysteresis component of friction. The effect of surface roughness was also observed by Bongaerts et.al [113] in the lubricated friction in the PDMS-PDMS contact. However, the distinct shifting of $\Omega\eta$ (an equivalent quantity to Gu) towards higher values at the CoFmin was not observed here, although the starting value of Gu into the transitional flat region in the Stribeck curve is slightly higher for the rougher surface than for the smoother surface, as seen in Table 5.7. The observation indicates that a higher roughness prevents the spread of fluid into the contact zone.
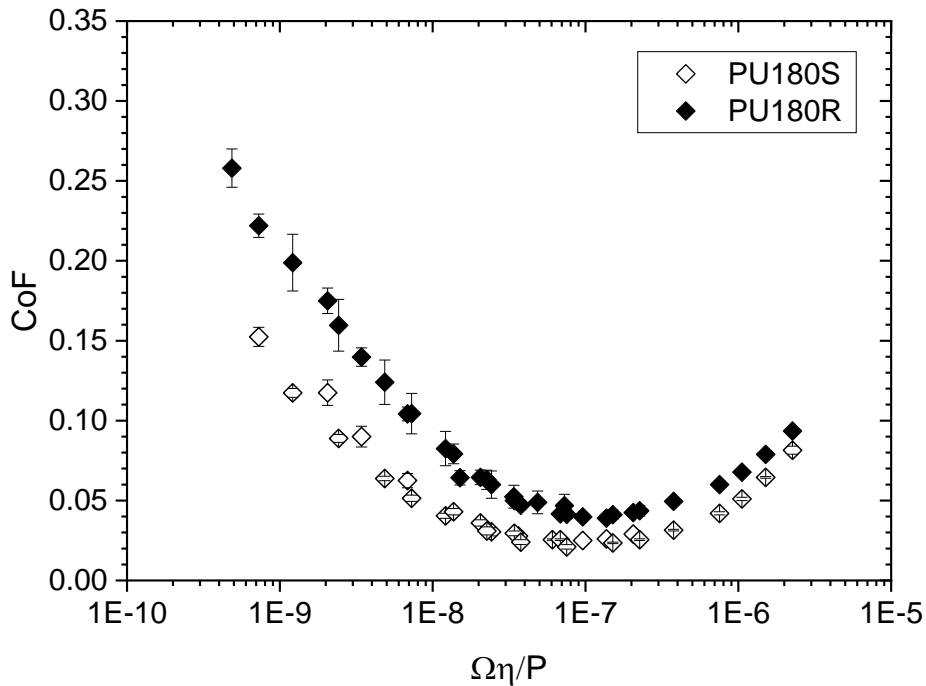

Figure 5.12 Stribeck curves for two TPU surfaces with different R_a and R_{tm} and a similar S_m. PU180R -the rougher surface; PU180S -the smoother surface.

5.2.4   Intermediate summary

The wet slip resistance of thermoplastic polyurethane elastomer was assessed using a three-ball-on-plate accessory on a rotational rheometer to measure the lubricated CoF (coefficient of friction). The Stribeck curves show the frictional properties of the steel-on-TPU tribo-system in the mixed lubrication and EHL (elastohydrodynamic lubrication) regimes and demonstrate the following effect of surface characteristics on the friction:

(1) On surfaces with varying S_m (the average spacing parameter) and similar R_a (arithmetical mean roughness) and R_{tm} (mean peak-to-valley roughness), the CoF decreases with increasing S_m until approaching the same minimum level of friction as obtained on an untreated smooth referential surface. The starting values of Gu (the Gumbel number) into the transitional region for the surfaces with larger S_m are slightly lower than for the surfaces with smaller S_m, indicating that a larger spacing between surface asperities promotes fluid entrainment into the contact zone and hence reduces friction. An explanation is provided for the descending trend of the CoF with increasing S_m by the sliding frequency dependence of hysteresis friction. A smaller S_m is associated with higher deformation frequency of the elastomer during wet sliding and may cause more hysteresis energy loss contributing to the friction. A correlation exists with the higher values of loss modulus or loss factor at the relevant temperature in the temperature dependent DMA curves.

(2) On surfaces with varying roughness (R_a and R_{tm}) and a similar S_m, the CoF increases with increasing R_a or R_{tm}. The surface roughness of TPU can influence the friction in both the mixed and EHL regimes while the effect is more noticeable in the mixed lubrication regime. The results indicate that the deformation of the elastomer during wet sliding, which is affected by the material surface characteristics, takes place in all tested lubricating conditions.

(3) The frictional properties in the mixed lubrication regime (approaching the boundary lubrication regime) are responsible for the wet slip-resistant performance of the elastomer material. Changing the surface parameter in either vertical or horizontal direction can change the CoF by a factor of 2-3 under a defined test condition in the mixed lubrication regime. Therefore, it is necessary to treat TPU surfaces in such a manner that they have similar surface characteristics in the frictional measurement. The hot-pressing method and sandpaper with the grade between P240 to P120 are taken for the surface roughening because the friction of the obtained TPU surfaces in

5.2 Effect of surface characteristics of TPU on the coefficient of friction

this roughness regime was not strongly influenced by the variation in the surface
parameters.

5.3 Effect of the hardness of TPU on the coefficient of friction

5.3.1 The material and surface properties of TPU samples

In order to investigate the effect of material bulk hardness on the lubricated friction, polyether diol based TPU samples with five different levels of hardness were produced by changing the amount of the chain extender 1,4-butanediol in the formulation. The nomenclature of the TPU samples in Table 5.9 consists of the capital letters PU followed by the resulting sample's Shore A hardness. The study in Section 5.2 has shown that the roughness of elastomeric contacting surface has substantial influence on the lubricated friction. To prevent the study on the effect of hardness from being interfered by roughness variation, all the TPU samples were pretreated by a hot-pressing protocol to obtain the same level of surface roughness parameters (S_m, R_a and R_{tm}). The values of S_m, R_a and R_{tm} for these surfaces are shown in Table 5.9. Figure 5.13 presents a white-light-interferometry image of the PU88A surface on behalf of all the surfaces used in this part of the work.
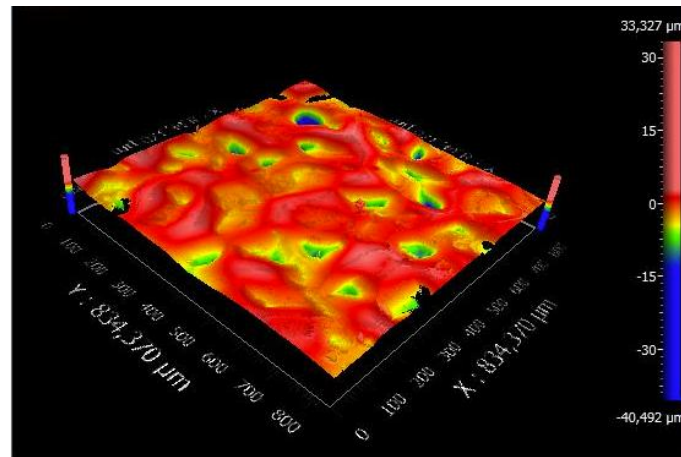

Figure 5.13 White-light-interferometry image of the PU88A surface which was roughened by sandpaper imprinting with the grade P180

5.3 Effect of the hardness of TPU on the coefficient of friction

Table 5.9 Material properties and surface characteristics of the TPU samples with different hardnesses

Nomenclature*	Shore A hardness	S_m (µm)	R_a (µm)	R_{tm} (µm)	E (MPa)	P (kPa)	$T_{g, G"max}$ (ºC)	$tan\delta$ at 10 ºC	$G"$ (MPa) at 10 ºC	Hysteresis at 10% max.strain
PU81A	81	169 ±13	1.95 ±0.16	6.56 ±0.93	19.1	848	-50	0.074	0.500	6.7
PU86A	86	203 ±5	2.17 ±0.36	7.44 ±0.58	37.8	1339	-45	0.106	1.535	9.2
PU88A	88	187 ±32	2.05 ±0.15	7.03 ±0.68	50.7	1628	-45	0.130	2.647	10.8
PU91A	91	216 ±30	2.04 ±0.24	7.04 ±0.57	89.3	2374	-40	0.166	6.717	16.4
PU97A	97	208 ±37	2.21 ±0.44	7.72 ±1.43	140.3	3206	-40	0.175	11.83	21.0

Note: The relevant trade names for the five samples are Elastollan® 1180A10 (PU81A), 1185A10 (PU86A), 1190A10 (PU88A), 1195A10 (PU91A) and 1198A (PU97A), respectively.
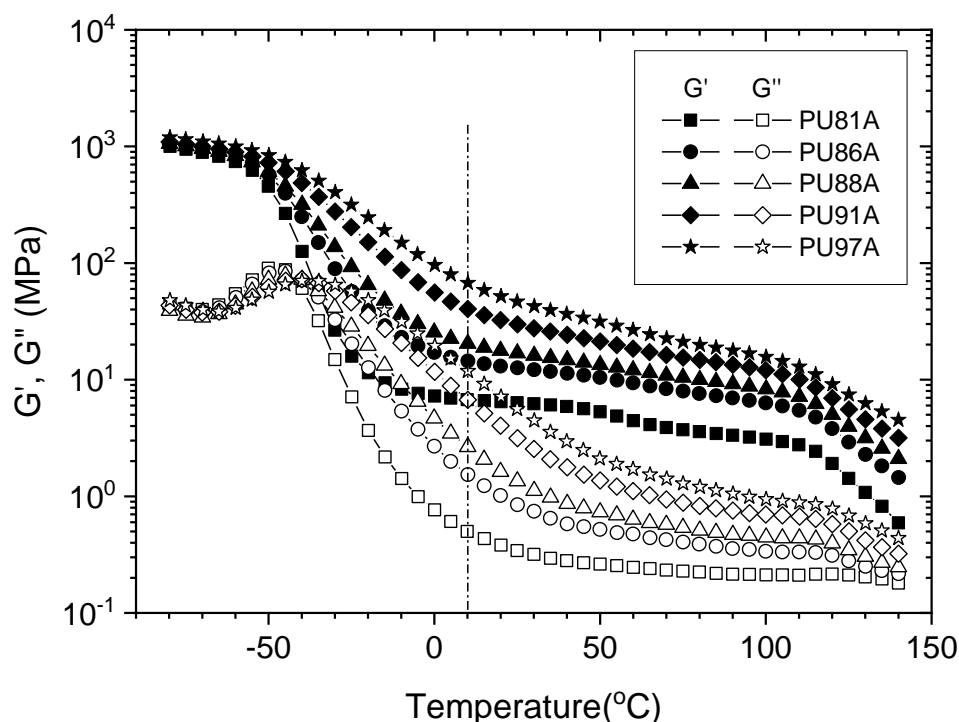
Figure 5.14 Storage moduli and loss moduli of the TPU samples with different levels of hardness as a function of temperature; f = 1 Hz.

Figure 5.14 presents the storage moduli (G') and loss moduli (G'') of the TPU samples with different levels of hardness in a temperature ramp DMA test. The loss factor (*tan δ*) of the samples as a function of temperature was shown in Figure 5.15. The polyurethanes with lower amount of HSC have a lower hardness at room temperature (25°C). The DMA curves exhibit a relatively sharp transition from the glassy to the rubbery state for the TPUs with a lower hardness. With increasing amount of HSC, the hard domains eventually form the continuous phase and the soft domains are dispersed in the continuous hard domain matrix. In this case, the polyurethanes show a gradual transition to the rubbery state [2]. The values of G' and G'' in the rubbery state increase with increasing hardness. The storage modulus provides information regarding the stiffness of the polyurethane, while the loss modulus and loss factor are indicators of the polymer ability to internally dissipate the energy under the test conditions. The peaks in the G'' and *tan δ* plots shift towards higher temperatures and broaden as the hardness increases [118]. The broaded peaks are associated with the less defined composition of the soft domains as well as more hard domains being involved in the glass transition [4].

The upturn in *tan δ* at the high temperature, which is associated with the softening of the hard domains, is earlier and higher for the TPU with lower hardness.
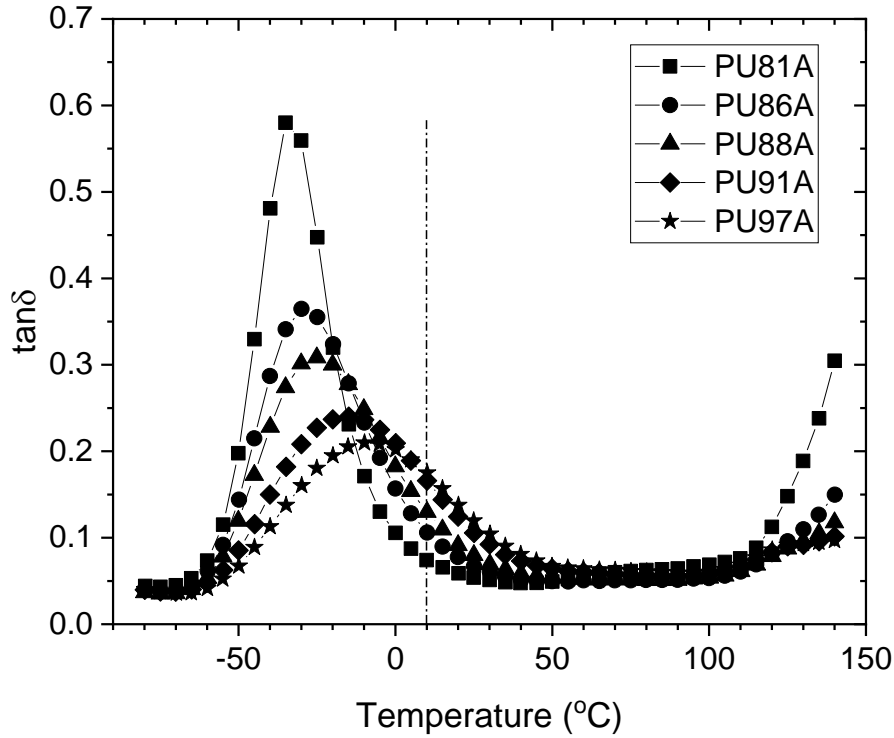

Figure 5.15 Loss factor of the TPU samples with different levels of hardness as a function of temperature; f= 1 Hz.

In addition to the DMA measurements, tensile hysteresis measurements also have been performed. Both measurements present information on the viscoelastic behavior of the TPUs, albeit at a different frequency and deformation. The DMA spectra were recorded at a frequency of 1 Hz; the duration of one hysteresis cycle in the tensile testing in our experiment amounted to 50 seconds.

5.3 Effect of the hardness of TPU on the coefficient of friction
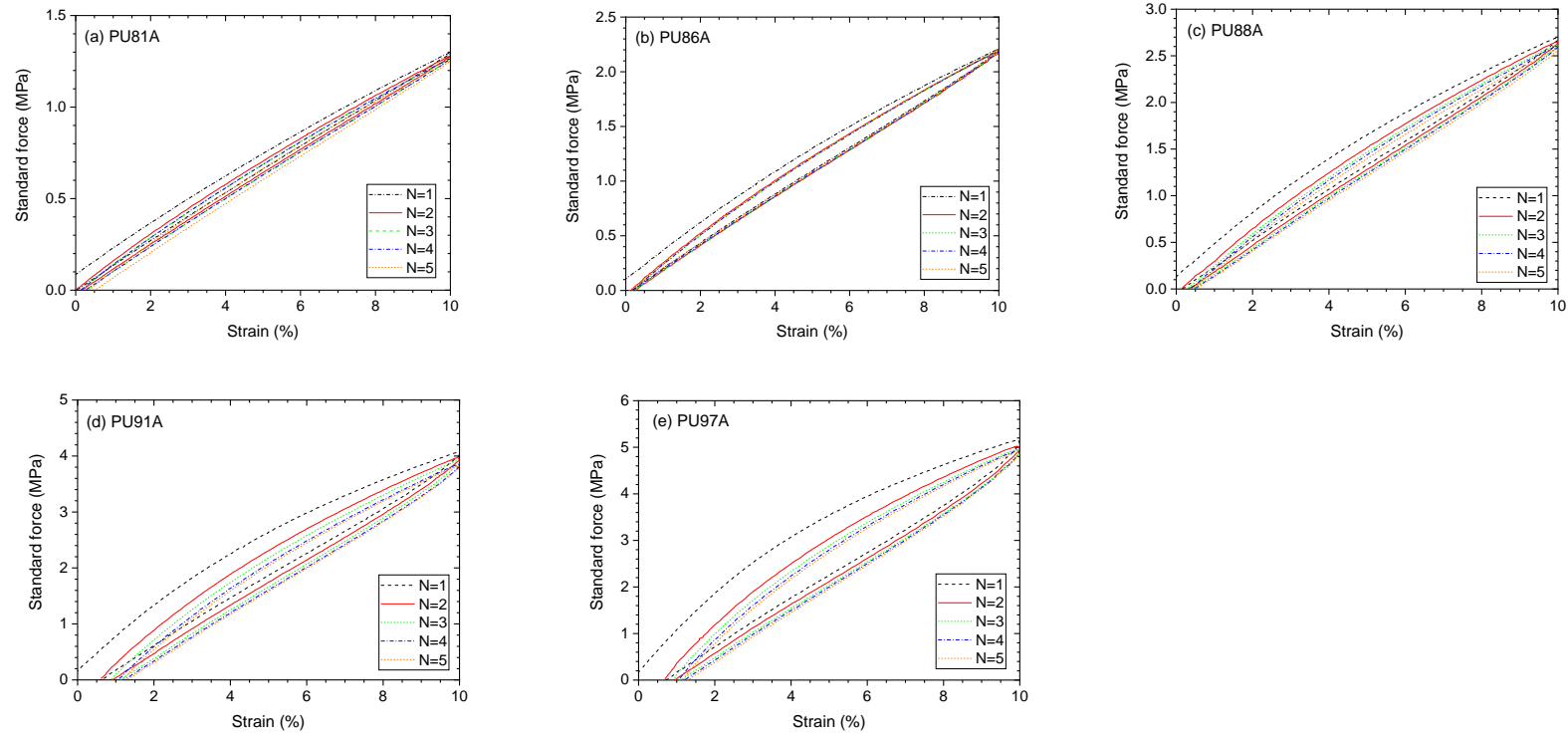
Figure 5.16 Tensile load/unload cycles for the TPUs with increasing levels of hardness from (a) to (e). (a) PU81A; (b) PU86A; (c) PU88A; (d) PU91A; (e) PU97A. maximum strain =10%.

In the cyclic tensile test, due to the viscoelasticity of TPU, a phase shift occurs between strain and stress and in the stress-strain coordinates, the geometrical locus of operational point becomes a loop, known as hysteresis loop. As shown in Figure 5.16, the maximum hysteresis and residual strain, which are strongly dependent on the hard segment content, occurs during the first cycle. The hysteresis losses in the second and subsequent cycles are significantly lower than that in the first cycle. After five load/unload cycles the stress-strain curves tend to stabilize to a fixed trajectory [119]. The hysteresis at 10% maximum strain was calculated for the five TPUs and listed in Table 5.9. Materials with a larger HSC content show a larger hysteresis. Similar observations have been made before [120][121]. The hysteresis of polyurethane is associated with mechanisms such as plastic deformation of the hard segment domains, irreversible disruption of the molecular structure and irreversible hard segment orientation. At low HSC content, the hard domains are majorly distributed within the continuous soft domain without significant aggregation, so alignment and break-up of the low amount of hard domain structure is not a relevant feature, resulting in lower levels of hysteresis. At high HSC contents, elongation of the now present crystalline, interconnected hard domains produces plastic deformation and disruption of the hydrogen-bonded or/and crystalline hard segment structure, which is reflected in a larger hysteresis [4]. The high hysteresis at very low HSC content because of insufficient physical crosslinks to prevent the polymer from flowing under stress [120] is not observed in this work.

During the initial 10 to 20 seconds of the frictional measurement, sometimes a slight decrease in the torque (therefore in the CoF) can be seen, and it bears some resemblance to the material hysteresis: how fast the CoFs decrease to the steady state depends on material hysteresis. Because the minimum sampling interval of the rheometer of 1 second is still too large for the transitional frictional study and hence only a few data points in the running-in phase were available, the running-in phenomena in the frictional measurement were not further investigated.

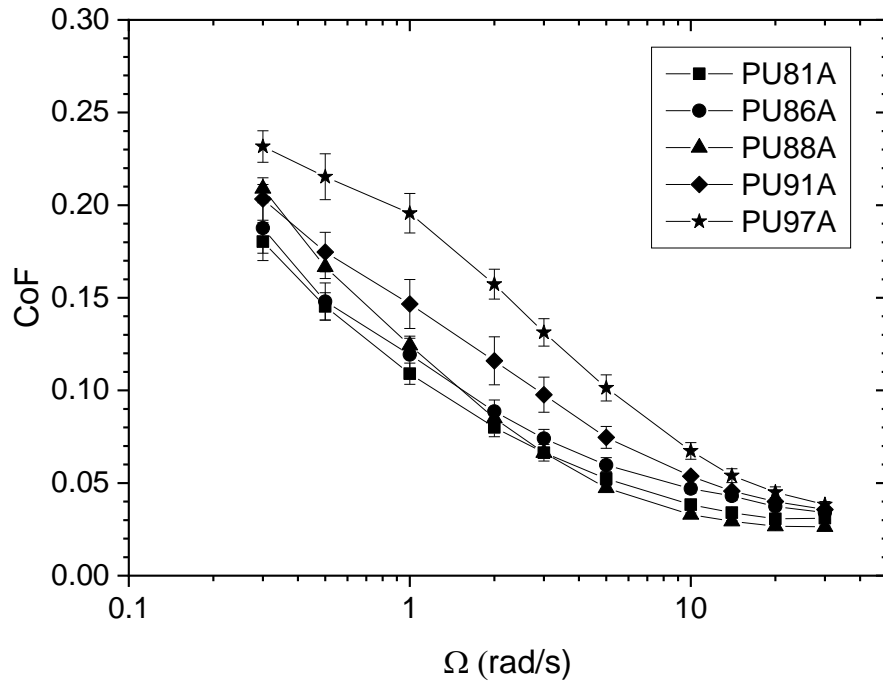### 5.3.2 The coefficients of friction in the mixed lubrication regime

Figure 5.17 Friction of the TPUs with different hardnesses as a function of angular sliding velocity. The tribo-system is lubricated by 40 wt% glycerin-water solution.

The CoFs of the TPU samples with different levels of hardness were measured using 40 wt% glycerin as the lubricant. In the plot of the CoF against the angular sliding velocity (Figure 5.17) the CoF decreases with increasing velocity, which indicates the system is in the mixed lubrication regime. The TPU friction can be differentiated in the regime; the sample with a higher hardness shows higher friction over the whole range of measured velocities. More viscous glycerin water mixtures were not used in the measurement, because it would have shown the friction in the EHL regime where very few solid to solid contacts exist and the CoFs of all the materials would converge, which was not of interest in the present work.
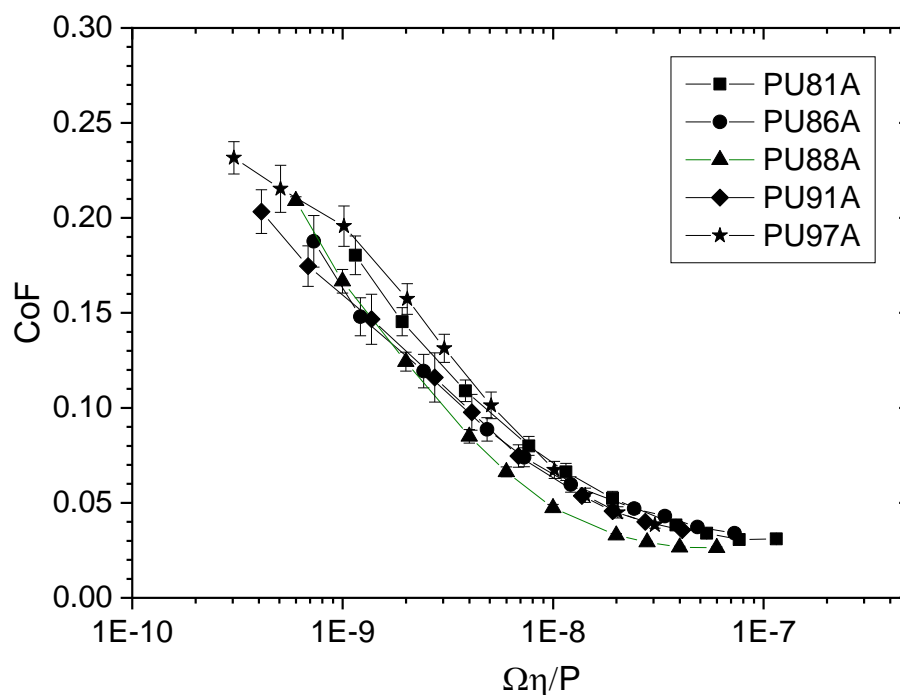
Figure 5.18 Stribeck curves of the TPUs with different hardnesses as a function of angular sliding velocity. The lubricant is 40 wt% glycerin-water solution.

The Young's moduli of the TPUs, which are calculated using the shear storage moduli[5] in the DMA curves, increase with the TPU hardness. The values of Young's moduli and the average contact pressures for the five samples are presented in Table 5.9. The Stribeck curves are shown in Figure 5.18. When the CoFs are plotted against the Gumbel number, the abovementioned friction-speed curves can be horizontally translated and collapsed onto a master curve. Under a defined axial force, the curve for softer TPU which has a lower contact pressure shifts to the right while the curve for harder TPU which has a higher contact pressure shifts to the left. The convergence of the single friction-speed curves confirms that the Stribeck curve can describe the effect of operational conditions such as sliding velocity, lubricant viscosity and contact pressure on the friction for the TPU based tribo-system. The master Stribeck curve is proved applicable for the series of polyether-based TPUs with a relatively high hardness range.

---

[5] Refer to Appendix A.1

5.3.3 The correlation between the viscoelastic properties of TPU and the coefficient of friction

In Figure 5.17, the CoFs of the TPUs at the sliding velocity of 11 mm/s ($\Omega = 1$ rad/s) can be distinguished. Therefore, they are used for demonstrating the existence of a correlation to the viscoelastic properties of the present series of TPUs. Following the course of reasoning as described in Section 5.2.2.2, the sliding frequency at the speed of 11 mm/s and the relevant temperature on the temperature dependent DMA curve for the five tested surfaces are calculated and shown in Table 5.10. The CoFs at the sliding velocity of 11 mm/s is associated with the viscoelastic properties at the relevant temperature of about 10 °C in the temperature dependent DMA curves as f_{ref} of 1 Hz. The results are similar due to a fixed sliding velocity and the similar values of S_m for the surfaces.

Table 5.10 Relevant frequencies of dynamic deformation during wet sliding and corresponding relevant temperatures in the temperature dependent DMA curves according to the TTS.

Sample	Average value of S_m (µm)	Sliding frequency (Hz) as v=11 mm/s, T=27 °C	Relevant temperature(°C) on the temperature dependent DMA curve
PU81A	169	66	10
PU86A	203	55	10
PU88A	187	60	10
PU91A	216	52	11
PU97A	208	54	10

The glass transition temperatures (T_g) at the maximum of G'' and the values of $tan\,\delta$ and G'' at the temperature of 10 °C for the five samples are presented in Table 5.9. The values of G'' and $tan\,\delta$ at 10 °C are located in the tail end of the α-glass transition of the TPUs (Figure 5.14 and Figure 5.15, respectively, the relevant temperature of 10 °C is marked in both graphs by a dashed line). The physical quantities increase with the increasing TPU hardness. Hence, the TPUs become more damping at the relevant temperature as the hardness increases.

In the following four graphs from Figure 5.19 to Figure 5.22, the CoFs of the TPU surfaces at the sliding velocity of 11 mm/s are plotted against the T_g, $tan\,\delta$ and G'' at 10°C and hysteresis at 10% maximum strain, respectively (Table 5.9). The CoFs do not have an explicit correlation with T_g, however, have a monotonically increasing relationship with $tan\,\delta$, G'' or

the hysteresis. The friction appears not to be linearly dependent on the $tan\ \delta$ (poor R^2 value of 0.696) while a linear correlation seems to exist between the friction and G'' or the lower part of the hysteresis (R^2 values of 0.990 and 0.945, respectively). Increasing values of $tan\ \delta$ or G'' suggest that during the wet sliding, more energy of the material is likely to be dissipated in the form of heat and contributes to the hysteresis friction. The component of hysteresis friction caused by the deformation and relaxation of surface asperities is well controlled at a similar level because the surfaces have similar roughness parameters. Therefore, the ranking of the friction primarily reveals the diversity in the dynamic mechanical properties of the TPUs. As for the TPU mechanical hysteresis at 10% maximum strain, it has a monotonically increasing relationship with the $tan\ \delta$ at 10 °C. The hysteresis, like $tan\ \delta$, is also related with energy dissipation in the polymer bulk, although the form of motion and duration of the experiment is different: the former is subject to cyclic stretching and relaxation at a selected strain level that causes non-linear viscoelastic deformation of the material; the latter is subject to continuous oscillation under a small deformation amplitude at a fixed frequency of 1 Hz. The indentation depth encountered in the wet sliding test was calculated to range from 28 μm for the softest TPU to 7 μm for the hardest TPU, respectively (See Appendix A.1) and corresponds to about 1.4 to 0.3 % compression of the present series of TPU samples.
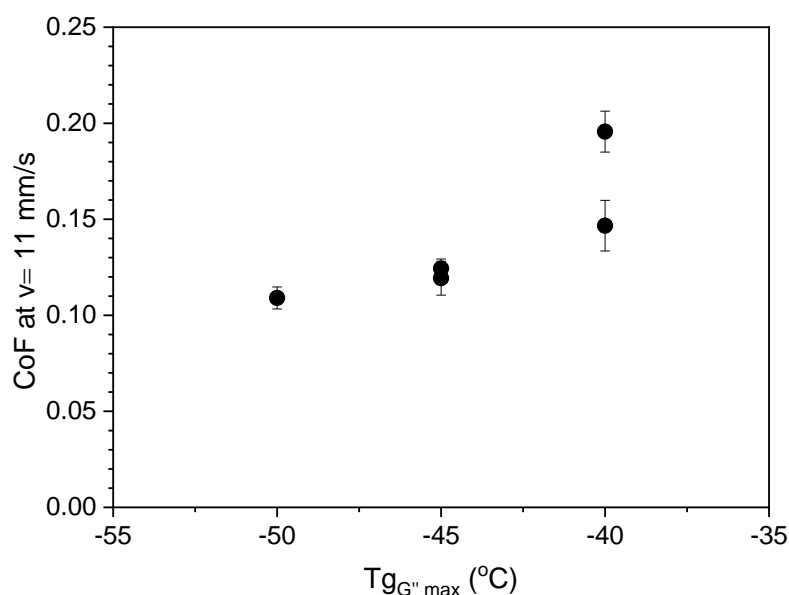

Figure 5.19 Plot of CoF at the sliding velocity of 11 mm/s against the glass transition temperature
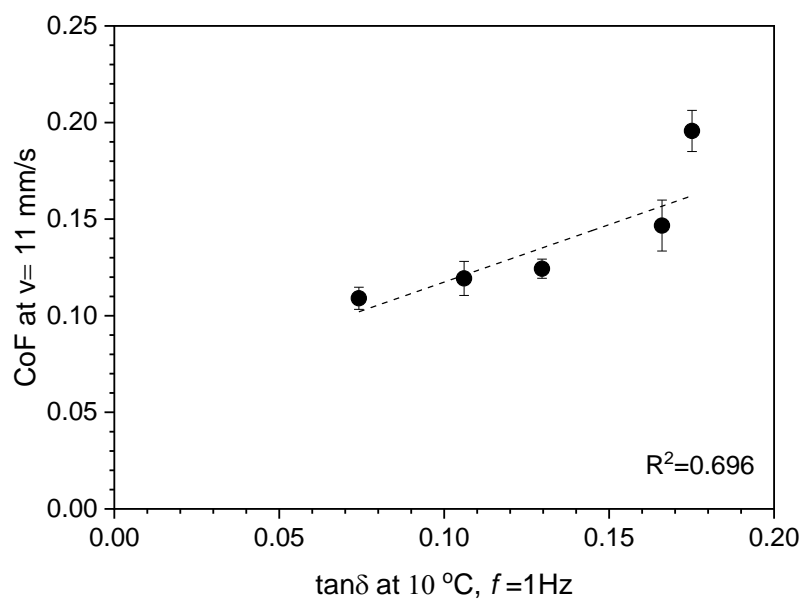
Figure 5.20 Plot of CoFs at the sliding velocity of 11 mm/s for the TPUs vs. the $\boldsymbol{tan\ \delta}$ at T = 10 °C; f = 1 Hz.
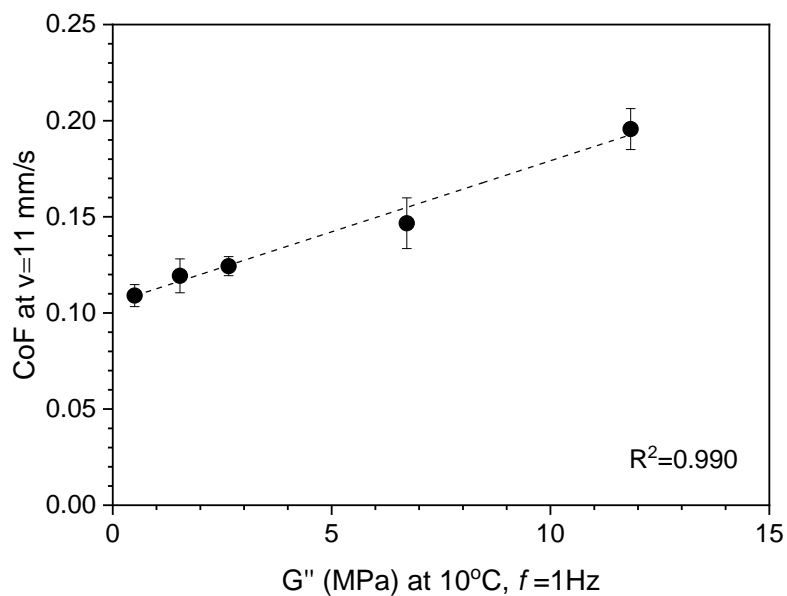
Figure 5.21 Plot of CoFs at the sliding velocity of 11 mm/s for the TPUs vs. the $\boldsymbol{G}''$ at T = 10 °C and f = 1 Hz.
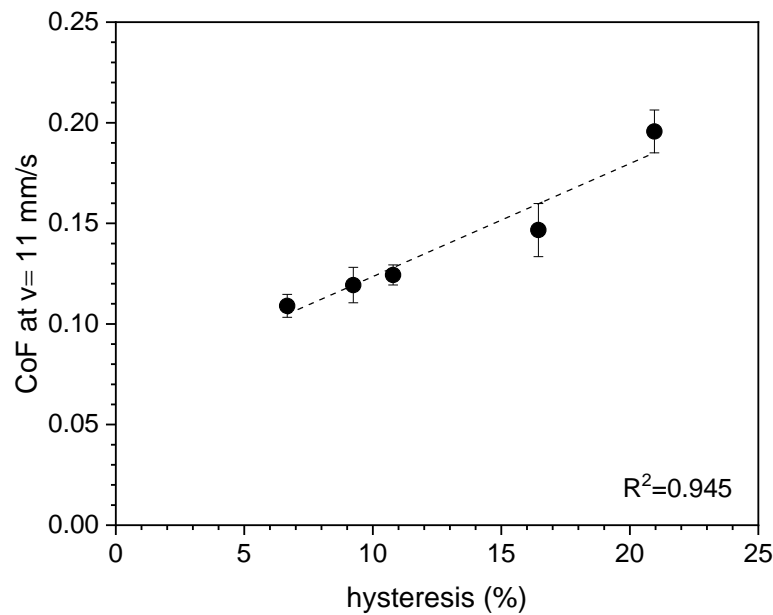
Figure 5.22 Plot of CoFs at the sliding velocity of 11 mm/s for the TPUs vs. the material hysteresis (maximum strain of 10%)

Previous studies on elastomers often reported the opposite results that increased shoe material hardness significantly reduced the hysteresis friction [42][87][122][123]. Softer elastomers experience more deformation while mechanically interlocking with the asperities in the surface, which may contribute to the hysteresis friction. However, in those studies, the softer material was also rougher than the harder material, and hence the surface roughness may have helped to increased the hysteresis. The empirical rules that soling materials with more hardness and solidity makes the shoe more prone to slipping [124] may be the consequence of the combined effect of shoe hardness and roughness.

The frictional test was also carried on a TPU with Shore 64D in hardness, manufactured using a high amount of the chain extender. Due to the close contact and the high contact pressure between the steel ball and the relatively stiff TPU surface, the tips of the steel balls were quickly worn out and the repeatability of the measurement was unsatisfactory. The result for the hard TPU sample is not included in the discussion, but the data is shown in Appendix A.2 for reference.

5.3.4　Intermediate summary

The lubricated friction of five TPU samples with different hardnesses was investigated using the three-ball-on-plate tribo-rheometer. To prevent the surface roughness from interfering the results, the samples were pre-treated with a hot-pressing process to obtain the same level of roughness. Within the tested range of hardnesses, the CoFs in the mixed lubrication regime increase with increasing TPU bulk hardness, and the following correlations with dynamic mechanical properties of TPU are summarized below:

Through the time-temperature superposition, the CoFs at the sliding velocity of 11 mm/s are associated with the viscoelastic properties of TPUs at the relevant temperature of ca.10 ºC in the temperature dependent DMA curves at a deformation frequency of 1 Hz. The CoFs show linear correlations with the $tan\ \delta$ and G'' at 10 °C and also with the material hysteresis at 10% maximum strain. The friction appears to have curved dependence on the $tan\ \delta$ while a linear correlation seems to exist between the friction and the G'' or the lower part of the hysteresis at 10% maximum strain.

6. Experimental

6.1 Material

6.1.1   Manufacture of the thermoplastic polyurethane elastomers

The thermoplastic polyurethane elastomer sheets were prepared from 4,4'-methylene diphenyl diisocyanate (MDI) as isocyanate, 1,4-butanediol as chain extender and polytetrahydrofuran (PTHF) as polymer glycol. Different levels of hardness were obtained by changing the content of the chain extender. The TPUs were produced by BASF Polyurethanes GmbH using a band casting process. The reaction mixture was continuously fed to a conveyor belt through a mixing head regulated to a prescribed temperature to polymerize the mixture. The casts were chopped and passed through an extruder to make pellets which were subsequently injection-molded to obtain uniform sheets. The sheets were annealed at 100 °C for 20 hours in order to get optimum properties.

6.1.2   Surface roughening of the thermoplastic polyurethane elastomer

The surfaces of the TPU sheets were subjected to hot-pressing and were roughened by sandpaper imprinting using five grades of different abrasive grit to obtain different surface parameters. The finest grade was P800 (particle size = 21.8 µm), the next was P400 (particle size = 35.0 µm), then P240 (particle size = 58.5 µm) and P180 (particle size = 82 µm), and the coarsest grade was P120 (particle size = 125 µm) [125]. During the hot pressing, a TPU sheet was pre-heated to a temperature of 100 ºC for 20 minutes. The upper surface of the TPU sheet was pressed against a piece of sandpaper for 90 seconds, and then was taken off the heating plates and cooled down to the room temperature. Hence the pattern of the sandpaper was transferred to the TPU surface. In the study of the effect of surface characteristics on the CoF, a pressure between 50 bar to 95 bar was carefully adjusted to achieve two groups of surface characteristics: (i) the five surfaces with varying S_m and a similar level of R_a and R_{tm} by applying different sandpaper grades; (ii) the two surfaces with varying R_a and R_{tm}, and a similar S_m by using a single type of sandpaper P180 under varying load. Another smooth surface was used as the reference in friction measurements without the hot-pressing treatment. All the surfaces used in the study of the effect of TPU hardness on the CoF were pretreated with the sandpaper P180 in order to have the consistent values of S_m, R_a and R_{tm}. Subsequently, the TPU sheets were washed in a 5-minute ultrasonic water bath treatment to

remove the residual grit on the surfaces. They were cut to obtain round disks with a diameter of 40 mm for friction measurements.

6.1.3 Polyoxymethylene disk

The POM (RCT®-SH) used in this work was purchased from Reichelt Chemietechnik GmbH. The 500×500 mm plate had a thickness of 2 mm and a R_q of 0.043±0.005 µm. It was cut to obtain round disks with a diameter of 40 mm.

6.2 Methods

6.2.1 Surface roughness parameters measurement

The surface roughness parameters of the TPUs were characterized by a white-light interferometric optical profiler (Nexview®, Zygo Corporation). The evaluation length (l_N) was 4 mm, and the cut-length (l_r) was 0.8 mm. The lateral resolution is 0.811 µm. The surface parameters obtained on one TPU sheet were recorded by averaging the 10 readings from 10 randomly chosen locations. All the sample surfaces were judged as being isotropic in terms of surface characteristics.

6.2.2 Hardness measurement

The bulk hardness of the samples was measured by the durometer HBA100-0 (Sauter) at the room temperature. The testing protocol was based on the DIN ISO 7619-1 standard for the measurement of hardness in Shore for thermoplastic elastomers. The specimen was placed on a hard-flat substrate underneath the indenter. The steel indenter is either configured as a frustum cone (Shore A) or a needle pin (Shore D) (see Figure 6.1). With Shore A, the point of the indenter dents in the material, whereas with Shore D it penetrates the material. The depth of indentation or penetration was measured on a scale of 0 to 100, with higher values indicating a harder material. The testing time was 15 seconds, as shore hardness reduces as testing continues. Each data was determined by taking an average of five readings in different spots. The durometer was calibrated with the referential elastomer blocks before the measurements. The measurement tolerance was ±2 HD.
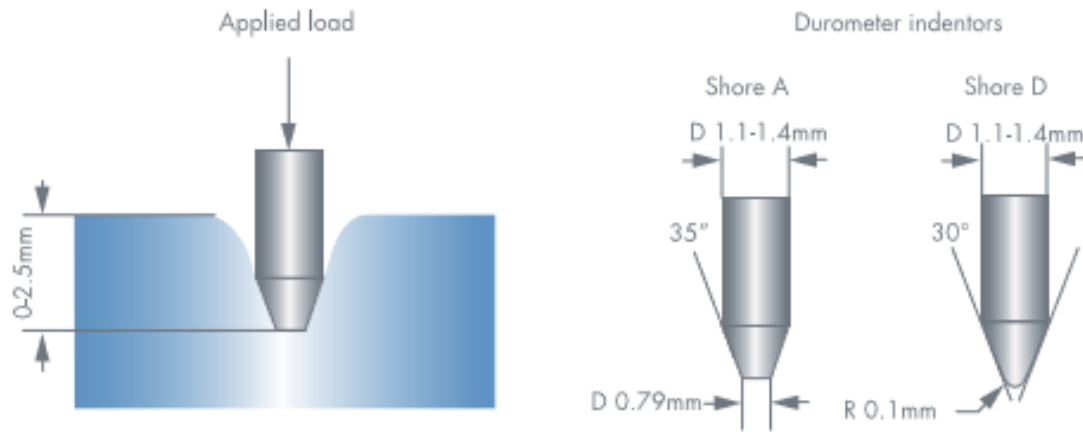
6. Experimental

Figure 6.1 Indentor and press foot for a Shore A type durometer and a Shore D type durometer (Reprinted from Ref.[126])

6.2.3 Dynamic mechanical analysis (DMA)

The dynamic viscoelastic properties (storage modulus, loss modulus and loss factor) of the TPUs were obtained using an ARES rheometer (TA Instruments Inc.) in torsional oscillation mode at a frequency of 1 Hz and a deflection of 0.3%. The dimensions of the sample were 12 × 2 × 50 mm^3. The range of temperature was between -80 °C and 140 °C and the heating was done in steps of 5°C.

6.2.4 Cyclic tensile testing

Tension experiments were performed using a Zwick Roell Z1.0 testing machine with the type of load cell Xforce P. Type S2 specimens as defined in Standard DIN 53504:1994-05 [127] were used. One specimen was held on the machine between two clamps with the rough strips to grip the slippery material better. A force of 0.5 N was preloaded to fully stretch the specimen at a pre-load speed of 50 mm/min. A typical cycle of the tensile test consists of an imposed traction to a set maximum strain of 10% at a strain rate of 10 mm/min followed by a return to zero load. Another four cyclic tests were followed by performing subsequent loading and unloading trials immediately following the initial loading.

Random spots were painted on the narrow part of a specimen to record the strain during the stretching and relaxation of the material. The camera videoXtens determined the displacement of several spots on the specimen. The displacement of those spots in the loading direction over time permitted to calculate the strain rate and the strain. The displacement along the transverse direction was very small and so was not taken into account.

77

6. Experimental

6.2.5 Friction measurement

Friction measurements were made using a combined motor and transducer Discovery Hybrid Rheometer 2 ("DHR-2", TA Instruments Inc.) with a three-ball-on-plate tribo-rheometry accessory previously designed at BASF SE. The test protocol was defined as follows. The steel balls were carefully cleaned with acetone before use to remove organic residue on the ball surface. Subsequently, the balls were rinsed with deionized water. The POM disks were cleaned by a piece of cloth wetted with a 50 wt% ethanol-water solution while the TPU disks were cleaned by a piece of cloth wetted with cyclohexane, both rinsed thoroughly with flowing deionized water after the cleaning and allowed to dry for a day prior to use. The sample disk was mounted in the reservoir and fully immersed with the test fluid. The reservoir was refilled with new test fluid after every 20 minutes during the test. The test conditions for a whole series of friction measurement on one type of material are listed in the table below. The friction was measured on one sample at ten angular velocities. Within the velocity range, it can be reasonably assumed that the interfacial heating effect related to the local increase in contact temperature is negligible [49]. Each measurement at a single velocity lasted for 120 seconds and the result was taken as the averaged value of the CoF recorded in the last 100 seconds. The series of measurements for one lubricant viscosity was repeated on two or three samples. The results in the repetitive measurements were averaged and the standard deviations were shown by the error bars on the data points (see Figure 5.3 for example). After all friction measurements were done on one sample another single measurement was made immediately using the same sample at v =33.5 mm/s and the obtained CoF was compared with the one measured previously at v =33.5 mm/s for a check of repeatability. No significant changes in the CoF were found, showing the trivial effect of surface wear. The same set of TPU surfaces were used for each lubricant viscosity without replacing with a new set of TPU surfaces to minimize surface variability.

6. Experimental

A copy of Table 5.1 from Section 5.1.2 Test conditions

Test variable	Abbreviation (unit)	Setting
Angular sliding velocity	Ω (rad/s)	Ω = 0.3; 0.5; 1; 2; 3; 5; 10; 14; 20 and 30 rad/s
Corresponding linear sliding velocity	v (mm/s)	v = 3.3; 5.6; 11.2; 22.3; 33.5; 55.8; 111.5; 156.1; 223.0 and 334.5 mm/s
Axial force (load)	F_A (N)	F_A=1.0 ±0.1 N
Lubricant	glycerin-water mixtures	40 wt%; 60 wt%; 86.6 wt% glycerin in water
Environment temperature and humidity	T (°C); H (%RH)	24-33 °C; 21-53% RH

6.2.6   Viscosity measurement

The dynamic viscosities of the glycerin-water mixtures used in this work were measured by an Anton Paar MCR302 rheometer with a cone-plate measuring device (50 mm; 0.3°) at 25°C. The shear rate equals 500 s^{-1}. Considering the friction measurements were done at a room temperature range of 24-33°C, the viscosities of the test fluids at 30°C were also measured, and the influence on the shape of the Stribeck curve and the conclusions by the minor changes in the viscosity was negligible. Therefore, the set of viscosities measured at 25°C was used for the data analysis throughout the work.

6.2.7   Light microscopy

The micrographs of the steel balls were taken using the Leica DMi8A microscope (Leica Microsystems GmbH).

6.2.8   Surface free energy measurement

Wettability of polymer surface can be assessed by the surface free energy of the polymer. The work which has to be expended in order to increase the size of the surface of a phase is referred to as the surface free energy (or surface energy). According to Young equation, there is a relationship between the surface free energy σ_s of the solid, the contact angle θ, the surface tension of the liquid σ_l and the interfacial tension γ_{sl} between the two phases:

Equation 6.1

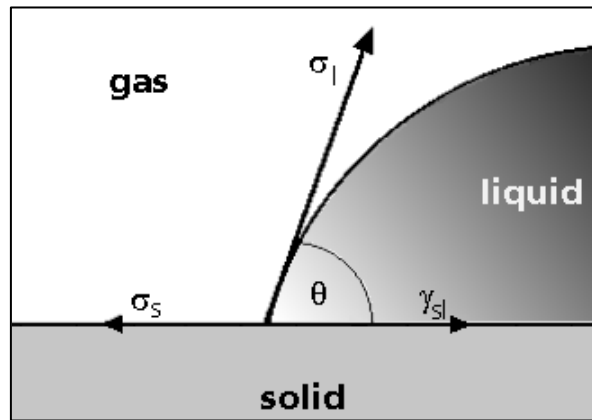$$\sigma_s = \gamma_{sl} + \sigma_l \cdot cos\theta$$

Figure 6.2 Schematic diagram of contact angle on a solid surface

The surface free energy of solid and the surface tension of liquid can be easily measured, but the problem is that the unknown γ_{sl} cannot be measured directly. To be able to solve the equation, more assumption of the relationship between σ_s, γ_{sl} and σ_l has to be made.

A number of models, for example, Zisman, Fowkes, OWRK and Wu, exist with which the surface energy can be calculated with given contact angle data. With most models, a second equation which has the following general form is set up to calculate the interfacial tension:

Equation 6.2

$$\gamma_{sl} = \sigma_s + \sigma_l - [interaction\ between\ phases]$$

The models differ in the way in which the interactions are interpreted and which interaction components of the individual phases are made responsible for producing the surface tension or surface free energy.

In this work, the contact angles of water, ethylene glycol and 1-bromonaphthalene on a TPU surface were measured by DSA 20 (KRÜSS GmbH). The surface free energy was calculated by applying the Owens, Wendt, Rabel and Kaelble (OWRK) method [128] [129][130]. The surface energy of each phase was split up into a polar and a disperse fraction:

Equation 6.3

$$\sigma_l = \sigma_l^P + \sigma_l^D$$

6. Experimental

$$\sigma_s = \sigma_s^P + \sigma_s^D$$

The method took a second equation for the interfacial tension

$$\gamma_{sl} = \sigma_s + \sigma_l - 2\left(\sqrt{\sigma_s^D \cdot \sigma_l^D} + \sqrt{\sigma_s^P \cdot \sigma_l^P}\right)$$

The equation was combined with Young equation and was adapted by transposition to the general equation for a straight line

$$y = mx + b$$

The transposed equation is shown below:

$$\frac{(1 + cos\theta) \cdot \sigma_l}{2\sqrt{\sigma_l^D}} = \sqrt{\sigma_s^P} \cdot \sqrt{\frac{\sigma_l^P}{\sigma_l^D}} + \sqrt{\sigma_s^D}$$

The polar and disperse fractions of the surface free energy were calculated with the aid of a single linear regression from the contact angle data of the three liquids with known disperse and polar fractions of the surface tension. In a linear regression of the plot of y against x, σ_s^P was obtained from the square of the slope of the curve m and σ_s^D from the square of the ordinate intercept b. (see Figure 6.3)
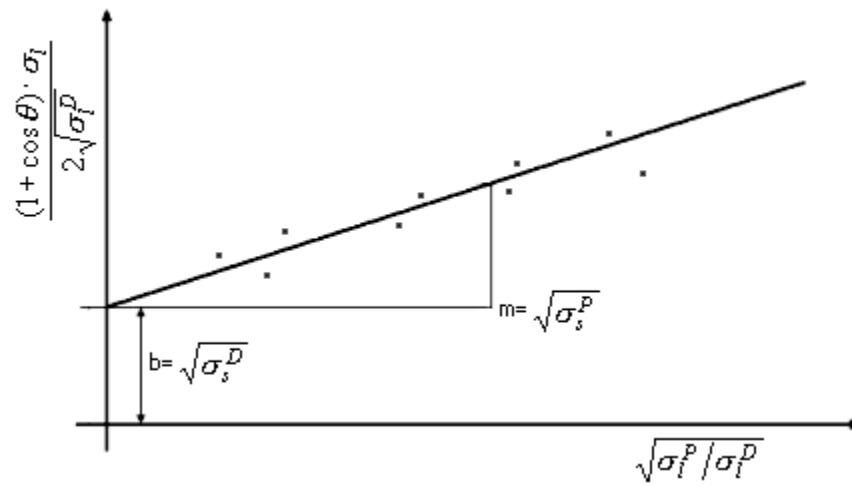
Figure 6.3 Determination of the disperse and polar fractions of the surface free energy (Reprinted from Ref.[128])

7. Literature

[1]   O. Bayer, W. Siefken, H. Rinke, L. Orthner, and H. Schild, "Verfahren zur Herstellung von Polyurethanen bzw. Polyharnstoffen (Process for the preparation of polyurethanes or polyureas)," DE728981, 1937.

[2]   Z. S. Petrović and J. Ferguson, "Polyurethane elastomers," *Prog. Polym. Sci.*, vol. 16, pp. 695–836, 1991.

[3]   H. W. Engels *et al.*, "Polyurethanes: Versatile materials and sustainable problem solvers for today's challenges," *Angew. Chemie - Int. Ed.*, vol. 52, no. 36, pp. 9422–9441, 2013.

[4]   Cristina Prisacariu, "Mechanical aspects of polyurethane elastomers," in *Polyurethane Elastomer: From Morphology to Mechanical Aspects*, SpringerWienNewYork, 2011, p. 255.

[5]   M. S. Redfern and B. Bidanda, "Slip resistance of the shoe-floor interface under biomechanically-relevant conditions," *Ergonomics*, vol. 37, no. 3, pp. 511–524, 1994.

[6]   D. P. O'Hara, B. J. Duggan, G. M. Comer, D. J. Goldhardt, and L. M. Sanmiguel, "US 6464686B1, Polyurethane feeding tube and assciated adaptors," 2002.

[7]   R. A. Beck and R. W. Truss, "Effect of chemical structure on the wear behaviour of polyurethane-urea elastomers," *Wear*, vol. 218, no. 2, pp. 145–152, 1998.

[8]   "Polyurethanes in Footwear." [Online]. Available: http://www.polyurethanes.org/en/where-is-it/footwear.

[9]   "Unit2-Sustainable materials and components for footwear (online course 'How to implement sustainable manufacturing in footwear- New occupational profile and training opportunities' www.step2sustainability.eu)," 2016.

[10]   R. M. Karkalić, J. R. Radulović, and D. B. Jovanović, "Characteristics of polyurethane and elastomer parts for shoe industry produced by liquid injection," *Mil. Tech. Cour.*, vol. 65, no. 4, pp. 948–968, 2017.

[11]   "Elastopan-footwear systems." [Online]. Available: http://www.polyurethanes.basf.com/pu/solutions/en/content/group/Arbeitsgebiete_und_ Produkte/Systeme/Elastopan-Schuhsysteme.

[12]   "polyurethane boots." [Online]. Available: http://www.ecoboots.com.br/en/polyurethane.

[13]   A. Schallamach, "A theory of dynamic rubber friction," *Wear*, vol. 6, no. 5, pp. 375–382, 1963.

[14]   D. F. Moore, *The friction and lubrication of elastomers*. Pergamon Press Ltd., 1972.

[15]   S. Bahadur, "Friction of polymers," in *Encyclopedia of tribology*, Q. J. Wang and Y.-W. Chung, Eds. Springer, Boston, MA, 2013, pp. 1365–1372.

[16] D. F. Moore and W. Geyer, "A review of adhesion theories for elastomers," *Wear*, vol. 22, no. 2, pp. 113–141, 1972.

[17] D. I. James, *Abrasion of rubber*. London: MacLaren & Sons, Ltd., 1967.

[18] R. H. Thurston, *Friction and Lubrication.Determinations of the Laws and Co-efficients of Friction by New Methods and with New Apparatus*. New York: The Railroad Gazette, 1879.

[19] R. Stribeck, "Die Wesentlichen Eigenschaften der Gleit- und Rollenlager (the main characteristics of the sliding and roller bearings)," *Zeitschrift des Vereins Dtsch. Ingenieure*, vol. 36(Band46), pp. 1341-48,1432-38,1463-70, 1902.

[20] M. Woydt and R. Wäsche, "The history of the Stribeck curve and ball bearing steels: The role of Adolf Martens," *Wear*, vol. 268, no. 11–12, pp. 1542–1546, 2010.

[21] L. Gümbel, "Das Problem der Lagerreibung (The problem with the bearing friction)," *Mitteilungsblatt des Berliner Bezirksvereins Dtsch. Ingenieure (VDI)*, no. 5, pp. 87-104,109-120, 1914.

[22] M. D. Hersey, "The laws of lubrication of horizontal journal bearings," *J. Washingt. Acad. Sci.*, vol. 4, no. 19, pp. 542–552, 1914.

[23] H. Tian, N. Saka, and N. P. Suh, "Surfaces boundary lubrication studies on undulated titanium surfaces," *Tribol. Trans.*, vol. 32, no. 3, pp. 289–296, 2008.

[24] I. M. Feng, W. L. Perilstein, and M. R. Adams, "Solid film deposition and non-sacrificial boundary lubrication," *ASLE Trans.*, vol. 6, no. 1, pp. 60–66, 1963.

[25] N. K. Myshkin, M. I. Petrokovets, and A. V. Kovalev, "Tribology of polymers: Adhesion, friction, wear, and mass-transfer," *Tribol. Int.*, vol. 38, no. 11-12 SPEC. ISS., pp. 910–921, 2005.

[26] I. V. Kragelskii, M. N. Dobychin, and V. S. Kombalov, *Friction and Wear*. Oxford: Pergamon Press, 1982.

[27] M. Godet, "The third-body approach: A mechanical view of wear," *Wear*, vol. 100, no. 1–3, pp. 437–452, 1984.

[28] B. N. J. Persson, "Rubber friction : role of the flash temperature," *J. Phys. Condens. Matter*, vol. 18, pp. 7789–7823, 2006.

[29] P. M. Lugt and G. E. Morales-Espejel, "A review of elasto-hydrodynamic lubrication theory," *Tribol. Trans.*, vol. 54, no. 3, pp. 470–496, 2011.

[30] H. A. Spikes and A. V. Olver, "Basics of mixed lubrication," *Lubr. Sci.*, vol. 16, no. 1, pp. 1–28, 2006.

[31] A. Kovalchenko, O. Ajayi, A. Erdemir, G. Fenske, and I. Etsion, "The effect of laser surface texturing on transitions in lubrication regimes during unidirectional sliding contact," *Tribiology Int.*, vol. 38, pp. 219–225, 2005.

[32] E. Cuilli, "Friction in lubricated contacts: from macro- to microscale effects," in *Fundamentals of Tribology and Bridging the Gap Between the Macro- and Micro/Nanoscales*, B. Bhushan, Ed. Springer, Dordrecht, 2001.

[33]   J. E. Shigley, *Mechanical Engineering Design*, 1st ed. McGraw-Hill, 1988.

[34]   S. Dizdar and S. Andersson, "Influence of pre-formed boundary layers on wear transition in sliding lubricated contacts," *Wear*, vol. 213, no. 1–2, pp. 117–122, 1997.

[35]   J. P. Davim, Ed., *Technology in Manufacturing Technology*. Heidelberg: Springer,Berlin, 2013.

[36]   I. Hutchings, *Tribology: Friction and Wear of Engineering Materials*, 1st ed. Butterworth-Heinemann, 1992.

[37]   B. N. J. Persson, "Theory of rubber friction and contact mechanics," *J. Chem. Phys.*, vol. 115, p. 3840, 2001.

[38]   J. H. H. Bongaerts, K. Fourtouni, and J. R. Stokes, "Soft-tribology: Lubrication in a compliant PDMS-PDMS contact," *Tribol. Int.*, vol. 40, no. 10-12 SPEC. ISS., pp. 1531–1542, 2007.

[39]   M. Scaraggi, G. Carbone, and D. Dini, "Experimental evidence of micro-EHL lubrication in rough soft contacts," *Tribol. Lett.*, vol. 43, no. 2, pp. 169–174, 2011.

[40]   A. Krzeminski, S. Wohlhüter, P. Heyer, J. Utz, and J. Hinrichs, "Measurement of lubricating properties in a tribosystem with different surface roughness," *Int. Dairy J.*, vol. 26, no. 1, pp. 23–30, Sep. 2012.

[41]   L. Strandberg, "The effectof conditions underfoot on falling and overexertion accidents," *Ergonomics*, vol. 28, no. 1, pp. 131–147, 1985.

[42]   M. J. H. Cowap, S. R. M. Moghaddam, P. L. Menezes, and K. E. Beschorner, "Contributions of adhesion and hysteresis to coefficient of friction between shoe and floor surfaces: effects of floor roughness and sliding speed," *Tribol. - Mater. Surfaces Interfaces*, vol. 9, no. 2, pp. 77–84, 2015.

[43]   D. P. Manning, C. Jones, F. J. Rowland, and M. Roff, "The Surface Roughness of a Rubber Soling Material Determines the Coefficient of Friction on Water-Lubricated Surfaces," *J. Safety Res.*, vol. 29, no. 4, pp. 275–283, 1998.

[44]   W. R. Chang, I. J. Kim, D. P. Manning, and Y. Bunterngchit, "The role of surface roughness in the measurement of slipperiness," *Ergonomics*, vol. 44, no. 13, pp. 1200–1216, 2001.

[45]   F. Rowland, C. Jones, and D. Manning, "Surface roughness of footwear soling materials: relevance to slip resistance," *J. Test. Eval.*, vol. 24, no. 6, pp. 368–376, 1996.

[46]   J. A. Greenwood and J. B. P. Williamson, "Contact of nomimally flat surface," *Proceeding R. Soc. A*, vol. 295, no. 1442, pp. 300–319, 1966.

[47]   W. R. Chang, "The effects of surface roughness and contaminants on the dynamic friction between porcelain tile and vulcanized rubber," *Saf. Sci.*, vol. 40, no. 7–8, pp. 577–591, 2002.

[48]   K. A. Grosch, "The relation between the friction and viscoelastic properties of rubber," *Proceeding R. Soc. A*, no. 274, p. 21, 1963.

[49]   K. A. Grosch, "Relation between the friction and visco-elastic properties of rubber,"

Nature, vol. 197, no. 4870, p. 858, 1963.

[50]   K. Hanhi and B. Stenberg, "Friction and the dynamic mechanical and thermal properties of polyurethane elastomers. I: Solid polyurethanes.," *Cell. Polym.*, vol. 12, no. 6, pp. 461–493, 1993.

[51]   K. Hanhi and B. Stenberg, "Friction and the dynamic mechanical and thermal properties of polyurethane elastomers. II: Microcellular polyurethanes.," *Cell. Polym.*, vol. 13, no. 1, pp. 33–56, 1994.

[52]   S. Futamura, "Effect of Material Properties on Tire Performance Characteristics — Part II, Tread Material," *Tire Sci. Technol.*, vol. 18, no. 1, pp. 2–12, 1990.

[53]   H. Takino, R. Nakayama, Y. Yamada, S. Kohjiya, and T. Matsuo, "Viscoelastic Properties of Elastomers and Tire Wet Skid Resistance," *Rubber Chem. Technol.*, vol. 70, no. 4, pp. 584–594, 1997.

[54]   X. Pan, E. D. Kelley, and M. W. Hayes, "Bulk Viscoelastic Contribution to the Wet-Sliding Friction of Rubber Compounds," *J. Polym. Sci. Part B Polym. Phys.*, vol. 41, pp. 757–771, 2003.

[55]   X. Pan, "Significance of tuning bulk viscoelasticity via polymer molecular design on wet sliding friction of elastomer compounds," *Tribol. Lett.*, vol. 20, no. 3–4, pp. 209–219, 2005.

[56]   C. Wetzel, U. Windhövel, D. Mewes, and O. Ceylan, "Slipping on pedestrian surfaces: Methods for measuring and evaluating the slip resistance," *Int. J. Occup. Saf. Ergon.*, vol. 21, no. 3, pp. 256–267, 2015.

[57]   W. R. Chang, S. Leclercq, T. E. Lockhart, and R. Haslam, "State of science: occupational slips, trips and falls on the same level," *Ergonomics*, vol. 59, no. 7, pp. 861–883, 2016.

[58]   W. R. Chang *et al.*, "The role of friction in the measurement of slipperiness, Part 1: Friction mechanisms and definition of test conditions," *Ergonomics*, vol. 44, no. 13, pp. 1217–1232, 2001.

[59]   W. R. Chang *et al.*, "The role of friction in the measurement of slipperiness, Part 2: Survey of friction measurement devices," *Ergonomics*, vol. 44, no. 13, pp. 1233–1261, 2001.

[60]   R. Myung, J. L. Smith, and T. B. Leamon, "Slip distance as an objective criterion to determine the dominant parameter between static and dynamic CoFs," in *Proceedings of the Human Factors Society 36th Annual Meeting*, 1992, pp. 738–741.

[61]   L. Strandberg and H. Lanshammar, "The dynamics of slipping accidents," *J. Occup. Accid.*, vol. 3, no. 3, pp. 153–162, 1981.

[62]   M. Tisserand, "Progress in the prevention of falls caused by slipping," *Ergonomics*, vol. 28, no. 7, pp. 1027–1042, 1985.

[63]   R. Grönqvist, "On transitional friction measurement and pedestrian slip resistance," in *XIII Triennial Congress of the International Ergonomics Association, IEA.*, 1997, pp. 383–385.

[64]   R. Grönqvist, M. Hirvonen, and A. Tohv, "Evaluation of three portable floor slipperiness testers," *Int. J. Ind. Ergon.*, vol. 25, no. 1, pp. 85–95, 1999.

[65]   D. Mewes, "OSHwiki-Measuring the slip resistance of floorings and footwear," *2017*. [Online]. Available: https://oshwiki.eu/wiki/Measuring_the_slip_resistance_of_floorings_and_footwear.

[66]   S. Di Pilla, *Slip and Fall Prevention: A Practical Handbook*, 1st ed. CRC Press, 2003.

[67]   G. W. Harris and S. R. Shaw, "Slip resistance of floors: Users' opinions, Tortus instrument readings and roughness measurement," *J. Occup. Accid.*, vol. 9, no. 4, pp. 287–298, 1988.

[68]   "European Committee for Standardization (CEN). Determination of slip resistance of pedestrain surfaces -methods of evaluation (Technical Specification No. CEN/TS16165:2012)." Brussels, 2012.

[69]   "German Institute for Standardisation (DIN). Testing of floor coverings -determination of the anti-slip property -method for measurement fo the sliding friction coefficient. Standard No. DIN 51131:2014." Berlin: Beuth, 2014.

[70]   R. H. Smith, *Analyzing friction in the design of rubber products and their paired surfaces*. Boca Raton, Florida: CRC Press, Taylor & Francis Group, 2008.

[71]   S. Di Pilla, *Slip, Trip, and Fall Prevention: A Practical Handbook, Second Edition*, 2nd ed. CRC Press, Taylor & Francis Group, 2009.

[72]   "BS 7976-2:2002+A1:2013 Pendulum testers. Method of operation."

[73]   "ASTM E303 - 93(2013) Standard Test Method for Measuring Surface Frictional Properties Using the British Pendulum Tester."

[74]   R. Grönqvist, J. Roine, E. Järvinen, and E. Korhonen, "An apparatus and a method for determining the slip resistance of shoes and floors by simulation of human foot motions," *Ergonomics*, vol. 32, no. 8, pp. 979–995, 1989.

[75]   T. Jones, A. Iraqi, and K. Beschorner, "Performance testing of work shoes labeled as slip resistant," *Appl. Ergon.*, vol. 68, no. December 2017, pp. 304–312, 2018.

[76]   K. E. Beschorner, M. S. Redfern, W. L. Porter, and R. E. Debski, "Effects of slip testing parameters on measured coefficient of friction," *Appl. Ergon.*, vol. 38, no. 6, pp. 773–780, 2007.

[77]   W. R. Chang, R. Grönqvist, M. Hirvonen, and S. Matz, "The effect of surface waviness on friction between Neolite and quarry tiles," *Ergonomics*, vol. 47, no. 8, pp. 890–906, 2004.

[78]   K. W. Li and C. J. Chen, "The effect of shoe soling tread groove width on the coefficient of friction with different sole materials, floors, and contaminants," *Appl. Ergon.*, vol. 35, no. 6, pp. 499–507, 2004.

[79]   K. W. Li, H. H. Wu, and Y. C. Lin, "The effect of shoe sole tread groove depth on the friction coefficient with different tread groove widths, floors and contaminants," *Appl. Ergon.*, vol. 37, no. 6, pp. 743–748, 2006.

[80]   I. J. Kim, "Investigation of Floor Surface Finishes for Optimal Slip Resistance
        Performance," *Saf. Health Work*, vol. 9, no. 1, pp. 17–24, 2018.

[81]   M. Wilson, "Development of SATRA slip test and tread pattern design guidelines," in
        Slips, Stumbles, and Falls: Pedestrian Footwear and Surfaces, ASTM STP1103, B.
        Gray, Ed. 1990, pp. 113–123.

[82]   "ISO 13287:2012(E) Personal protective equipment - Footwear - Test method for slip
        resistance."

[83]   S. Leclercq, M. Tisserand, and H. Saulnier, "Assessment of the slip-resistance of floors
        in the laboratory and in the field: Two complementary methods for two applications,"
        Int. J. Ind. Ergon., vol. 13, no. 4, pp. 297–305, 1994.

[84]   C. M. Powers, J. R. Brault, M. A. Stefanou, Y. J. Tsai, J. Flynn, and G. P. Siegmund,
        "Assessment of walkway tribometer readings in evaluating slip resistance: A gait-based
        approach," *J. Forensic Sci.*, vol. 52, no. 2, pp. 400–405, 2007.

[85]   J. D. Clarke, K. Hallas, R. Lewis, S. Thorpe, G. Hunwin, and M. J. Carré,
        "Understanding the friction measured by standardised test methodologies used to
        assess shoe-surface slip risk," *J. Test. Eval.*, vol. 43, no. 4, p. 20120334, 2015.

[86]   C. T. Moore, P. L. Menezes, M. R. Lovell, and K. E. Beschorner, "Analysis of shoe
        friction during sliding against floor material: role of fluid contaminant," *J. Tribol.*, vol.
        134, no. 4, p. 041104, 2012.

[87]   C. M. Strobel, P. L. Menezes, M. R. Lovell, and K. E. Beschorner, "Analysis of the
        contribution of adhesion and hysteresis to shoe-floor lubricated friction in the boundary
        lubrication regime," *Tribol. Lett.*, vol. 47, no. 3, pp. 341–347, 2012.

[88]   M. J. H. Cowap, S. R. M. Moghaddam, P. L. Menezes, and K. E. Beschorner,
        "Contributions of adhesion and hysteresis to coefficient of friction between shoe and
        floor surfaces: effects of floor roughness and sliding speed," *Tribol. - Mater. Surfaces
        Interfaces*, vol. 9, no. 2, pp. 77–84, 2015.

[89]   N. Selway, V. Chan, and J. R. Stokes, "Influence of fluid viscosity and wetting on
        multiscale viscoelastic lubrication in soft tribological contacts," *Soft Matter*, vol. 13, no.
        8, pp. 1702–1715, 2017.

[90]   J. de Vicente, J. R. Stokes, and H. A. Spikes, "Rolling and sliding friction in compliant,
        lubricated contact," *Proc. Inst. Mech. Eng. Part J J. Eng. Tribol.*, vol. 220, no. 2, pp.
        55–63, 2006.

[91]   H. P. Kavehpour and G. H. McKinley, "Tribo-rheometry: From gap-dependent
        rheology to tribology," *Tribol. Lett.*, vol. 17, no. 2, pp. 327–335, 2004.

[92]   P. Heyer and J. Läuger, "A flexible platform for tribological measurements on a
        rheometer," *XV Int. Congr. Rheol. AIP Conf. Proc.*, vol. 1027, pp. 1168–1170, 2008.

[93]   P. Heyer and J. Läuger, "Correlation between friction and flow of lubricating greases in
        a new tribometer device," *Lubriction Sci.*, vol. 21, pp. 253–268, 2009.

[94]   J. M. Kim, F. Wolf, and S. K. Baier, "Effect of varying mixing ratio of PDMS on the
        consistency of the soft-contact Stribeck curve for glycerol solutions," *Tribol. Int.*, vol.
        89, pp. 46–53, Sep. 2015.

[95]   K. Kieserling, S. Schalow, and S. Drusch, "Method Development and Validation of Tribological Measurements for Differentiation of Food in a Rheometer," *Biotribology*, vol. 16, no. January, pp. 25–34, 2018.

[96]   A. He *et al.*, "Tribological Performance and Lubrication Mechanism of Alumina Nanoparticle Water-Based Suspensions in Ball-on-Three-Plate Testing," *Tribol. Lett.*, vol. 65, no. 2, pp. 1–11, 2017.

[97]   U. A. Mannan and R. A. Tarefder, "Tribological and rheological characterisation of asphalt binders at different temperatures," *Road Mater. Pavement Des.*, vol. 19, no. 2, pp. 445–452, 2018.

[98]   S. M. Goh, P. Versluis, I. A. M. Appelqvist, and L. Bialek, "Tribological measurements of foods using a rheometer," *Food Res. Int.*, vol. 43, no. 1, pp. 183–186, 2010.

[99]   P. T. M. Nguyen, B. Bhandari, and S. Prakash, "Tribological method to measure lubricating properties of dairy products," *J. Food Eng.*, vol. 168, pp. 27–34, 2016.

[100] F. C. Godoi, B. R. Bhandari, and S. Prakash, "Tribo-rheology and sensory analysis of a dairy semi-solid," *Food Hydrocoll.*, vol. 70, pp. 240–250, 2017.

[101] Y. Zhu, B. Bhandari, and S. Prakash, "Tribo-rheometry behaviour and gel strength of κ-carrageenan and gelatin solutions at concentrations, pH and ionic conditions used in dairy products," *Food Hydrocoll.*, vol. 84, pp. 292–302, 2018.

[102] F. C. Godoi, B. R. Bhandari, and S. Prakash, "Tribo-rheology and sensory analysis of a dairy semi-solid," *Food Hydrocoll.*, vol. 70, pp. 240–250, 2017.

[103] TA Instruments, "The Discovery Hybrid Rheometer," 2016.

[104] L.-H. Sun, Z.-G. Yang, and X.-H. Li, "Study on the friction and wear behavior of POM/Al2O3 nanocomposites," *Wear*, vol. 264, no. 7–8, pp. 693–700, 2008.

[105] M. Esfahanian and B. J. Hamrock, "Fluid-film lubrication regimes revisited," *Tribol. Trans.*, vol. 34, no. 4, pp. 628–632, 1991.

[106] J. Halling, *Principles of Tribology*. London: The Macmillan Press Ltd, 1975.

[107] D. Downson, C. M. Taylor, T. H. C. Childs, M. Godet, and D. G., Eds., "Thin Films in Tribology (ed. Downson D., Taylor C. et al.)," in *Proceeding of the 19th Leeds-Lyon Symposium on Tribology*, 1993, p. iii-vi.3–749.

[108] B. J. Harmrock, S. R. Schmid, and B. O. Jacobson, *Fundamentals of Fluid Film Lubrication,2nd Edition*. CRC Press, 2004.

[109] A. Srivastava, "PhD thesis. Dynamic Friction Measurement and Modeling at the Micro/Nano Scale," 2006.

[110] M. G. Larson and S. J. Timpe, "Static and dynamic friction characteristics of a steel on polyoxymethylene interface under dry and lubricated contact conditions," in *Proceedings of the ASME 2012 International Mechanical Engineering Congress & Expostition IMECE2014-38345*, 2014.

[111] J. Jeong and M. Cho, "Tribological performance of laser-textured polyoxymethylene

under boundary lubricated sliding condition," *J. Frict. Wear*, vol. 38, no. 6, pp. 462–468, 2017.

[112] Zygo, "Understand surface texture parameters, CMP-0514C," 2013.

[113] J. H. H. Bongaerts, K. Fourtouni, and J. R. Stokes, "Soft-tribology: Lubrication in a compliant PDMS-PDMS contact," *Tribol. Int.*, vol. 40, no. 10-12 SPEC. ISS., pp. 1531–1542, 2007.

[114] A. Le Gal, X. Yang, and M. Klüppel, "Evaluation of sliding friction and contact mechanics of elastomers based on dynamic- mechanical analysis," *J. Chem. Phys.*, vol. 123, no. 1, p. 014704, 2005.

[115] R. J. Young and P. A. Lovell, *Introduction to Polymers*, 3rd ed. Routledge, 2011.

[116] X. Pan, "Relationship between the dynamic softening transition and wet sliding friction of elastomer compounds," *J. Polym. Sci. Part B Polym. Phys.*, vol. 42, pp. 2467–2478, 2004.

[117] M. L. Williams, R. E. Landel, and F. D. Ferry, "The temperature dependence of relaxation mechanisms in amorphous polymers and other glass-forming liquids," *J. Am. Chem. Soc.*, vol. 77, pp. 3701–3707, 1955.

[118] L. S. T. J. Korley, B. D. Pate, E. L. Thomas, and P. T. Hammond, "Effect of the degree of soft and hard segment ordering on the morphology and mechanical behavior of semicrystalline segmented polyurethanes," *Polymer (Guildf).*, vol. 47, no. 9, pp. 3073–3082, 2006.

[119] H. J. Qi and M. C. Boyce, "Stress – strain behavior of thermoplastic polyurethanes," *Mech. Mater.*, vol. 37, pp. 817–839, 2005.

[120] S. Abouzahr, G. L. Wilkes, and Z. Ophir, "Structure-property behaviour of segmented polyether-MDI-butanediol based urethanes: effect of composition ratio," *Polymer (Guildf).*, vol. 23, no. 7, pp. 1077–1086, 1982.

[121] H. Cho *et al.*, "Deformation mechanisms of thermoplastic elastomers: Stress-strain behavior and constitutive modeling," *Polymer (Guildf).*, vol. 128, pp. 87–99, 2017.

[122] S. Derler, F. Kausch, and R. Huber, "Analysis of factors influencing the friction coefficients of shoe sole materials," *Saf. Sci.*, vol. 46, pp. 822–832, 2008.

[123] R. Mohan, B. N. Das, and R. Sundaresan, "Effect of Hardness and Surface Roughness on Slip Resistance of Footwear Rubber Sole," *J. Test. Eval.*, vol. 43, no. 6, pp. 1574–1586, 2015.

[124] Y.-J. Tsai and C. M. Powers, "Increased shoe sole hardness results in compensatory changes in the utilized coefficient of friction during walking," *Gait Posture*, vol. 30, pp. 303–306, 2009.

[125] "FEPA-standard 43-1984 R 1993: Grit Sizes for Coated Abrasives; 32GB; 33GB."

[126] INNOVATEST, "Shore durometers." 2015.

[127] "DIN 53504: Prüfung von Kautschuk und Elastomeren – Bestimmung von Reißfestigkeit, Zugfestigkeit, Reißdehnung und Spannungswerten im Zugversuch." p.

20, 2017.

[128] KRÜSS, "Drop shape analysis theory, user manual V100501." 2002.

[129] D. K. Owens and R. C. Wendt, "Estimation of the surface free energy of polymers," *J. Appl. Polym. Sci.*, vol. 13, pp. 1741–1747, 1969.

[130] D. H. Kaelble, "Dispersion-Polar Surface Tension Properties of Organic Solids," *J. Adhes.*, vol. 2, pp. 66–81, 1970.

[131] V. L.Popov, *Contact Mechanics and Friction: Physical Principles and Applications*. Springer, 2010.

[132] R. W. Warfield and F. R. Barnet, "Elastic constants of bulk polymers NOLTR 71-226,Neval Ordnance Laboratory Report," White Oak, Silver Spring, Maryland, 1972.

[133] A. Martin, A. Buguin, and F. Brochard-Wyart, "Dewetting At Soft Interfaces," *Phys. Rev. Lett.*, vol. 80, no. 15, pp. 3296–3299, 1998.

A. Appendix

A.1 Calculating the contact parameters using Hertzian contact theory

In Hertzian contact theory, an elastic medium fills an infinitely large half-space. Under the influence of the forces that act on the free surface, the medium is deformed. The xy-plane is placed on the free surface of the medium; the filled area corresponds to the positive z-direction. The displacement from the force acting at the origin in the z-direction and the contact pressure can be defined in the analytical form. Here I only show the equations which can be directly used for the calculation in this work. The derivation of the formulas is omitted and can be found in textbooks about contact mechanics [131].
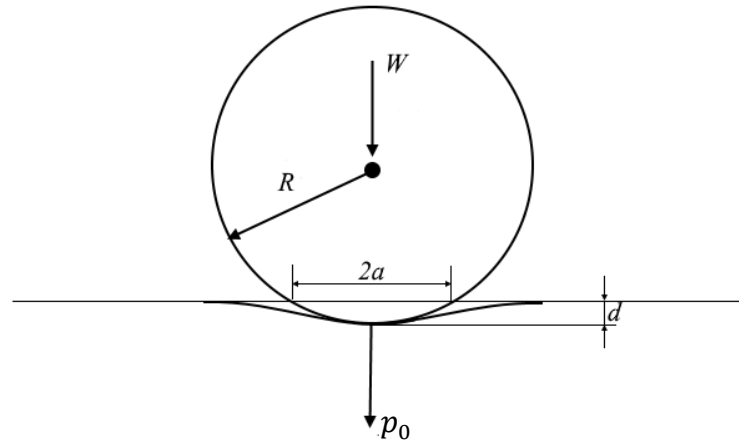
Figure A.1 Schematic diagram of a rigid sphere in contact with an elastic half-space. W-the normal force; p_0- the maximum contact pressure; a- the contact radius; d- the indentation depth

In Figure A.1 a contact between a rigid sphere and an elastic half-space is shown schematically. The displacement of the points on the surface in the contact area between an initially even surface and a rigid sphere of radius R in term of the coordinate r is

Equation A.1

$$u_z = d - \frac{r^2}{2R}$$

where d denotes the indentation depth.

The vertical displacement can also be expressed as

Equation A.2

$$u_z = \frac{\pi p_0}{4 E_e a}(2a^2 - r^2), \quad r \le a.$$

where p_0 is the maximum contact pressure; a is the contact radius; E_e is the effective elastic modulus of the tribopair and is defined by

Equation A.3

$$\frac{1}{E_e} = \frac{1 - {v_1}^2}{E_1} + \frac{1 - {v_2}^2}{E_2}$$

E_1, E_2, v_1, v_2 denote the Young's moduli and the Poisson's ratios of the two contacting bodies. In this work, the DMA tests was considered as a more reliable method than tensile testing to determine the modulus of elasticity (Young's modulus) because the deformation was much smaller (0.3% of strain) and the sensitivity was higher. Since only the torsional DMA test was available, the shear storage modulus G' was used as an approximate value of shear modulus G and G was converted into Young's modulus E using the following expression:

Equation A.4

$$E = 2G(1 + v)$$

The Poisson's ratio is 0.44 for POM and 0.50 for TPU [132]. The Young's modulus and Poisson's ratio of the steel ball are 208 GPa and 0.30.

Equation A.5 is used to find the parameters a and p_0 that cause exactly the displacement

Equation A.5

$$\frac{1}{E_e} \frac{\pi p_0}{4a}(2a^2 - r^2) = d - \frac{r^2}{2R}$$

The variables a and d must, therefore, fulfill the following requirements:

Equation A.6

$$a = \frac{\pi p_0 R}{2 E_e} \quad, \quad d = \frac{\pi p_0 a}{2 E_e}$$

It follows for the contact radius

A. Appendix

$$a^2 = Rd$$

and for the maximum pressure in the center of the contact area

$$p_0 = \frac{2}{\pi} E_e \left(\frac{d}{R}\right)^{1/2}$$

In addition, the total force is already know as

$$W = \int_0^a p(r) 2\pi r \, dr = \frac{2}{3} p_0 \pi a^2$$

substituting from *Equation A.7*, *Equation A.8* into *Equation A.9*, the normal force is obtained:

$$W = \frac{4}{3} E_e R^{1/2} d^{3/2}$$

if d is expressed as a function of W, it will follow as

$$d = \left(\frac{3W}{4E_e}\right)^{2/3} \left(\frac{1}{R}\right)^{1/3}$$

With *Equation A.7*, *Equation A.8* and *Equation A.10*, the maximum pressure in the center of the contact area as well as the contact radius can be calculated as a function of the normal force:

$$p_0 = \left(\frac{6WE_e^2}{\pi^3 R^2}\right)^{1/3}$$

$$a = \left(\frac{3WR}{4E_e}\right)^{1/3}$$

In the frictional measurement, the normal force applied on the rotational shaft of the rheometer is 1.0 N with a sensitivity of ±0.1 N. Assuming distributed evenly onto the three steel spheres, the normal force applied on each sphere is approximately 0.33 N. The *average* contact pressure is used to contruct the Stribeck curve and can be calculated as:

<div align="right">*Equation A.14*</div>

$$P = \frac{the\ normal\ force\ applied\ on\ one\ steel\ sphere}{the\ contact\ area} = \frac{W}{\pi a^2} \approx \frac{F_A}{3\pi a^2}$$

With *Equation A.11*, *Equation A.13* and *Equation A.14*, d, a and P can be calculated accordingly. Table A.1 shows these contact parameters for the materials mentioned in this work. The effect of surface roughness is not considered in the calculation.

Table A.1 Mechanical properties and the physical quantities involved in Hertzian contact for the polymer samples

Material	Shore hardness	Young's modulus E (MPa)	E_e (MPa)	P(kPa)	d(µm)	a(µm)
POM	82D	2811	3433	22325	1.1	69
PU81A	81A	19.1	25.4	848	28	354
PU86A	86A	37.8	50.4	1339	18	282
PU88A	88A	50.7	67.6	1628	14	255
PU91A	91A	89.3	119.1	2374	10	211
PU97A	97A	140.3	186.9	3206	7	182

A.2 Frictional measurement on a hard TPU sample Elastollan® 1164D

In this work, the lubricated friction for a TPU sample with high hard block content-Elastollan® 1164D was also measured. Its hardness reached to 64 Shore D. Due to the high contact pressure in the contact zone, the CoFs recorded at the sliding velocity of 33.5 mm/s kept increasing over time (Table A.2). Signs of wear on the TPU surface were not observed with the naked eyes. However, some scratches were visible on the tips of the steel balls under the microscope (Figure A.2). The fact that the steel balls had been scratched by an elastomer is quite counter-intuitive. The consequent increasing roughness of the steel surface resulted in the continuous increase in the CoF. The Stribeck curve for 1164D (E_{1164D}= 583.7 MPa; P_{1164D} = 8281 kPa) was plotted and compared with the curve for the sample PU86A (Figure A.3). The frictional measurement started at the lowest velocity and then the velocity went up step by step. Due to the surface wear, the CoFs plotted against increasing *Gu* show an upward trend. If the surface wear had not happened, a steady record of the CoF should have been expected, demonstrating the friction of the tribo-system in the boundary lubrication regime.

Figure A.2 Photomicrographs showing the scratches on the tips of a steel ball after the frictional measurement on the 1164D surface
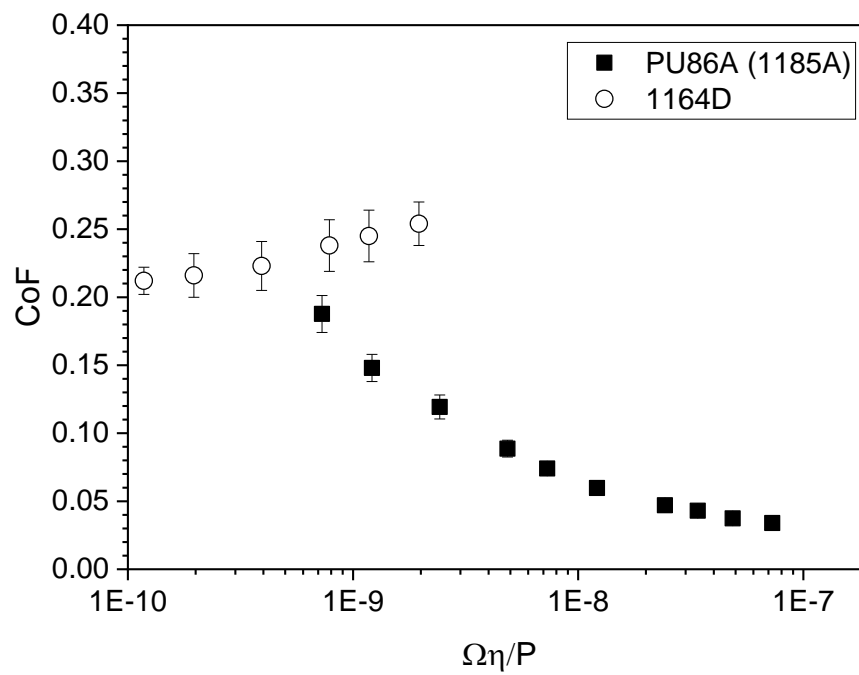
Figure A.3 Stribeck curves for a relatively hard TPU sample 1164D and PU86A

Table A.2 Repeated frictional measurement: after all friction measurements were done on one sample another single measurement was made immediately using the same sample at v of 33.5 mm/s and the obtained CoF was compared with the one measured previously at v of 33.5 mm/s.

Material	Lubricating condition	CoF in the beginning of the test series	CoF in the middle of the test series	CoF at the end of the test series
1164D	40 wt% glycerin	0.135 ($\pm$0.010)	0.245 ($\pm$0.019)	0.262 ($\pm$0.050)

A.3 The surface free energies of the TPUs with different hardnesses and dewetting at soft interfaces

In the mixed lubrication regime, the asperities in the contacting surfaces are not fully separated by the fluid, and direct solid to solid contact exists. There may be electrostatic or van der Vaals forces bonding the molecules in the surface layer of the elastomer and the rigid body. Therefore, besides hysteresis friction which plays a major role in the friction of elastomers on rough surface, adhesion friction is also a possible contribution to the lubricated CoF. Adhesion friction is proportional to the real contact area which is determined by surface energy between two surfaces, asperity radius, combined elastic modulus of two surfaces and normal contact force. A change in surface energy between the contacting surfaces can impact on the dewetting of the lubricant film. The lubricant film dewets by nucleation and growth of a dry patch [133]. The stability of the intercalated liquid film is controlled by the spreading coefficient

Equation A.15

$$S = \gamma_{SR} - (\gamma_{SL} + \gamma_{RL})$$

which compares interfacial energies between "dry" contacts γ_{SR} and lubricated contacts $\gamma_{SL} + \gamma_{RL}$. When S is negative, the system gains energy by excluding the intercalated liquid.
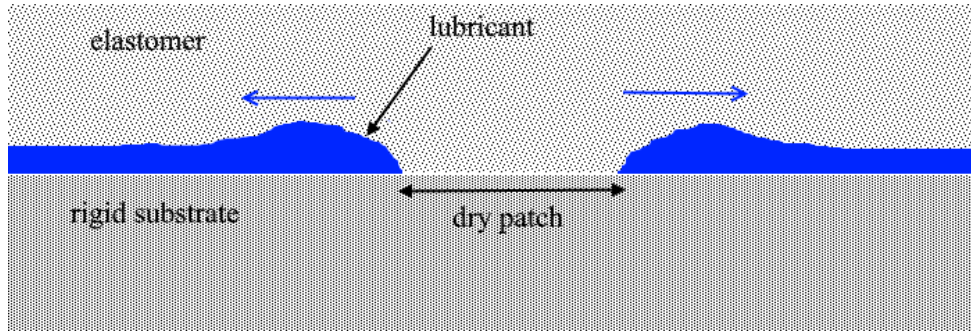
Figure A.4 Dewetting in a lubricant layer intercalated between a rigid substrate and an elastomer

The dewetting rate is fast for a large negative S and a soft elastomer. A high surface roughness of elastomer can trigger the emergence and growth of dry patches. The surface free energies of the five TPU surfaces, as shown in Table A.3, do not have significant difference. Therefore, no obvious difference in spreading coefficient is expected. Considering the five surfaces have a similar level of roughness, the stiffness of the elastomer becomes the most critical factor in determining the surface's dewetting ability. Thus, the lubrication film is more likely to dewet on the soft elastomer surface and the effect may contribute to the total friction. However, the ranking of the CoFs seems not to be strongly influenced by the possible dewetting mechanism, and in general, the CoFs still increase with increasing hardness.

Table A.3 Surface free energy of the five TPU samples with varying hardness used in Section 5.3

Material	Surface free energy (mN/m)	Dispersive part (mN/m)	Polar part (mN/m)
PU81A	37.69 ±3.35	36.90 ±3.25	0.79 ±0.79
PU86A	34.13 ±1.54	33.80 ±1.49	0.33 ±0.36
PU88A	35.40 ±2.12	32.38 ±1.86	3.02 ±1.02
PU91A	29.88 ±3.74	27.58 ±3.57	2.30 ±1.21
PU97A	31.08 ±3.26	29.39 ±3.10	1.70 ±1.01

A.4 List of hazardous substances

List of hazardous substances used in this work according to the Material Safety Data Sheets (MSDS) of the commercially available substances.

Substances	CAS	GHS Pictogram	Signal word	Hazard statements	Precautionary statements
Ethanol	64-17-5		Danger	H225, H319	P210, P233, P240, P241, P280, P303+P361+P353, P337+P313, P370+P378, P403+P325, P501
Cyclohexane	110-82-7		Danger	H225, H304, H315, H336, H400	P210, P233, P261, P273, P280 P301+P310, P303+P361+P353, P304+P340+P312, P331, P370+P378
Isopropanol	67-63-0		Danger	H225, H319, H336	P210, P233, P261, P280, P303+P361+P353, P304+P340+P312, P337+P313, P370+P378, P403+P233, P403+P235
Thermoplastic Polyurethane Elastollan® Series	Not a hazardous substance or mixture according to GHS classification criteria.				

A. Appendix

Glycerin	56-81-5	Not a hazardous substance or mixture according to GHS classification criteria.
Polyoxymethy-lene	9002-81-7	Not a hazardous substance or mixture according to GHS classification criteria.

B. Acknowledgement

B. Acknowledgement

C. Declaration on oath

I hereby declare on oath, that I have written the present dissertation by my own and have not used other than the acknowledged resources and aids. The submitted written version corresponds to the version on the electronic storage medium. I hereby declare that I have not previously applied or pursued for a doctorate (Ph.D. studies).

15 August 2019

_____

Xiangyun Kong